

Report Number CCEER-89-2

**Dynamic Response Analysis of the  
Dominion Road Bridge Test Data**

James Andrew Richardson  
Bruce Douglas

---

**Center for Civil Engineering Earthquake Research**  
Department of Civil Engineering/258  
University of Nevada  
Reno, NV 89557

March 1989

## ACKNOWLEDGEMENTS

The project upon which this dissertation is based was jointly funded by United States and New Zealand research agencies. In the United States, the National Science Foundation financially supported the project under two grants through the Earthquake Hazards Mitigation Program under the direction of Drs. J. B. Scalzi and S. C. Liu. In New Zealand, the National Roads Board contributed funds through the Structures Committee of the Road Research Unit.

People associated with many different organizations cooperated to make the project a successful one, including: Professor Bruce Douglas and Dr. Mehdi Saiidi from the University of Nevada-Reno; Dr. Ian Buckle from Computech Engineering Services, Inc.; and Dr. John Butterworth and Mr. Mike Jones from the University of Auckland. The following organizations also contributed to the project: Central Laboratories and Head Office of the New Zealand Ministry of Works and Development; Auckland City Council Department of Public Works; and Kinematics, Inc. of California.

I would like to thank my wife, my family and my friends for their encouragement while I worked on this dissertation. I am especially grateful for the unwavering support of my parents, to whom I dedicate this dissertation.

and three rotational) were measured on both the superstructure and the foundations of the bridge.

Natural frequencies and three-dimensional mode shapes of the bridge are extracted from the time history data using unique applications of traditional Fourier Transform methods.

Also, a method to separate the responses of vibrations modes closely spaced in frequency is developed.

Finally, a computer model of the bridge response is constructed. The values of the boundary element springs used to represent the foundations were calculated based on geotechnical methods. The model parameters most affecting the model response were identified and their values adjusted in order to bring the model response into reasonable agreement with the measured response. The optimal values of these model parameters were determined using a system identification algorithm.

4.4	CURVE FITTING METHODS . . . . .	100
4.4.1	Preliminaries . . . . .	102
4.4.1.1	Interference . . . . .	102
4.4.1.2	Smoothing . . . . .	104
4.4.2	Curve Fitting Algorithms . . . . .	110
4.4.2.1	Method A . . . . .	116
4.4.2.2	Method's B, C and D . . . . .	118
4.4.3.3	Comparison of Curve Fitting Methods . . . . .	121
4.4.3.4	Implementation on Dominion Road Data . . . . .	126
4.5	FREQUENCY RESPONSE OF PARTIAL TIME HISTORIES	128
4.6	SUMMARY . . . . .	134
5.	<b>ESTIMATION OF FOUNDATION STIFFNESSES</b> . . . . .	169
5.1	SITE CONDITIONS . . . . .	170
5.2	LATERAL FOUNDATION STIFFNESSES . . . . .	173
5.3	ROTATIONAL STIFFNESSES . . . . .	176
5.4	COUPLED RESPONSES . . . . .	180
6.	<b>BRIDGE MODEL VERIFICATION</b> . . . . .	188
6.1	THE ANALYTICAL MODEL . . . . .	188
6.1.1	Node and Element Layout . . . . .	189
6.1.2	Material and Element Properties . . . . .	189
6.1.2.1	Deck Properties . . . . .	190
6.1.2.2	Elastomeric Pad Properties . . . . .	190
6.1.2.3	Column Properties . . . . .	193
6.1.3	Boundary Elements . . . . .	194
6.2	PRELIMINARY PARAMETER IDENTIFICATION . . . . .	195
6.3	PARAMETER IDENTIFICATION METHOD . . . . .	197
6.3.1	Overview of System Identification Algorithm . . . . .	199
6.3.2	Definition of the Error Function . . . . .	200
6.3.3	Optimization Routine . . . . .	203
6.3.3.1	Parameter Check . . . . .	204
6.3.3.2	Computation of Search Direction . . . . .	206
6.3.3.3	Line Search . . . . .	208
6.3.3.4	Convergence Check . . . . .	208
6.3.4	Evaluation of Reliability . . . . .	209
6.4	RESULTS OF PARAMETER IDENTIFICATION . . . . .	209
6.4.1	Selection of Parameters for Optimization . . . . .	210
6.4.2	Optimized Parameter Values . . . . .	213
6.4.3	Model Verification . . . . .	216

## LIST OF TABLES

<u>Table</u>		<u>Page</u>
Table 2-1	Schedule of accelerometers depicted in Figure 2-13 to yield response components. . . . .	23
Table 3-1	Summary of experimental mode shapes. . . . .	65
Table 4-1	Excitation methods used in full scale testing. . . . .	141
Table 4-2	Artificial time history simple oscillator properties for test of modal separation algorithms. . . . .	141
Table 4-3	Initial values for test of modal separation algorithms. . . . .	141
Table 4-4a	Results of test of modal separation algorithms on long duration time history. . . . .	142
Table 4-4b	Results of test of modal separation algorithms on short duration time history. . . . .	142
Table 4-5	Ratios of final to initial amplitude for free vibration time histories used for Figures 4-17 through 4-20. . . . .	143
Table 4-6	Results of modal separation methods A and B on three consecutive four second segments of longitudinal direction reference accelerometer at station 20. . . . .	143
Table 5-1	Summary of pile dimensions. . . . .	183
Table 5-2a	Unconfined compressive strength vs. depth below top of pile for Foundations B, C & D. . . . .	184
Table 5-2b	Unconfined compressive strength vs. depth below top of pile for Foundations F, G & I. . . . .	185

## LIST OF FIGURES

<u>Figure</u>		<u>Page</u>
Figure 2-1	Plan and elevation of the Dominion Road Bridge. . . . .	24
Figure 2-2	Cross section of the box girder. . . . .	25
Figure 2-3	Elevation and plan view of the superstructure to column top connection. . . . .	26
Figure 2-4	Load rams in place at Pier J. . . . .	27
Figure 2-5	Orientation of loads for Load Pattern One. . . . .	28
Figure 2-6	Orientation of loads for Load Pattern Two. . . . .	28
Figure 2-7	Hydraulic pump and quick release valve assembly. . . . .	29
Figure 2-8	A typical dial gauge setup, near Pier F. . . . .	30
Figure 2-9	Electrical displacement gauge at Abutment A. . . . .	31
Figure 2-10	Scaffolding erected midspan between Piers H and I. . . . .	32
Figure 2-11	Accelerometer measurement stations for the bridge deck and foundations. . . . .	33
Figure 2-12	A typical accelerometer layout for a bridge deck measurement station. . . . .	34
Figure 2-13	Accelerometer orientation for all bridge deck measurement stations. . . . .	35
Figure 3-1	Fourier modulus spectrum of analytical time history, demonstrating leakage. . . . .	66

<u>Figure</u>	<u>Page</u>
Figure 4-2	One quadrant of the surface formed by the real and imaginary components of the Laplace Transform of a damped simple oscillator . . . . . 145
Figure 4-3	The modulus, real component and imaginary component of the frequency response of two oscillators well separated in frequency. . . . . 146
Figure 4-4	The modulus, real component and imaginary component of the frequency response of two oscillators closely spaced in frequency. . . . . 147
Figure 4-5	The modulus, real component and imaginary component of the frequency response of two simple oscillators . 148
Figure 4-6	FFT modulus of an unsmoothed time history (solid line) and of an identical but smoothed time history (dashed line). . . . . 149
Figure 4-7	Hamming smoothing window (solid line) vs. Hanning smoothing window (dashed line). . . . . 149
Figure 4-8	Magnified view of 3.0 to 4.0 Hz portion of Figure 4-7. . . . . 150
Figure 4-9	FFT modulus of smoothed (solid) and unsmoothed (dashed) free vibration time history with relatively low damping. . . . . 150
Figure 4-10	FFT modulus of smoothed (solid) and unsmoothed (dashed) free vibration time history with relatively high damping. . . . . 151
Figure 4-11	Typical transverse response time history, (longitudinal reference accelerometer at station 20). . . . . 152
Figure 4-12	FFT modulus of smoothed (dashed) and unsmoothed (solid) time history of Figure 4-11. . . . . 152

<u>Figure</u>	<u>Page</u>	
Figure 4-25	FFT moduli of first four-second segment (dotted), second four-second segment (dashed) and third four-second segment (dot-dashed) of longitudinal reference accelerometer time history. . . . .	164
Figure 4-26	Same curves as Figure 4-24 but with normalized amplitudes. . . . .	164
Figure 4-27	Magnified view of 3.0 to 5.0 Hz region of Figure 4-25. . . . .	165
Figure 4-28	FFT modulus of the initial four-seconds of bridge response at the beginning of the day. . . . .	165
Figure 4-29	FFT modulus of the initial four-seconds of bridge response in the middle of the day. . . . .	166
Figure 4-30	FFT modulus of the initial four-seconds of bridge response at the end of the day. . . . .	166
Figure 4-31	FFT modulus of the initial four-seconds of bridge response at the beginning of the next day. . . . .	167
Figure 4-32	FFT moduli of first four-second segment (dotted), second four-second segment (dashed) and third four-second segment (dot-dashed) of vertical reference accelerometer time history. . . . .	167
Figure 4-33	Same curves as Figure 4-32 but with normalized amplitudes. . . . .	168
Figure 5-1	Plan of pile layout. . . . .	187
Figure 5-2	Schematic of vertical pile top load vs. pile top displacement. . . . .	187
Figure 6-1	Schematic showing the directions of the two degrees of freedom for the flexibility matrix of equation 6.2. . . . .	226

## 1. INTRODUCTION

A combined crew from the United States and New Zealand measured the dynamic response of an existing highway bridge to large amplitude lateral loads. The purpose of the field test was to learn about the behavior of bridges during earthquakes. Unique features of the bridge test include the large load amplitude, the complexity of the bridge and the many response components measured.

The snap back and quick release method, used previously by Douglas [20,21,22,23], was used to excite the bridge. Large controlled static loads were applied laterally to the bridge superstructure and released simultaneously. The resulting free vibration response was measured. Accelerations of up to 25% of gravity were measured, on the order of response expected due to a moderate magnitude earthquake.

The bridge was a 910 foot long, 10-span highway overpass. The second half of the bridge followed a 70° curve. Because of the curve, all six response components (three translational and three rotational) were measured at each measurement station. Measurement stations were located at each quarter-span deck section and at the base of each pier.

effect on the modeled response were optimized in the system identification procedure. The final optimized response compared very well with the measured response. The optimized model successfully predicted the measured static response as well as the measured response of experimental modes four and six.

### 1.1 BACKGROUND

The design of bridges to withstand earthquakes has undergone dramatic change in recent years. The 1971 San Fernando earthquake stimulated much research in this country in areas relating to the seismic design of bridges. Many of the results from this ongoing research have been incorporated in AASHTO's Guide Specifications for Seismic Design of Highway Bridges [1], published in 1983.

Other recent publications on seismic bridge design include two Federal Highway Administration publications [2,3] and two publications from the Applied Technology Council [4,5].

These seismic design guidelines for highway bridges are based upon a knowledge base which has expanded greatly in the last 17 years. Areas of uncertainty still exist, however. For example, it is now recognized that the bridge

nearby. Several investigators have studied the recorded response of the Meloland overpass, including Douglas [9], Werner [10], Gates [11] and Shepherd [12]. Also, the recorded response of a highway bridge near Hollister, California to a moderate magnitude earthquake was studied by Wilson [13].

The responses of bridges to man-made loads and ambient wind loads have also been measured and studied. A good review of full scale dynamic testing of civil engineering structures in general is provided by Srinivasan [14]. Many investigators have measured the vertical response of bridges. However, relatively few have measured the lateral dynamic response, which is of most interest in seismic bridge design.

McLamore [15], Buckland [16] and Abdel-Ghaffar [17] have measured the lateral response of suspension bridges. Abdel-Ghaffar obtained an impressive 91 modes from his ambient measurements of the Golden Gate Bridge. In addition, his calculated frequencies and mode shapes agreed very well with the measured frequencies and mode shapes.

Shepherd [18] measured the longitudinal and transverse dynamic responses of a bridge in New Zealand excited by counter rotating eccentric weights. The individual

foundation stiffness values predicted by Norris [24] agreed with the experimental foundation stiffness values measured at several load levels.

The pull-back and quick-release method was used in the bridge experiment of this project. Loads applied to the superstructure were just below the elastic capacity of the piers. Five deck response components (three translational and two rotational) and up to six foundation response components were measured on the ten-span, curved highway overpass.

## 1.2 OBJECTIVE AND SCOPE

The objective of this study was to examine the three-dimensional dynamic response of a curved highway overpass by analyzing the data from the Dominion Road bridge test, according to the following plan:

- 1) determine the natural frequencies and mode shapes of the bridge from the recorded acceleration time histories;
- 2) develop a method to separate the closely spaced vibration modes expected in the data;
- 3) construct a linear bridge response model based on the available structural drawings and soil data, and on the current knowledge of the engineering properties of materials; and

researched and ideas and techniques from these areas were used to formulate a mode separation method specifically suited for Dominion Road bridge test data.

Finally, an analytical model of the Dominion Road bridge response was constructed. Chapter Five describes the application of a geotechnical method developed by Norris [24] to predict the model foundation stiffnesses. Chapter Six describes the construction of the structural model.

The values of the model parameters which produce the best fit between the model response and the measured mode one bridge response were determined. A system identification algorithm was developed specifically for this purpose.

12. Shepherd, R. and Lisiecki, L., "The Response of a Bridge to Strong Ground Shaking", Proceedings 7th European Conference on Earthquake Engineering, Athens, Greece, 1982.
13. Wilson, J. C., "Analysis of the Observed Earthquake Response of a Multiple Span Bridge," EERL Report No. 84-01, California Institute of Technology, Pasadena, California, 1984.
14. Srinivasan, M.G., Kot, C.A. and Hsieh, B.S., Dynamic Testing of As-Built Civil Engineering Structures - A Review and Evaluation, Office of Nuclear Regulatory Research, U. S. Nuclear Regulatory Commission, Washington, D.C., (NUREG/CR-3649), 1984.
15. McLamore, V.R., Hart, G.C., Stubbs, I.R., "Ambient Vibration of Two Suspension Bridges," Journal of the Structural Division, ASCE, Vol. 97, No. ST 10, Oct. 1971, pp. 2567-2582.
16. Buckland, P.G., Hooley, R., Morgenstern, B.D., Rainer, J.H. and Van Selst, A.M., "Suspension Bridge Vibrations Computed and Measured," Journal of the Structural Division, ASCE, Vol. 105, No. ST 5, May 1979, pp 859-874.
17. Abdel-Ghaffar, A.M., Scanlan, R.H., "Ambient Vibration Studies of the Golden Gate Bridge: I. Suspended Structure," Journal of the Engineering Mechanics, Vol. 111, No. 4, April 1985, pp.463-482.
18. Shepherd, R. and Charleson, A.W., "Experimental Determination of the Dynamic Properties of a Bridge Substructure," Bulletin of the Seismological Society of America, Vol. 61, No. 6, Dec. 1971, pp. 1529-1548.
19. Pardoen, G.C., Carr, A.J. and Moss, P.J., "Bridge Modal Identification Problems," Proceedings of the Second ASCE-EMD Specialty Conference on the Dynamic Response of Structures: Experimentation, Prediction and Control, January 1981, Atlanta GA.
20. Douglas, B.M., Quick Release Pullback Testing and Analytical Seismic Analysis of a Six Span Composite Girder Bridge, Report No. FHWA-RD-76-173, Federal Highway Administration, Office of Research and Development, Washington, D.C., 1976.

## 2. THE BRIDGE TEST

The field experiment was performed in January, 1985 by a combined crew from the University of Auckland, the University of Nevada, Reno, the Central Laboratories of the New Zealand Ministry of Works and Development, and Computech Engineering Services, Inc., of Berkeley California. The bridge tested was Ramp B of the Dominion Road interchange, located in Auckland, New Zealand. Buckle [1] describes the bridge test and preliminary results from it.

### 2.1 THE BRIDGE

Ramp B of the Dominion Road interchange, (hereafter called the Dominion Road bridge), is a 910' foot long, 10 span overpass. The southern part of the bridge is straight, the middle section is curved and the northern end is straight and is oriented at an angle of 70 degrees relative to the southern end (Figure 2-1). The prestressed concrete, continuous box girder (Figure 2-2) is supported on single reinforced concrete columns of from 18 feet to 29 feet in height. Each column is supported on cast-in-place reinforced concrete piles which extend an average of 30 feet to bear on hard sandstone.

side of the bridge at each of Piers D, E and G. At Pier J two rams were located, one on either side of the bridge.

Two load configurations were used in order to excite as many of the bridge's modes of vibration as possible. For Load Pattern One, the rams at D, E, G and the ram on the north side of the bridge at J were loaded as indicated in Figure 2-5. For Load Pattern Two, the rams at D, E, G and the ram on the south side of the bridge at J were loaded as indicated in Figure 2-6.

The steel rams sat atop hydraulic jacks which in turn were supported by steel brackets bolted to specially constructed reinforced concrete reaction pads. The hydraulic jacks were activated by hand pumps manned by students from the University of Auckland. A pressure gauge in the hydraulic line connecting the pump to the jack enabled the load to be controlled, (Figure 2-7). Each ram had a calibration curve determined in the laboratory which related the hydraulic pressure in the line leading into the ram to force exerted by the ram head.

The bridge was loaded to two load levels in order to observe the effect of load level on bridge response. The high amplitude load was calculated to cause a strain in the column reinforcing steel just below the yield strain. The

caps at the base of Piers C, D, E and F. A typical dial gauge setup is shown in Figure 2-8.

Electrical displacement gauges were constructed by technical support staff at the University of Auckland. A typical gauge was constructed by mounting electrical resistance strain gauges on a metallic strip. Rigid pieces were attached perpendicular to the strip at either end to produce a "c" shaped device. One end of the "c" was attached to the bridge and the other to a non-moving reference. Bridge movement caused the ends of the "c" to open or close, which caused a strain in the metallic strip, which in turn caused a change in the electrical resistance of the strain gauges. The electrical resistance was measured by hand held resistance meters for static deflection measurements. Three electrical displacement gauges were located at each abutment and pier top. One gauge was oriented to measure the lateral deflection of the bottom of the box girder and the other two were orientated to measure the vertical deflection of each corner of the bottom of the box girder. These gauges measured the relative deflection of the box girder with respect to the abutment or the pier top. Electrical displacement gauges at Abutment A are shown in Figure 2-9.

Electrical displacement gauges were also attached to a scaffolding located midspan between Piers H and I, (Figure

The orientation of the coordinate system used for the analysis of the bridge is indicated in Figure 2-11. The origin of the coordinate system is at measurement station one, the centerline of Abutment A. The X, Y and Z axes correspond to the bridge's longitudinal, radial and vertical axes, respectively. Each component of displacement or acceleration is assigned a degree of freedom (DOF). DOF's one, two and three correspond to translation along the X, Y and Z axes, respectively. DOF's four, five and six correspond to rotations about the X, Y and Z axes, respectively.

A typical accelerometer layout for a bridge deck station is shown in Figure 2-12. The orientation of these accelerometers are indicated schematically in Figure 2-13. Measurements were obtained at four locations across the bridge deck for each measurement station. The acceleration measurements were combined as indicated in the third column of Table 2-1. Five acceleration components were measured at each of the 47 measurement stations on the bridge deck. Each set of reference accelerometers was composed of three individual accelerometers, located and oriented similar to accelerometers 1, 2 and 3 in Figure 2-13.

Accelerometers were located at Foundations C, D, E, F, G, H, I and J to obtain up to six acceleration components for each

Two complete data sets were created, one at a filter corner setting of 5 Hz and the other at a filter corner setting of 25 Hz. The strategy was to amplify the bridge response in the zero to 5 Hz range after filtering out the higher amplitude response above 5 Hz. The strategy proved most effective for measuring foundation response, where the response at frequencies greater than 5 Hz sometimes overshadowed the response at frequencies less than 5 Hz.

Response Component	DOF	Accelerometers
Longitudinal	1	$(1 + 6) / 2$
Radial	2	2
Vertical	3	$(4 + 5) / 2$
Rotation about Long. axis	4	$(3 - 7)/(10.5 \text{ ft.})$
Rotation about Radial axis	5	not computed for deck
Rotation about Vertical axis	6	$(6 - 1)/(25.5 \text{ ft.})$

Table 2-1. Schedule of accelerometers depicted in Figure 2-13 to yield response components.

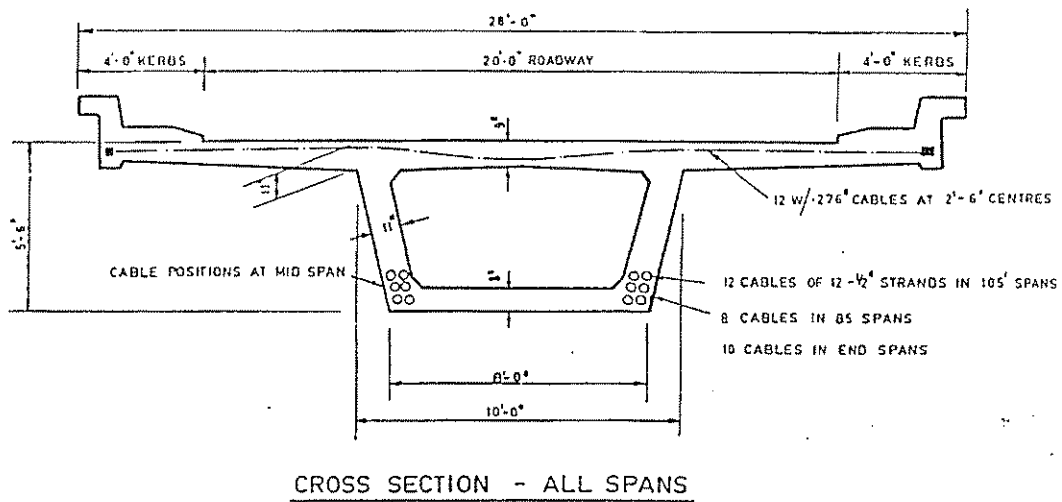


Figure 2-2. Cross section of the box girder.

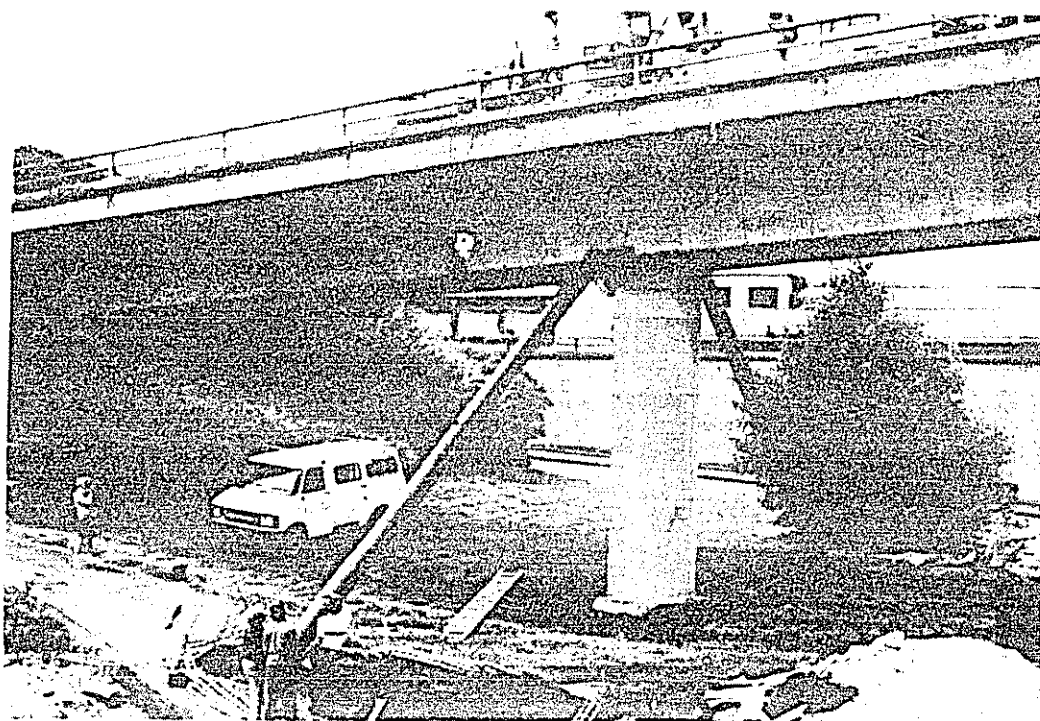


Figure 2-4 Load rams in place at Pier J.



Figure 2-7 Hydraulic pump and quick release valve assembly.

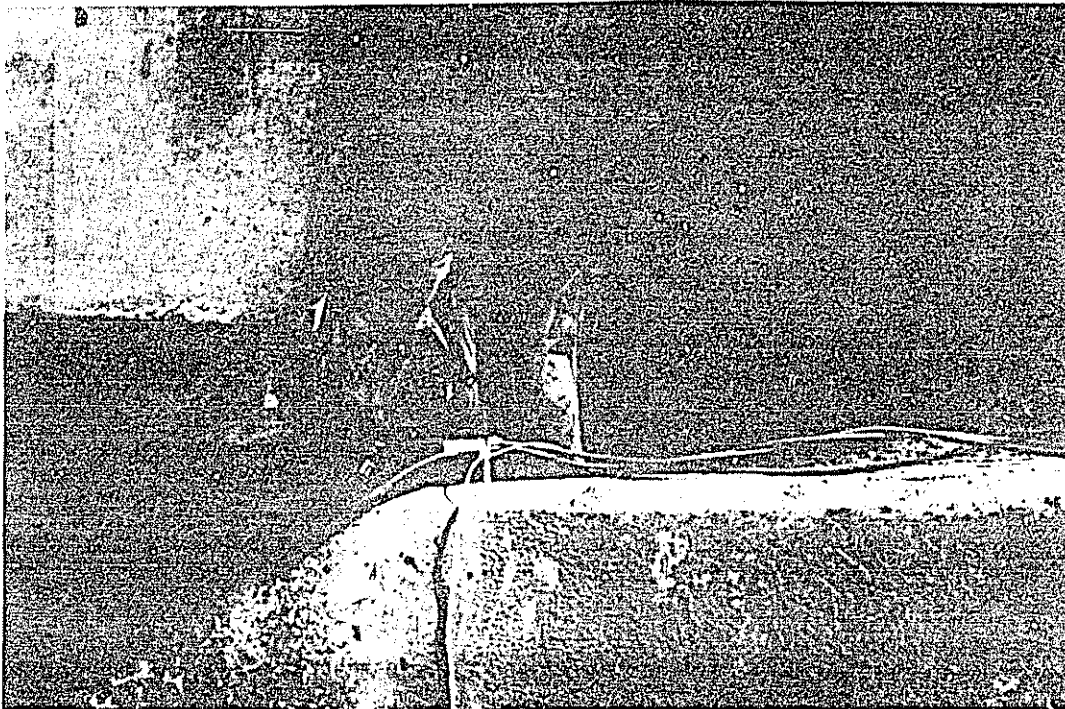


Figure 2-9 Electrical displacement gauge at Abutment A.

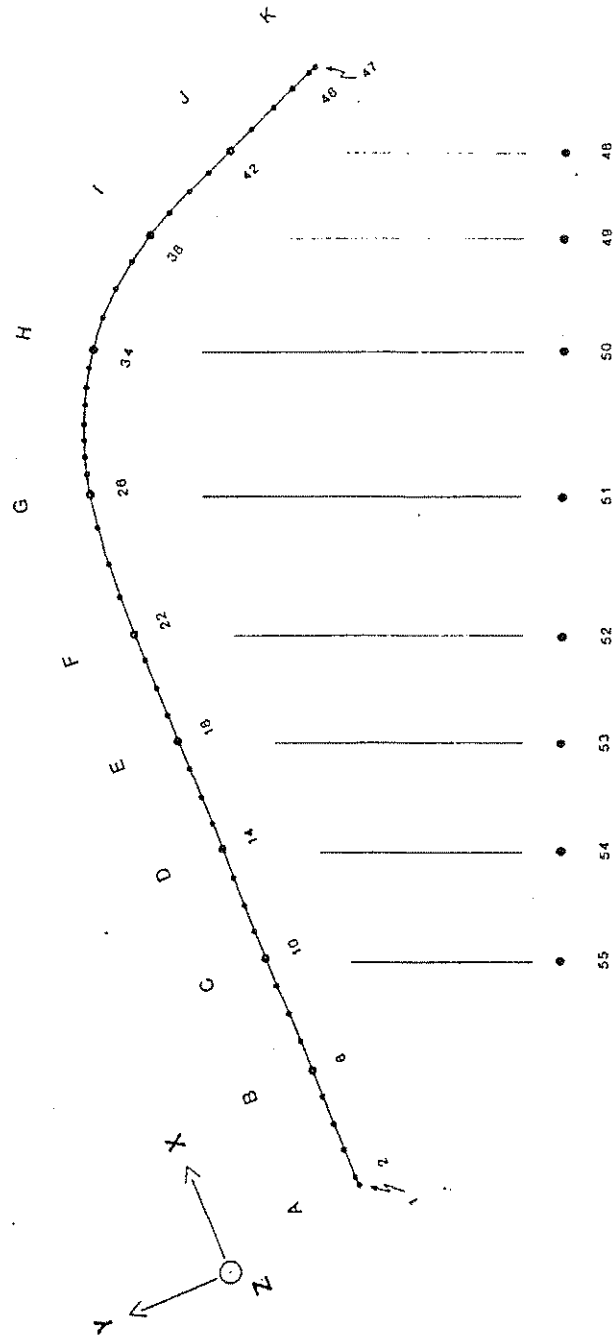


Figure 2-11. Accelerometer measurement stations for the bridge deck (nos. 1 through 47) and the foundations (nos. 48 through 55).

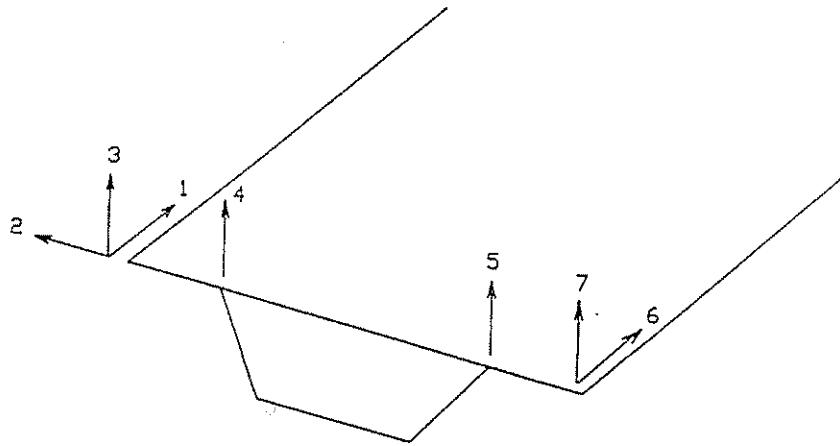


Figure 2-13. Accelerometer orientation for all bridge deck measurement stations.

Transform of a series of numbers. The FFT is used in this dissertation to transform a discrete function of time (e.g. an acceleration time history) into a discrete function of frequency (here termed a frequency response function). This section reviews two problems which arise when using the FFT: leakage and aliasing. The common remedies to these problems are also discussed.

A good reference on the Fourier Transform is the text by Bracewell [1]. Reference 2 is the article in which Cooley and Tukey originally presented the Fast Fourier Transform. Trifunac and Udvardia [3] present the basic methodology of applying the Discrete Fourier Transform to digital data. Trifunac [4] applies the procedure to obtain the natural frequencies and mode shapes from experimental data. Bergland [5] discusses common FFT signal processing pitfalls.

The FFT is derived from the Fourier Transform but differs from it in several subtle but important ways. These differences arise out of two approximations necessary to implement the Fourier Transform on a digital computer.

The Fourier Transform is defined as

$$Y(f) = \int_{-\infty}^{\infty} y(t) e^{-i2\pi ft} dt \quad (3.1)$$

cycles per T). The area beneath the curve in Figure 3-1 in the vicinity of 1.0 Hz is the same as the area beneath the curve in the vicinity of 1.5 Hz. However, some of the area from the lobe at 1.5 Hz has "leaked" over to adjacent frequencies.

Leakage can be reduced by lengthening the duration of the integral, T, thereby increasing the number of frequencies that are periodic over this interval. Leakage can also be reduced by "smoothing" the time history. Smoothing the time history by multiplying it by a bell shaped curve reduces the discontinuity between the ends of the time history. Unlike the first method of reducing leakage, smoothing involves a trade-off where decreased side lobe amplitude is gained at the expense of increased main lobe width. Smoothing is discussed in more detail in Section 4.4.1.2 of this dissertation.

The second approximation to the Fourier Transform is to make the transform a discrete process. The Discrete Finite Fourier Transform, (or simply, the Discrete Fourier Transform, (DFT)), is defined as

$$Y^{**}(f_j) = \sum_{k=0}^{N-1} y(t_k) e^{-i2\pi f_j t_k} \quad (3.4)$$

Components in  $y(t)$  of frequency higher than  $f_{\text{folding}}$  will appear at  $f_{\text{alias}}$ , where

$$f_{\text{alias}} = f_{\text{folding}} - (f_{\text{true}} - f_{\text{folding}}) \quad (3.7)$$

To prevent aliasing,  $y(t)$  should be low pass filtered with the corner frequency less than the folding frequency.

The Fast Fourier Transform (FFT) is an efficient algorithm for computing the DFT. The FFT is most efficient when  $N$  is an integer power of 2. The FFT requires  $2N \log_2 N$  multiplications compared to the  $N^2$  multiplications required by the DFT. For large  $N$ , the computational savings are substantial.

### 3.1.2 FFT on Dominion Road Data

The FFT was used on the Dominion Road data to obtain natural frequencies and mode shapes. The subset of the Dominion Road data analyzed was the data filtered at a corner frequency of 25 Hz, Load Patterns One and Two. A value for  $N$  of 16384 ( $2^{14}$ ) was used. As there were approximately only 4000 data points in the time histories, data points 4001 through 16384 were set to zero. "Padding" the end of the time history with zeroes reduces the "picket fence

PSD data for the bridge deck, the foundations and the relative deck vs. column top responses.

### 3.2.1 Power Spectral Density Plots

The initial attempt at efficient data display of the voluminous PSD data was the construction of a three dimensional perspective plot. A mesh surface was generated representing power spectral density along the vertical axis and frequency and bridge measurement station along the horizontal axes. Power spectral density (PSD) is defined here as the square of the FFT modulus. Figure 3-2 depicts a PSD surface for the lateral bridge deck response between 1.0 and 2.0 Hz. The figure is composed of Fourier spectra from 43 of the 47 bridge deck measurement stations. (Only the measurement stations located at the quarter-span deck locations between Piers G and H were used.) The data were collected from the 24 separate bridge releases necessary to completely measure the bridge deck.

The perspective plot has a couple of practical deficiencies. One, it is not possible to choose a view point which does not obscure some of the surface; and two, it is difficult to extract quantitative information from the plot. A

### 3.2.2 Bridge Deck P.S.D. Data

The PSD contour plots proved useful not only in locating natural frequencies but also in detecting data irregularities due to both processing errors and real physical phenomena.

The PSD contour plots were first scanned for anomalous responses. Responses differing from neighboring responses by a factor of two would indicate probable error in recording the gain setting for that channel and that particular release. No such anomalies were detected.

A pattern of gradually changing frequency and amplitude was detected in a large number of PSD contour plots. Assuming the Dominion Road bridge behaved as a constant linear elastic system, the PSD contours of the nonmoving reference channels *should* appear as constant amplitude ridges normal to the frequency axis. Note that 32 individual releases were required to measure the complete bridge. During these 32 releases, (which spanned a three day period), the six reference accelerometers were not moved while the remaining 14 accelerometers were marched down the bridge.

of a day's testing and then returned to its initial condition overnight.

One explanation of this phenomenon may be that the foundation soils change stiffness during the many releases of a day's testing, then return to their initial state overnight. Thixotropy, the condition where disturbed soils regain a portion of their undisturbed strength over time, may account for such behavior.

Also, the field test was conducted in the middle of the New Zealand summer. A change in the properties of various bridge components due to thermal effects may explain the observed cyclic change in bridge response.

Whatever the cause, the nonuniform frequency response of the bridge from release to release caused problems in trying to determine the frequency response of the bridge. The primary use of determining the frequency response of the bridge was to compare it to the frequency response of analytical models -- linear elastic analytical models for this dissertation. Therefore, an average response was determined. The average response was used to determine the properties of an analytical bridge model.

than the magnitude of the deck response. It is anticipated that a computer model of the bridge that has been verified by fitting it to experimental frequency response data would be helpful in determining whether local foundation modes were excited.

#### *3.2.4 Column Top vs. Deck Relative Displacement PSD Data*

All of the displacement time histories recorded for the column top vs. deck relative displacements in the data set were plotted and examined in order to determine the quality of the data. The lateral relative displacement time histories were the most noise free. Relative displacements recorded over Piers B through H were of good quality. A typical "good" time history is shown in Figure 3-7a, the lateral relative displacement at Pier B. Relative displacements at Abutment A, Pier I and Pier J were of poor quality. Figure 3-8a is the lateral relative displacement at Abutment A. The lateral relative displacement at Abutment K (Figure 3-9a) had the poorest quality. Many noise spikes can be observed in this time history.

The relative rotations about the longitudinal axis were of fair to good quality at all locations except Piers E and F and Abutment K. The relative rotation at Pier C, (Figure 3-10a), is a typical time history.

### 3.3 DETERMINATION OF MODE SHAPES

The determination of mode shapes for the Dominion Road bridge was not straightforward. The problem of drifting frequencies described in a previous section greatly complicated the process of extracting mode shapes from the FFT data. Also, it was observed in some preliminary mode shapes that sections of the mode shape were not in phase with the rest of the mode shape. A mode shape in which all components do not simultaneously equal zero is complex valued.

This section begins with a discussion of complex mode shapes, what they are and how they were handled. Then the problem of drifting frequencies is discussed and the procedure by which the mode shapes were constructed is described. Finally, the mode shapes are presented and noteworthy observations on the mode shapes are discussed.

#### 3.3.1 *Complex Mode Shapes*

Complex mode shapes can be computed analytically. An undamped eigenanalysis computes real valued eigenvectors (mode shapes). The eigenvalues (natural frequencies) and eigenvectors from an undamped eigenanalysis apply to

complex-valued experimental mode shapes with real-valued analytical-model mode shapes?

The first step in coping with complex mode shapes is to identify when a mode shape is real (imaginary component equals zero) and when a mode shape is complex (nonzero imaginary component). A convenient method of displaying a complex mode shape proved to be plotting the amplitude (as a solid line) and the real component (as a dashed line) on the same plot. Where the amplitude and real component overlaid each other, the imaginary component was zero and that portion of the mode shape was therefore real-valued. Where the real component was less than the amplitude, the imaginary component was therefore nonzero and the mode shape was complex-valued.

It was observed that many times the southern section of the bridge was not "in-phase" with the northern section of the bridge. When a reference channel located in the straight section was used to compute the mode shape, the straight section was in-phase and the curved section was out-of-phase. And when a reference channel located in the curved section was used, the straight section was out-of-phase and the curved section was now in-phase.

reference channel from the curved part of the bridge is used, but adjusted by the factor  $\frac{R_s}{R_c}$ . The resulting mode shape ordinates on the right hand side of Equations 3-8a and 3-8b have the same modulus but different phase angles.

The modified method was not used to compute any of the mode shape plots included in the appendix because only the modulus of the mode shapes was used in the bridge model verification work presented in Chapter 6.

### **3.3.2 *Coping with Drifting Frequencies***

The natural frequencies of the bridge changed slightly with each successive release of the bridge. Evidence of this shift in the bridge response was seen in virtually every PSD contour plot. The frequency "fingerprint" of the bridge was in some instances very different between the beginning and end of a day's testing. See for example Figure 3-4 and note the sudden appearance of a natural frequency at 1.65 Hz toward the end of each day's testing.

It is not possible, of course, to make an analytical model produce frequencies and mode shapes which change as you progress down the bridge. The task then was to obtain the

A mode shape ordinate,  $C$ , for the  $i^{\text{th}}$  DOF and the  $k^{\text{th}}$  measurement station was computed as

$$C_{ik} = \frac{M_{ijk}}{R_{1jm}} \quad . \quad \begin{array}{l} i = 1, 2, \dots, 6 \\ k = 1, 2, \dots, 55 \end{array} \quad (3.9)$$

where  $M_{ijk}$  represents the complex valued frequency response of the  $i^{\text{th}}$  DOF, at the  $j^{\text{th}}$  frequency and for the  $k^{\text{th}}$  measurement station; and  $R_{1jm}$  represents the complex valued frequency response of the  $1^{\text{th}}$  reference channel, at the  $j^{\text{th}}$  frequency and for the  $m^{\text{th}}$  release. The  $m^{\text{th}}$  release was related to the  $k^{\text{th}}$  measurement station as follows:

$$\begin{aligned} m &= \text{integer value of } \frac{(k+1)}{2} \text{ , } k = 1, 2, \dots, 47 \\ m &= 24 + (k-47) \text{ , } k = 48, 49, \dots, 55 \end{aligned}$$

The  $j^{\text{th}}$  frequency was the frequency at which the Fourier modulus of the guide channel frequency response was maximum within the frequency interval.

The peak response picking algorithm allowed reasonable mode shapes to be constructed from irregular data. As the natural frequencies of the bridge gradually changed, the mode shapes of the bridge gradually changed also. Therefore, the mode shapes produced by the peak picking algorithm represent an average bridge response. The average mode shapes appear reasonable for natural frequencies which changed little during the course of a day's testing. Mode

determined from the 0. to 10. Hz range of the frequency response data, Load Patterns One and Two. Each mode shape plot is organized as follows. There are six frames in each plot representing each of the six DOF's. For each frame, the solid and dashed lines represent the modulus and real components, respectively, of the bridge deck response, and the solid and open squares represent the modulus and real components, respectively, of the foundation response. The deck and foundation responses were plotted at separate scales. The number to the left of the frame indicates the deck response scale, from frame centerline to top of frame; and the number below it in parentheses indicates the foundation response scale. The horizontal axis is labeled A through K to represent the bridge pier locations. The bridge deck stations are given equal spacing; therefore, this axis is not to scale. Only the responses at the quarter-span measurement stations between Piers G and H are displayed for uniformity.

Table 3-1 summarizes the relevant information concerning each mode shape. For each mode, the average frequency and the dominant response are listed. Also, a subjective estimate of the "quality" of the mode shape is included in the table. The quality of a particular mode shape was judged on the basis of the relative strength and definition of its response in the PSD contour plots, and on the

### 3.3.5 Observations on Mode Shape Data

The first experimental mode was a lateral response mode. The PSD data indicated that this mode was excited more than any other lateral response mode. All four lateral response measurements (DOF's 1, 2, 4 and 6) were generally of excellent quality. The most serious loss of phase occurred in the last two and one half spans for DOF 1. In this section, the deck and foundation lagged the rest of the bridge by approximately 35 degrees or 0.1 seconds. Overall, the measured mode one response provides the most extensive and reliable response data of any mode.

The 19 mode shapes identified between zero and 10 Hertz were primarily either radial response or vertical response modes. The radial response was coupled with either DOF 4 (rotation about the longitudinal axis) or DOF 6 (rotation about the vertical axis). The vertical response was primarily uncoupled from the other responses. The PSD data indicated that there was a moderate amount of longitudinal response in many vertical response modes. The longitudinal movement was kinematically necessary in order to accommodate the vertical movement of the bridge deck.

rotational responses have been computed by dividing the transformed acceleration time histories by the distance (in feet) separating the accelerometers, as listed in Table 2-1. The responses of interest for experimental modes 15, 17 and 19, for example, are rotational responses.

A surprising result in the mode shape data were the magnitude of the foundation response in the vertical direction. The vertical mode at 5.00 Hz indicates that the response at Foundation D was nearly 100% of the deck response at Pier D and 12% of the maximum overall deck response. Other vertical mode shapes at higher frequencies also exhibited large magnitude vertical foundation response.

Another interesting result was the deflected shape of the bridge piers in mode one. The piers are in double curvature, indicating that a bending moment was applied by the deck to the pier tops in the same direction as the moment applied by the foundations to the pier bases.

In summary, the 19 experimental frequencies and mode shapes presented in this chapter and in Appendix B represent an extensive suite of measurements of the dynamic response of the Dominion Road bridge. These data will be especially useful for validating bridge response models. The mode one experimental data is used in Chapter Six for this purpose.

Mode	Avg. Freq. (Hz)	Dominant Response	Quality	Reliable DOF's	Guide Chan.	Ref. Chan.	Load Pattern
1	1.08	Radial	Excellent	1,2,4,6	REF 3	REF 3	Two
2	1.22	Radial	Poor	2,6	---	REF 2	Two
3	2.20	Longitud.	Fair	1	REF 2	REF 2	One
4	2.90	Radial	Good	2,6	REF 3	REF 3	One
5	3.65	Vertical	Excellent	3	REF 4	REF 4	One
6	4.15	Radial	Excellent	2,6	REF 6	REF 6	Two
7	4.50	Vertical	Excellent	3	DOF 3	REF 5	Two
8	5.00	Vertical	Good	3	DOF 5	REF 5	One
9	5.30	Vertical	Good	3	DOF 3	REF 6	One
10	5.70	Vertical	Good	3	REF 5	REF 5	One
11	6.50	Vertical	Good	3	REF 4	REF 4	Two
12	7.10	Vertical	Good	3	REF 1	REF 1	One
13	7.30	Radial	Excellent	2,6	DOF 2	REF 6	One
14	7.45	Vertical	Fair	3	DOF 3	REF 1	Two
15	7.70	Torsional	Poor	4	REF 1	REF 1	Two
16	8.25	Longitud.	Good	1	REF 5	REF 5	One
17	8.55	Torsional	Excellent	4	DOF 4	REF 4	One
18	9.10	Radial	Good	2,4	DOF 3	REF 3	Two
19	9.60	Radial	Good	6	DOF 6	REF 5	Two

Table 3-1. Summary of experimental mode shapes.

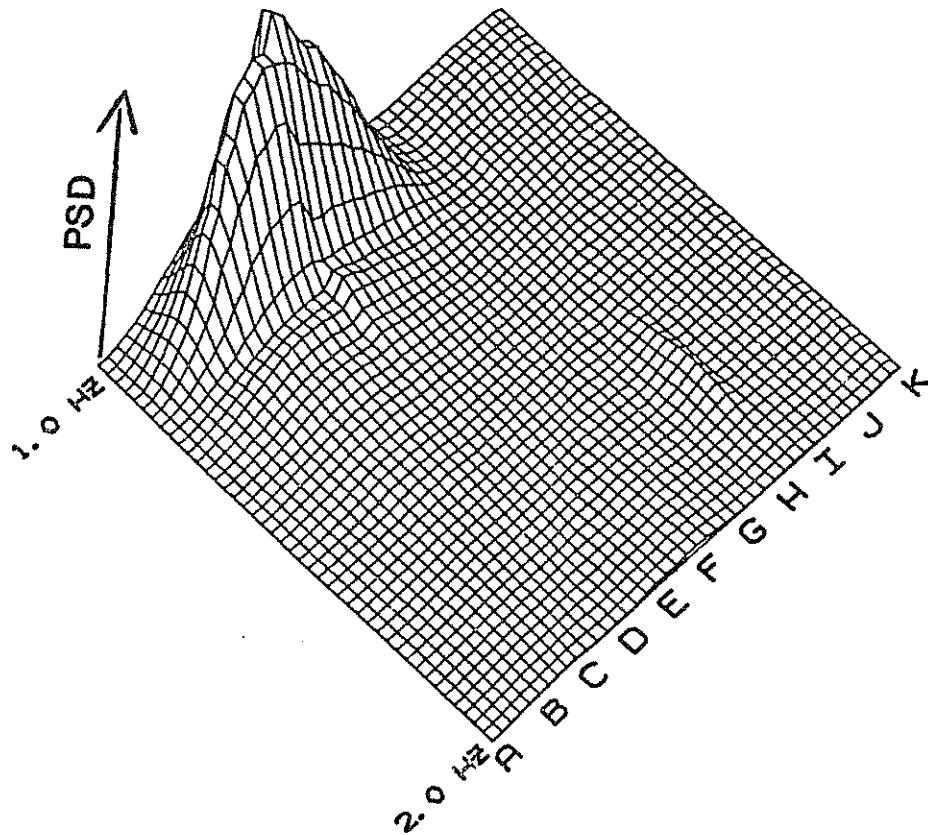


Figure 3-2 Power Spectral Density surface of the radial mode one response.

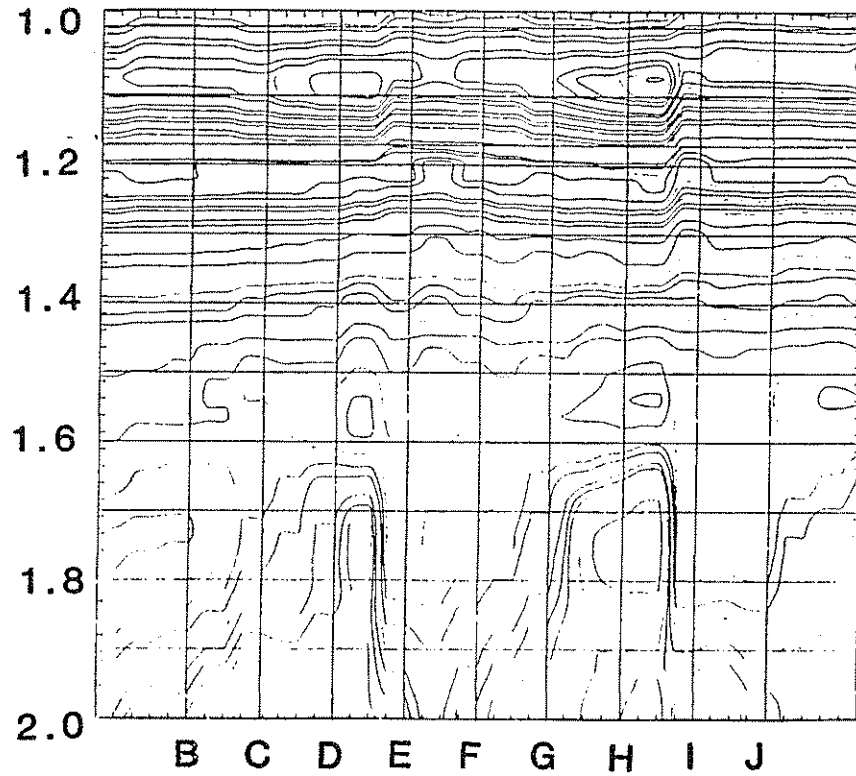


Figure 3-4 PSD contour plot of radial response reference accelerometer located at measurement station 20.

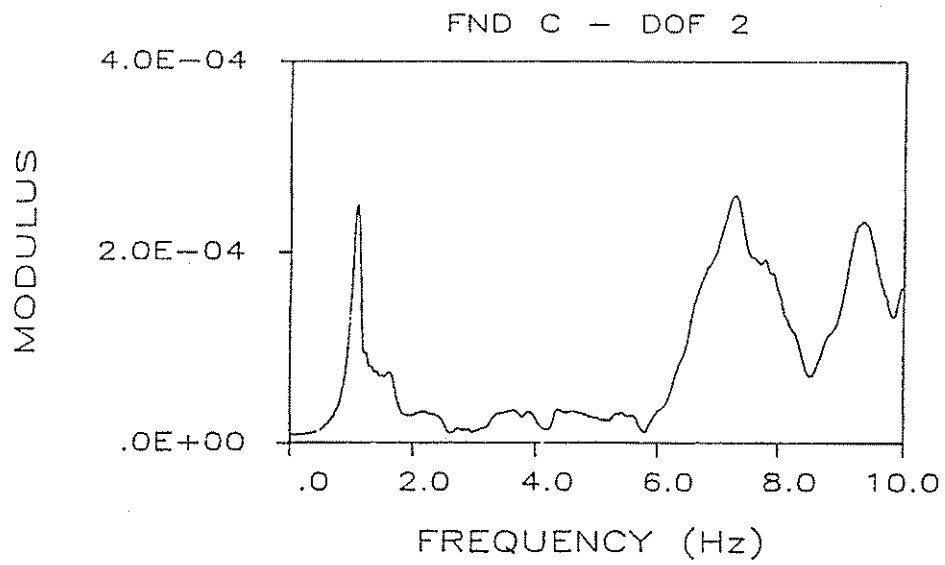


Figure 3-6 Fourier modulus spectrum for radial response on Foundation C.

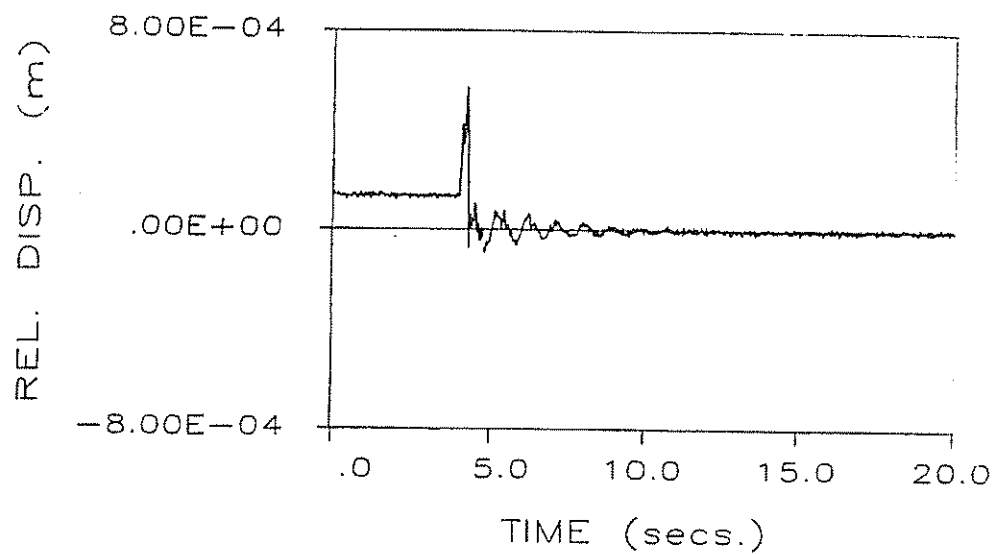


Figure 3-8a Time history of relative displacement at Abutment A.

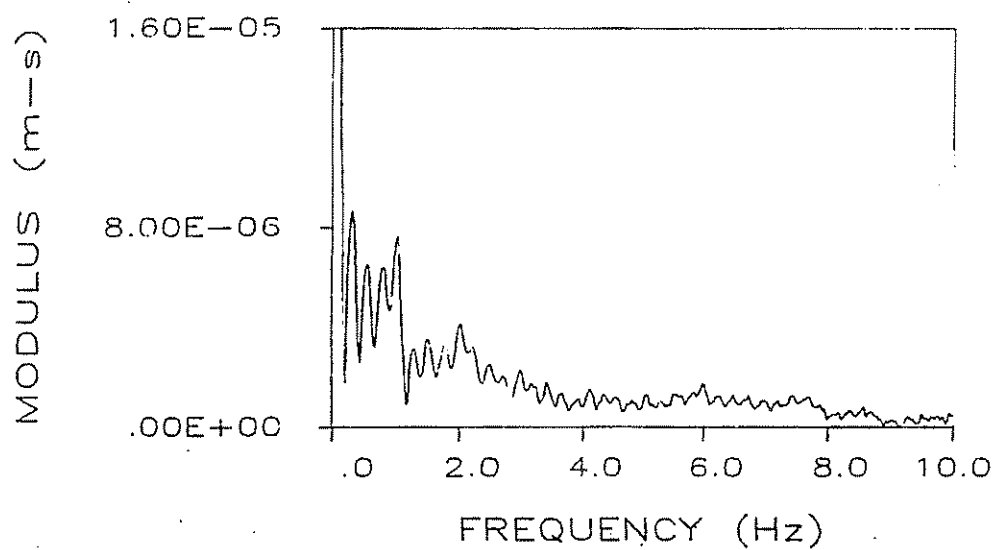


Figure 3-8b Fourier modulus of above time history.

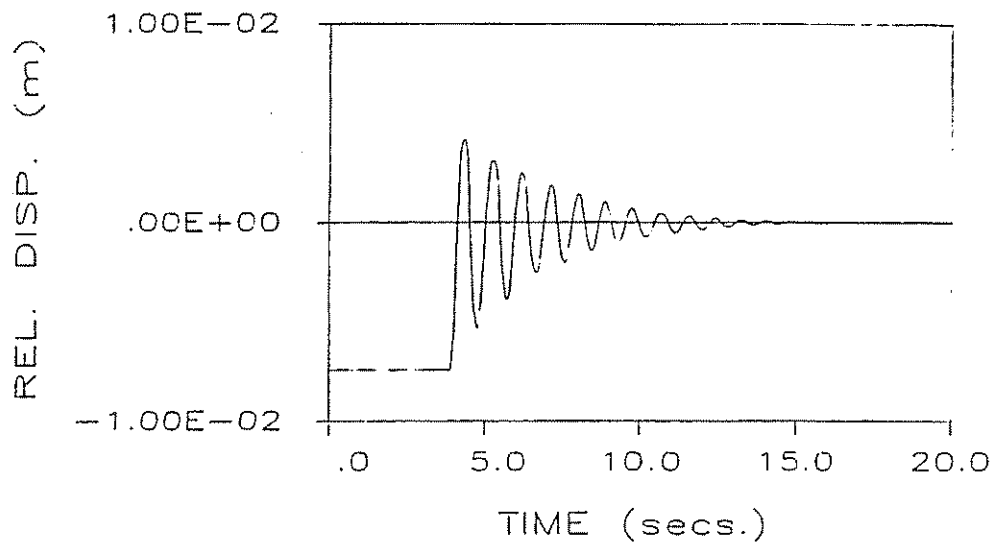


Figure 3-10a Time history of relative rotation between the bridge deck and the top of Pier C.

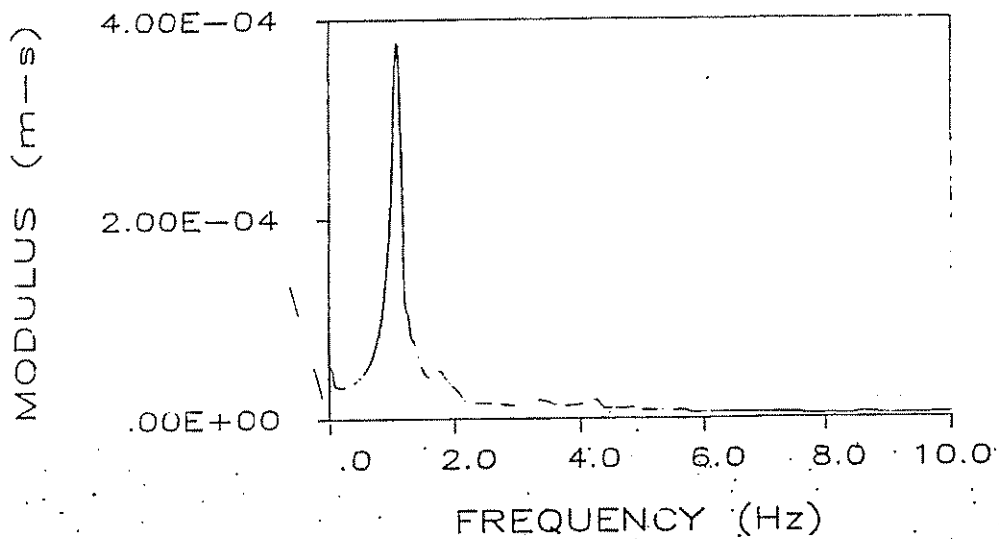


Figure 3-10b Fourier modulus of above time history.

This chapter begins with an overview and literature review of modal separation techniques. Three completely different approaches for separating closely spaced modes are then described. First, a straight forward time domain method was tried. Then, a modified Fast Fourier Transform (FFT) called the Chirp-Z Transform (CZT) was implemented and tested. Finally, a curve fitting method was developed and successfully used on Dominion Road bridge data.

The final section of this chapter shows that the frequency response of the bridge changed significantly during a single time history, (as well as over the course of a day's testing.) This section also demonstrates that the change in frequency response over a period of a day is concentrated in the initial (higher amplitude) portion of the time histories.

#### 4.1 OVERVIEW AND LITERATURE REVIEW

The topic of separation of closely spaced modes is discussed very little in the Civil Engineering literature. Most investigators use methods developed in other fields to compute the natural frequencies and mode shapes of their experimental data.

#### 4.1.1 Beck's Modal Minimization Method

James Beck, working at the California Institute of Technology under Paul Jennings, developed a method to compute the modal parameters of the response of a building during an actual earthquake [6]. Using the recorded foundation response as input, Beck's Modal Minimization method optimizes the response of a collection of simple oscillators to match the recorded response of the superstructure. Beck applied his method to the response of the 42 story steel frame Union Bank Building in Los Angeles during the 1971 San Fernando earthquake.

Beck's Ph.D. dissertation rigorously develops his modal parameter identification method, discussing often ignored but important topics as reliability of parameter estimates. He concludes that although it is not possible to establish definite error bounds for each parameter, it is possible to examine the relative reliability between parameters. Beck forms a "sensitivity" matrix composed of second derivatives of the error function with respect to the modal parameters. He notes that large diagonal and small off-diagonal terms imply "orthogonal" parameters, i.e. an error in one parameter would not cause errors in other parameters.

number of modes required to give a very good approximation of the relative displacement, velocity and acceleration are one, two and four modes, respectively," [6]. A method was needed for the Dominion Road data set which could efficiently identify dozens of modes in each of hundreds of time histories. For this purpose a method was sought which required a minimum of operator interaction and did not require reasonably accurate estimates of the modal frequencies.

#### *4.1.2 Modal Testing*

Modal testing is defined by Ewins [9] as, "...the testing of components or structures with the objective of obtaining a mathematical description of their dynamic or vibration behavior." A brief review of the development of modal testing is given by Smith [10] and a reasonably detailed coverage of the technology of modal testing is provided by D. J. Ewins in his book [9].

There are many different methods utilized in modal testing, each with its advantages and disadvantages. Factors affecting the method selection include economy, time constraints, location of structure (laboratory or field), required accuracy of results and the type of results needed.

predict the structure's response due to a set of forces of any frequency content, of any amplitude and applied at any location on the structure.

It is not the usual practice in field tests of large Civil Engineering structures to measure the driving force time history. The information lost by not recording the driving force time histories results in several deviations from modal testing procedures. The lack of driving force amplitude information means that modal participation factors can not be computed and that the amplitude of response vs. excitation amplitude can not be ascertained. Also, the lack of driving force frequency content information requires that the spectrum of the excitation be assumed.

The excitation force is assumed to be a random stationary process for the ambient wind and traffic excitation methods. If many ensembles (records) are averaged, the excitation force may be assumed to be an ergodic process. The spectrum of a random stationary ergodic process is uniform and is a constant for white noise excitation. The transfer function formed by dividing the transform of the measured response by the constant is simply the transform of the measured response, since the constant is not known and can be arbitrarily set to one. The resulting transfer function is a pseudo transfer function because it contains assumed

are listed in order of historical development (and computational complexity.)

Frequency Domain Methods

Time Domain Methods

peak picking

curve fit - one mode,  
one response

curve fit - multi-mode,  
one response

global curve fit -  
multi-mode,  
multi-response

complex exponential

Ibrahim Time Domain Method

The peak picking method of modal extraction determines the frequency, amplitude and phase from one value of the transfer function -- the value at which the peak amplitude occurs. A disadvantage of this method is that the information represented by adjacent transfer function values is not utilized.

The uni-mode curve fit method fits the analytically derived response curve of a simple oscillator to a section of the transfer function. The circle fit method can be classified as a uni-mode curve fit. The circle fit procedure is based on the fact that a SDOF response is represented as a circle on a Nyquist plot (a plot of real vs. imaginary response components.) This method works well when the experimental modes are well separated in frequency.

method [12] is used to find the frequencies and damping factors and the amplitude and phase values are then calculated from a least squares formulation. This method has been used primarily on damped free vibration data [13].

Ibrahim's time domain method [14] fits the time domain free vibration response of a collection of  $n$  simple oscillators, each multiplied by an  $M$  component shape function, to  $M$  time histories. The modal parameters for the entire structure are obtained then in one mighty crunch. Advantages of this method include:

- 1) the free vibration response is accurately modelled whereas Fourier methods model the response as a collection of *undamped*, infinite duration sinusoids
- 2) the response of the entire structure is modelled simultaneously allowing the best fit (in a least squares sense) of constant frequency modal parameter values
- 3) initial estimates of the natural frequencies are not required

Disadvantages of the Ibrahim time domain method include:

- 1) a large computer is required
- 2) the selection of  $n$ , the number of oscillators, is many times a trial and error process
- 3) spurious modes are not always easily differentiated from true response modes

remaining two parameters for this mode. Each mode was alternately optimized in this way until the error squared changed over the course of an entire cycle by less than a preset amount.

The above method was indeed stable and showed favorable initial convergence properties. Its final convergence, however, was extremely slow; but this could have been improved by implementing two of Beck's features. Beck determined the final value of each one dimensional optimization by fitting the equation of a parabola to the last three points of the incrementing process. Also, Beck only optimized frequency and damping for each mode. The objective function is a linear function of amplitude and phase and these parameters were determined directly (non-iteratively). These modifications to improve the convergence efficiency were not implemented because another disadvantage of the method was encountered.

It was observed that in order to separate a mode with a weak response from a mode with a strong response, all modes with responses stronger than the weak response mode need to be included in the fitting process. This disadvantage is inherent in all time domain approaches.

by the square of its frequency (in radians). The sum of these displacements compared reasonably well with the measured bridge displacements as seen in Figure 4-1.

Figure 4-1 is a plot of bridge release displacements, measured and computed. The triangles in the figure represent the measured static release displacements. The two triangles at each location represent the static measurements taken before and after the dynamic series of measurements. The most reliable static measurements were taken at the abutments and the bridge centerline, which were measured with dial gages. The other static measurements, considered less reliable, were measured by sighting through a transit located on the ground.

The bottom line on this method was that it was not an efficient way to separate closely spaced modes on the abundant Dominion Road data. A method was sought which would be unconditionally stable, require little operator input and be computationally efficient.

#### 4.3 CHIRP-Z TRANSFORM

The Fourier Transform utilizes the orthogonality property of sinusoids, i.e. the integral of the product of two sinusoids

### 4.3.1 The Chirp-Z Transform

The Chirp-Z Transform (CZT) is a special variation of a more general discrete transform called the Z-Transform. The Z-Transform is defined for the discrete function  $f_j$  as

$$F(z) = \sum_{j=-\infty}^{\infty} f_j z^{-j} \quad (4.1)$$

For  $f_j$  of finite extent

$$F(z) = \sum_{j=0}^{N-1} f_j z^{-j} \quad (4.2)$$

When  $z = e^{s_k \Delta t}$ , ( $s_k$  complex-valued), the Z-Transform is the discrete analogy of the Laplace Transform.

$$F(s_k) = \sum_{j=0}^{N-1} f_j e^{-s_k t_j} \quad (4.3)$$

where

$$t_j = j * \Delta t$$

$$s_k = k * \Delta s$$

In the equations below, the frequency and damping ratio constants of the simple oscillator are designated  $\omega$  and  $\xi$ , respectively. And the real and imaginary components of the Z-Transform variable  $s_k$  are designated  $v_k$  and  $w_k$ , respectively, (i.e.  $s_k = v_k + iw_k$ ).

$F(s_k)$  represents the DFT of  $f(t_j)$  when  $s_k = 0 + iw_k$

$$F(s_k) = F(w_k) = \sum_{j=0}^{N-1} f_j e^{-iw_k t_j} \quad (4.6)$$

The DFT is represented by the values of  $F(s_k)$  along the imaginary axis in Figure 4-2.

$F(s_k)$  represents the MFT of  $f(t_j)$  when  $s_k = -v_o + iw_k$

$$F(s_k) = \sum_{j=0}^{N-1} f_j e^{-(v_o + iw_k)t_j} \quad (4.7)$$

The MFT is represented by the values of  $F(s_k)$  along a line parallel to the imaginary axis and offset by  $v_o$  along the real axis in Figure 4-2.

$X(s_k)$  represents the Chirp-Z Transform, (or CZT), of  $f(t_j)$

would require  $N \cdot M$  additions and multiplications if computed straightforwardly. The CZT evaluates Equation 4.9 by a procedure which requires only approximately  $(N+M)(1+\log(N+M))$  additions and multiplications.

Equation 4.9 can be written

$$x_k = \sum_{j=0}^{N-1} x_j e^{-s_0 j \Delta t - k \Delta s j \Delta t} \quad (4.10)$$

Let

$$kj = 1/2[j^2 + k^2 - (k-j)^2]$$

then

$$x_k = \sum_{j=0}^{N-1} x_j e^{-s_0 j \Delta t} e^{-\Delta s j^2 \Delta t / 2} e^{\Delta s (k-j)^2 \Delta t / 2} e^{-\Delta s k^2 \Delta t / 2} \quad (4.11)$$

or

$$x_k = e^{-\Delta s k^2 \Delta t / 2} \sum_{j=0}^{N-1} g_j h_{k-j} \quad (4.12)$$

where

$$g_j = x_j e^{-s_0 j \Delta t - \Delta s j^2 \Delta t / 2}$$

$$h_j = e^{\Delta s j^2 \Delta t / 2}$$

The term involving the summation of  $g_j h_{k-j}$  is a convolution. The convolution operation is designated by the symbol  $*$ .

$$g * h = \sum_{j=0}^{N-1} g_j h_{k-j} \quad (4.13)$$

Before further tracking down the cause of the unexpected behavior, the CZT without using the high speed convolution technique, (Equation 4.9 evaluated straightforwardly) was tested on artificial data and on Dominion Road data.

The CZT exhibited marked improvement in resolution over the FFT on artificial time histories, but only when the sinusoids were periodic in the measurement window. Leakage occurred in the spectra of sinusoids not periodic in the measurement window. The cause of the leakage can be seen by rearranging Equation 4.9 as follows. Let  $s_0$  equal 0 to simplify, and separate the real and imaginary parts of  $\Delta s$ , (where  $\Delta s = (-\xi+i)\Delta\omega$ ), so that

$$F(s_k) = \sum_{j=0}^{N-1} f_j e^{\xi\Delta\omega kt_j} e^{i\Delta\omega kt_j} \quad (4.15)$$

Each value of  $f_j$  is multiplied by  $e^{\xi\Delta\omega kt_j}$ , before transformation. This effectively "straightens out" the decaying exponential of the time history,  $f_j$ , thereby increasing resolution but also canceling the "natural" smoothing of the time history and so increasing leakage effects.

initial estimates of the modal parameters, yet utilize powerful optimization routines that operate on the complete set of experimental transfer function values pertaining to the modes in question.

Multi-mode curve fitting procedures fit the analytical frequency domain expression of a collection of simple oscillators to the experimental transfer function. Initial estimates of the frequency and damping values for each oscillator as well as the frequency interval over which the fit is performed must be specified by an operator.

The most complete description of the multi-mode curve fitting procedure was given by Mark Richardson [2] when he was working for Hewlett-Packard. The curve fitting method employed in this dissertation utilized many features of the procedure described by Mark Richardson but also deviated from it in many ways. Specifically, the analytical frequency domain expression and the optimization routine were different from the procedure described by Mark Richardson.

The method explained in this section was successful in separating closely spaced modes of the Dominion Road data. The method utilizes the Discrete Fourier Transform (DFT) and the first subsection below presents some preliminary

extends beneath the peak of the other curve, obviously the amplitude of that peak in the summed curve will be in error.

The observed phenomenon of the shift in the frequencies of peak response of the modulus curve cannot be explained by superimposing the individual modulus curves. The phenomenon can be explained however by examining the real and imaginary components of the DFT. Figure 4-3 depicts the modulus, real component and imaginary component of the response of two oscillators well separated in frequency so that no significant interference effects occur. The dashed vertical lines at 1.0 Hz and 3.0 Hz represent the location of the simple oscillator frequencies. In this figure the real response components have the same shape for both oscillators, as do the imaginary response components. The modulus therefore has the same shape for both oscillators. Note that the peak response for each mode occurs at the location of the dashed lines in the figure.

Figure 4-4 is similar to Figure 4-3 except that the frequency of the second oscillator has been decreased so that now interference effects are exhibited. Note that the peak responses do not coincide with the dashed lines. The damping constant ( $\xi\omega$ ) of the second oscillator has been set equal to that of the first oscillator so that the response curves have the same shape. It is not possible to sum two

information on smoothing is presented because it is an oft misunderstood technique and it was used for the Fourier Modulus curves displayed in the last section of this chapter. A short review of what smoothing is and why it is useful, along with some examples of smoothed Dominion Road bridge data are presented below. Good background material on the Fourier Transform is provided by Bracewell [18], and a comprehensive treatment of smoothing windows is presented by Harris [19].

The reason time histories are smoothed prior to transformation by the FFT is due to the cyclic nature of the FFT. (The FFT is an efficient algorithm for computing the Discrete Fourier Transform (DFT) on a digital computer.) In the derivation of the DFT from the Fourier Transform, the time history was assumed to be periodic in time  $T$ , where  $T$  is the period of the DFT. The DFT assumes that the value of the time history at an arbitrary time  $t_1$  equals the value of the time history at  $T + t_1$ . The DFT treats the time history it acts upon as if the time history were written on a strip of paper and the ends of the paper were brought together to form a circle. Indeed, the DFT of a time history yields the identical modulus curve whether it begins at the beginning of the circular strip of paper or somewhere in the middle. (The phase of the DFT however will not be the same.)

Let the FFT of Equation 4.16 be designated as  $S(w)$  where

$$S(w) = \int_0^T s(t) e^{-iwt} dt \quad (4.17)$$

Evaluation of the integral yields

$$S(w) = \frac{4\pi^2}{2T^2} \frac{(-\sin(wT) + i2\sin(wT/2)2)}{w(w^2 - 4\pi^2/T^2)} \quad (4.18)$$

Evaluating  $S(w)$  at the discrete points

$$w = 0, \Delta w, 2\Delta w, \dots, (N-1)\Delta w$$

where

$$\Delta w = 2\pi/T$$

it is found that  $S(w)$  is nonzero for only three points:

$$w = 0, w = \Delta w \text{ and } w = (N-1)\Delta w.$$

Note that

$$(N-1)\Delta w = (N+N-1)\Delta w = -\Delta w$$

because of the cyclic properties of the DFT.

The values of  $S(w)$  evaluated at 0 and  $\pm\Delta w$  are:

$$S(-\Delta w) = -T/4$$

$$S(0) = T/2$$

$$S(+\Delta w) = -T/4$$

Therefore the time history may be effectively smoothed by convolving the complex values of the DFT of the time history with the sequence  $-T/4, T/2, -T/4$ .

most. Time histories of damped free vibration possess "natural" smoothing because the exponential decay smoothly reduces the final amplitude to zero. Figures 4-9 and 4-10 depict the FFT of artificial time histories with relatively low and high damping, respectively. The dashed and solid lines represent the FFT of unsmoothed and smoothed time histories, respectively. The time histories are composed of two simple oscillator responses with frequencies of 1.0 and 1.2 Hz. It can be seen that smoothing is much more beneficial for identifying the frequencies of the lightly damped response than for the more heavily damped response.

The effect of the Hamming smoothing window on experimental time histories is illustrated in Figures 4-11 through 4-14. A typical horizontal response time history of the Dominion Road bridge is shown in Figure 4-11, (of the reference accelerometer in the longitudinal direction at Station 20). The smoothed (dashed line) and unsmoothed (solid line) response modulus curves are plotted in Figure 4-12. A typical vertical acceleration time history is shown in Figure 4-13 (Station 28), and its smoothed and unsmoothed response modulus curves are plotted in Figure 4-14. The vertical response time history has a lower damping ratio than the transverse response time history. This fact and the fact that the vertical response is much more regular (as observed in the PSD contour plots) indicate that the

Because  $E_w$  and  $F_w$  are complex-valued, and because the optimization routine was written for real-valued functions,  $\epsilon$  was actually computed as the vector denoted below

$$\epsilon_w = \{\epsilon_{w_i}^R, \dots, \epsilon_{w_f}^R, \epsilon_{w_i}^I, \dots, \epsilon_{w_f}^I\} \quad (4.23)$$

where  $\epsilon_w^R$  and  $\epsilon_w^I$  represent the real and imaginary components, respectively, of  $\epsilon_w$ , and  $w_i$  and  $w_f$  are the initial and final frequencies in the frequency interval.

The analytically derived frequency response function,  $F_w$ , is a function of frequency  $w$  and the simple oscillator parameters  $\omega_k$ ,  $\xi_k$ ,  $A_k$  and  $B_k$ , where  $k = 1, 2, \dots, n$  and  $n$  equals the number of simple oscillators or modes.  $F_w$  is the time domain to frequency domain linear transform of  $f_t$ , where

$$f_t = \sum_{k=1}^n e^{-\xi_k \omega_k t} ( A_k \sin(\omega_{dk} t) + B_k \cos(\omega_{dk} t) ) \quad (4.24)$$

The function  $f_t$  is a nonlinear function of  $\omega_k$  and  $\xi_k$  and a linear function of  $A_k$  and  $B_k$ .  $F_w$  is also, therefore, a nonlinear function of  $\omega_k$  and  $\xi_k$  and a linear function of  $A_k$  and  $B_k$ . An iterative optimization routine for nonlinear least squares functions was implemented to find the  $\omega_k$  and

variable. It is an iterative method whereby the root of a function,  $y(x)$ , is found by successively incrementing  $x$  from some starting value. Referring to Figure 4-16, the value to increment  $x$  for the current iteration,  $\Delta x$ , is approximated by the equation

$$\Delta x = \frac{-F(x)}{\frac{dF(x)}{dx}} \quad (4.25)$$

The method is generalized to find the minimum of a function of  $N$  independent variables by the following substitutions

$$\begin{aligned} \Delta x &= \{\Delta p_1 \quad \Delta p_2 \quad \dots \quad \Delta p_N\} \\ F(x) &= \left\{ \frac{\delta \epsilon}{\delta p_1} \quad \frac{\delta \epsilon}{\delta p_2} \quad \dots \quad \frac{\delta \epsilon}{\delta p_N} \right\} = \text{Gradient Vector} \\ - \frac{dF(x)}{dx} &= \begin{bmatrix} \frac{\delta^2 \epsilon}{\delta p_1 \delta p_1} & \frac{\delta^2 \epsilon}{\delta p_1 \delta p_2} & \dots & \frac{\delta^2 \epsilon}{\delta p_1 \delta p_N} \\ \frac{\delta^2 \epsilon}{\delta p_2 \delta p_1} & \frac{\delta^2 \epsilon}{\delta p_2 \delta p_2} & \dots & \frac{\delta^2 \epsilon}{\delta p_2 \delta p_N} \\ \vdots & & & \vdots \\ \frac{\delta^2 \epsilon}{\delta p_N \delta p_1} & \frac{\delta^2 \epsilon}{\delta p_N \delta p_2} & \dots & \frac{\delta^2 \epsilon}{\delta p_N \delta p_N} \end{bmatrix} = \text{Hessian Matrix} \end{aligned} \quad (4.26)$$

The  $p_k$  represent the simple oscillator frequencies and

Four methods of computing the analytically derived frequency response function  $F_w$  were developed and tested. The analytical frequency response function was represented by:

- A) the FFT of an analytical discrete time history

$$F_w = \text{FFT} \left[ \sum_{k=1}^n f_t \right]$$

where  $f_t$  is defined in Equation 4.24

- B) the closed form solution of the Fourier Transform integral with finite upper limit

$$F_w = \int_0^T f(t) e^{-i\omega t} dt$$

- C) the closed form solution of the Fourier Transform integral, with infinite upper limit

$$F_w = \int_0^{\infty} f(t) e^{-i\omega t} dt$$

- D) the closed form solution of the Fourier Transform integral with infinite upper limit of a smoothed time history

$$F_w = \int_0^{\infty} S(t) f(t) e^{-i\omega t} dt$$

Method A proved to be the most precise method of separating closely spaced modes. Method B was nearly as precise but much more efficient. All of the four methods are described in the subsections below.

- 2)  $2n = N$  time histories,  $S_{kt}$  and  $C_{kt}$ , were computed, where  $n$  equals the number of simple oscillators in  $F_w$  and  $N$  equals the number of dependent parameters.

$$\begin{aligned} S_k^t &= e^{-\xi_k \omega_k t} \sin(\omega_{d_k} t), & k = 1, 2, \dots, n \\ C_k^t &= e^{-\xi_k \omega_k t} \cos(\omega_{d_k} t), & k = 1, 2, \dots, n \end{aligned} \quad (4.29)$$

where  $\omega_d$  represents the damped frequency.

- 3) the FFT of the  $N$  time histories were computed to yield  $N$  frequency response functions

$$\begin{aligned} S_k^w &= \text{FFT}[ S_k^t ], & k = 1, 2, \dots, n \\ C_k^w &= \text{FFT}[ C_k^t ], & k = 1, 2, \dots, n \end{aligned} \quad (4.30)$$

- 4) The  $A_k$  and  $B_k$  were computed by solving the set of  $N$  simultaneous equations generated by

$$\begin{aligned} \epsilon_{,A_k} &= 0, & k = 1, 2, \dots, n \\ \epsilon_{,B_k} &= 0, & k = 1, 2, \dots, n \end{aligned} \quad (4.31)$$

where

$$\begin{aligned} \epsilon &= \epsilon_w \epsilon_w \\ \epsilon_w &= E_w - F_w \\ F_w &= A_k S_k^w + B_k C_k^w \end{aligned}$$

- 5) The value of  $F_w$  was then computed and the value of the error function,  $\epsilon$ , was evaluated.

Fourier Transform. The analytical expression for the time domain response of a collection of  $n$  simple oscillators is

$$f(t) = \sum_{k=1}^N e^{-\xi_k \omega_k t} (A_k \sin(\omega_{dk} t) + B_k \cos(\omega_{dk} t)) \quad (4.32)$$

Method B evaluated  $F_w$  at discrete values of the following continuous function  $F(w)$

$$F(w) = \int_0^T f(t) e^{-iwt} dt \quad (4.33)$$

The integration limit  $T$  is the duration of the FFT of the experimental time history. Evaluation of the definite integral gives

$$F(w) = \sum_{k=1}^n a_k e^{\beta_k T} [A_k (\beta_k \sin(\omega_{dk} T) - \omega_{dk} \cos(\omega_{dk} T) + \omega_{dk}) + B_k (\beta_k \cos(\omega_{dk} T) + \omega_{dk} \sin(\omega_{dk} T) + \beta_k)] \quad (4.34)$$

where

$$a_k = \frac{1}{\omega_k^2 - w^2 + i2\xi_k \omega_k w}$$

$$\beta_k = -\xi_k \omega_k - iw$$

to the fact that the smoothing process increases the apparent resolution of the modulus curve only, and not of the real and imaginary components which are used in the curve fit process.

#### **4.4.3.3 Comparison of Curve Fitting Methods**

The performance of the three methods (Methods A, B and C) were compared by applying the methods to artificial data. The chief advantage of using artificial data (over real data) was that the properties of the modal parameters which the methods were attempting to determine were known exactly.

The artificial time history was composed of the responses of simple oscillators whose properties are listed in Table 4-2. These properties are similar to the properties of Modes One and Two of the Dominion Road data. An 8192 point FFT was applied to the artificial time history. The time increment of the time history was 0.005 seconds and therefore the frequency increment of the FFT was 0.02441 Hz. The frequency range over which the curve fit was performed spanned from 0.50 Hz to 1.50 Hz, resulting in 42 complex-valued frequency response "fitting" parameters or 84 real-valued fitting parameters.

number of function calls are listed in the second and third columns of the tables, respectively.

The relative precision of the methods was evaluated by comparing the final value and the gradient of the error function at the solution. The final value of the error function ( $\text{Error}^2$ ) and the Euclidian norm of the gradient vector ( $G^T G$ ) are listed in the third and fourth columns, respectively, for each method.

The accuracy of each method was evaluated by comparing its "predicted" simple oscillator properties against the "actual" simple oscillator properties listed in Table 4-1. The last four columns of Tables 4-4a and 4-4b list the frequencies, damping ratios, amplitudes and phase angles (in degrees) of each of the four simple oscillators fit to the artificial time history. If the frequency of the oscillator was outside the search range (0.5 to 1.5 Hz), the frequency, damping ratio and phase angle were not listed in the tables.

Method A was the top performer for precision. Method A exited the optimization routine having satisfied all convergence criteria. It had the lowest sum of the squared errors and the lowest Euclidian norm of the gradient vector at the solution. Its estimated modal parameter values

The effect of the exponential decay rate of a time history on the discrepancy between model and experimental transform for Method C can be observed in Figures 4-17 through 4-20. In these figures, the dashed lines represent the analytical model response function (Equation 4.35) and the solid lines represent the FFT of an "experimental" time history. The damping ratio of both the experimental time history and the analytical model have been set to provide the ratios of final time history amplitude to initial time history amplitude listed in Table 4-5.

It can be seen in the figures that Method C is not a good model for time histories with Final Amp./Initial Amp. ratios greater than or equal to .10. Method B meanwhile is an accurate model for time histories with any Final Amp./Initial Amp. ratio, as can be observed in Figure 4-21. This figure is identical to Figure 4-17 except that Method B (Equation 4.34) has been used to compute the analytical frequency response function.

Method B and Method C were about equally efficient in terms of computer CP time. Although Method B required slightly more CP time per function evaluation, its overall CP time requirement was equal to Method C's because Method B required fewer iterations to converge.

was not successful in separating Mode Two for DOF 1 and DOF 4, and it was not applied to DOF 3 and DOF 5 because these DOF's represent the vertical response which participated negligibly in Modes One and Two.

There are no data points in Figure 4-23 at certain bridge deck measurement stations. These stations were measured at the end of a day's testing. The power spectral density contour plot in Figure 4-24 reveals that the spectral peak which appears in the vicinity of 1.22 Hz at the beginning of a day's testing vanishes at the end of the day's testing. (Also, no peak is evident in the vicinity of 1.65 Hz at the beginning of a day's testing but one is evident at the end of a day's testing.) The mode shape plotted in Figure 4-23 represents the response of the bridge at the beginning of a day's testing.

Method B was used to separate Modes One and Two of the Dominion Road data for selected acceleration time histories. There were only slight differences between the results from Method B and Method A. Based on these results and those in Tables 4-4a and 4-4b, Method B is considered to be a suitable method to separate closely spaced modes.

Method B was not used to separate modes other than Modes One and Two in the Dominion Road data set because of the

the following manner. An experimental time history was divided into three consecutive four-second segments. The time history segments were smoothed, Fast Fourier Transformed and the modulus curves displayed. Modal separation Methods A and B were applied to the segments as well.

Figure 4-25 is a plot of Fourier amplitudes (or modulus) of three consecutive segments of an acceleration time history from the longitudinal reference accelerometer at station 20. The amplitude of the first, second and third segments are plotted as the dotted, dashed and dot-dashed lines, respectively. The same data is plotted in Figure 4-26 but the amplitude of each curve is normalized so that the maximum value of each curve is the same. Several observations can be made of the data displayed in Figure 4-26.

The frequency of Mode One (1.08 Hz) noticeably increases for successive time history segments. Also, a mode at 2.0 Hz is very pronounced in the first four-second segment and much less so for subsequent segments. This is expected based on the fact that for two oscillators having the same damping ratio, but with the frequency of the second oscillator twice the frequency of the first, the decay rate of the second oscillator is equal to the square of the decay rate of the

initial parameters were the same as those used previously and are listed in Table 4-2. The results are tabulated in Table 4-6.

The tabulated data was interpreted as follows for the first time history segment. The 1.05 Hz and the 1.13 Hz components represent a "wide" experimental mode one response. Two model modes were required to fit the experimental mode one response because the experimental mode one response drifted a little down the frequency axis as the time history progressed. (An analytical signal was constructed using the tabulated simple oscillator properties of these two model modes. The FFT modulus of this analytical time history matched the FFT modulus of the experimental time history perfectly.) The tabulated 1.22 Hz mode represents the experimental mode two response.

The tabulated data for the second time history segment requires a bit of imagination to interpret. Method A fit three model modes to this segment. The first two model modes (at .95 Hz and .99 Hz) have a physically impossible negative damping ratio. The frequency response of these two modes combined with the response of the large amplitude, large positive damping ratio model mode at 1.16 Hz yield a net frequency response which matches a "wide" experimental mode one response. The two model modes tabulated under

was accentuated in the initial high amplitude portion of the bridge response.

Figures 4-28, 4-29 and 4-30 present the initial bridge response at the beginning of the day, in the middle of the day and at the end of the day, respectively. The data in these figures was recorded from the same reference accelerometer as that of Figures 4-25 and 4-26. Observe the change in the bridge response in the vicinity of 2.1 Hz. A single mode occurred at this frequency at the beginning of the day. In the middle of the day, the mode had "split" into two modes, one at 1.9 Hz and one at 2.3 Hz. And by the end of the day, the modes were better defined and had separated further to 1.65 Hz and 2.35 Hz. Figure 4-31 represents the response of the same accelerometer at the beginning of the following day. The two modes in the vicinity of 2.1 Hz were now one mode and the other aspects of the bridge response were similar to the response at the beginning of the previous day.

The vertical response of the bridge appears more regular overall than the response in the horizontal direction. An interesting irregularity in the vertical response data, however, is represented in Figure 4-32. This figure represents the vertical response of the deck at Station 28. The dotted, dashed and dot-dashed lines represent the

Road bridge test data. The modal separation methods investigated in this chapter are summarized below.

The FFT is quick, efficient and unconditionally stable. Interpretation of its results is straightforward. The FFT models the data as a collection of constant amplitude, undamped, infinite duration sinusoids. The FFT of the damped, relatively short duration Dominion Road bridge time histories provided adequate results in most instances. The differences between model and data resulted in inadequate resolution in some instances, however. (e.g. to resolve modes one and two.)

Time domain methods model the data as a collection of finite duration, damped sinusoids. This accurate model is their strong point. The principal weakness of time domain modal separation methods centers around the fact that the sinusoidal responses are still coupled in the time domain. It is not possible to concentrate on just one frequency interval of the frequency response. To separate a weak mode from a nearby dominant mode for example, all modes with a larger amplitude must be included in the collection of sinusoids.

The CZT is a numerical discrete transform like the FFT. It models the data as a collection of infinite duration damped

produced by an experienced operator are more reliable than those from a fully automated routine.

The curve fitting method developed in this chapter was not used more to separate experimental modes because of the data irregularities demonstrated in the section on the frequency response of partial time histories. Nevertheless, this method would be a useful tool to separate closely spaced modes of other, more regular time history data. This modal separation method is especially well suited for short duration time history data.

10. Smith, S., "Modal Testing - A Critical Review," The Shock and Vibration Bulletin, No. 54, Part 1, June 1984, pp 65-75.
11. Srinivasan, M.G., Kot, C.A. and Hsich, B.J., Dynamic Testing of As-Built Civil Engineering Structures - A Review and Evaluation, Office of Nuclear Regulatory Research, U.S. Nuclear Regulatory Commission, Washington, D.C., (NUREG/CR-3649), 1984.
12. Hildebrand, F.B., Introduction to Numerical Analysis, McGraw-Hill, Inc., New York, 1956, pp457-462.
13. Spitznogle, F. R. and Quazi, A. H., "Representation and Analysis of Time-Limited Signals Using a Complex Exponential Algorithm," Journal of the Acoustical Society of America, Vol. 47, No. 75, Part 1, May 1970, pp 1150-1155.
14. Ibrahim, S. R. and Mikulcik, E. C., "A Method for the Direct Identification of Vibration Parameters from the Free Response," Shock and Vibration Bulletin, No. 47, Part 4, Sept. 1977.
15. Numerical Algorithm Group, Inc., Downers Grove, Illinois.
16. Douglas, B. M. and Richardson, J. A., "Maximum Amplitude Dynamic Tests of a Highway Bridge," Proceedings of the Eighth World Conference on Earthquake Engineering, San Francisco, July 1984, Vol.VI, pp 889-896.
17. Rabiner, L.R., Schafer, R.W. and Rader, C.M., "The Chirp Z-Transform Algorithm and Its Application," Bell System Technical Journal, Vol. 48, pp. 1249-1292, May 1969.
18. Bracewell, Ronald N., The Fourier Transform and its Application, McGraw-Hill Book Co., New York, 1978.
19. Harris, F.J., "On the use of Windows for Harmonic Analysis with the Discrete Fourier Transform," Proc. IEEE, Vol. 66, pp. 51-83, Jan. 1978.
20. Gill, P.E. and Murray, W., "Algorithms for the Solution of the Nonlinear Least Squares Problem," SIAM Journal of Numerical Analysis, Vol. 15, No. 5, Oct. 1978, pp. 997-992.

Excitation Method	Response Measured
sinusoidal steady state	forced steady state, free vib.
swept sine	general forced, free vib.
random	general forced, free vib.
pulse train	general forced, free vib.
impulse	general forced, free vib.
quick-release	general forced, free vib.
ambient wind	general forced
ambient traffic	general forced
earthquake	general forced

Table 4-1 Excitation methods used in full scale testing.

Mode	Frequency	Zeta	A	B
1	1.08	.03	0.	10.
2	1.24	.03	0.	1.

Table 4-2 Artificial time history simple oscillator properties for test of modal separation algorithms.

Mode	Frequency	Zeta
1	1.00	.03
2	1.10	.03
3	1.20	.03
4	1.30	.03

Table 4-3 Initial values for test of modal separation algorithms.

Figure	Final Amp./Initial Amp.
4-16	0.95
4-17	0.50
4-18	0.10
4-19	0.01

Table 4-5 Ratios of final to initial amplitude for free vibration time histories used for Figures 4-16 through 4-19.

Segment	Method A			Method B		
	Frq.	Zeta	Amp.	Frq.	Zeta	Amp.
1	1.05	.12	0.95	1.05	.12	2.10
	1.13	.07	1.90	1.13	.08	4.21
	1.22	.05	0.43	1.22	.05	0.94
2	0.95	-.02	0.12	1.05	.09	2.92
	0.99	-.04	0.32	1.14	.21	3.20
	1.16	.11	1.20			0.00
3	1.11	.09	0.28	1.11	.09	0.62
	1.25	.05	0.16	1.25	.05	0.35
	1.26	.02	0.05	1.26	.02	0.09

Table 4-6 Results of modal separation methods A and B on three consecutive four second segments of longitudinal direction reference accelerometer at station 20.

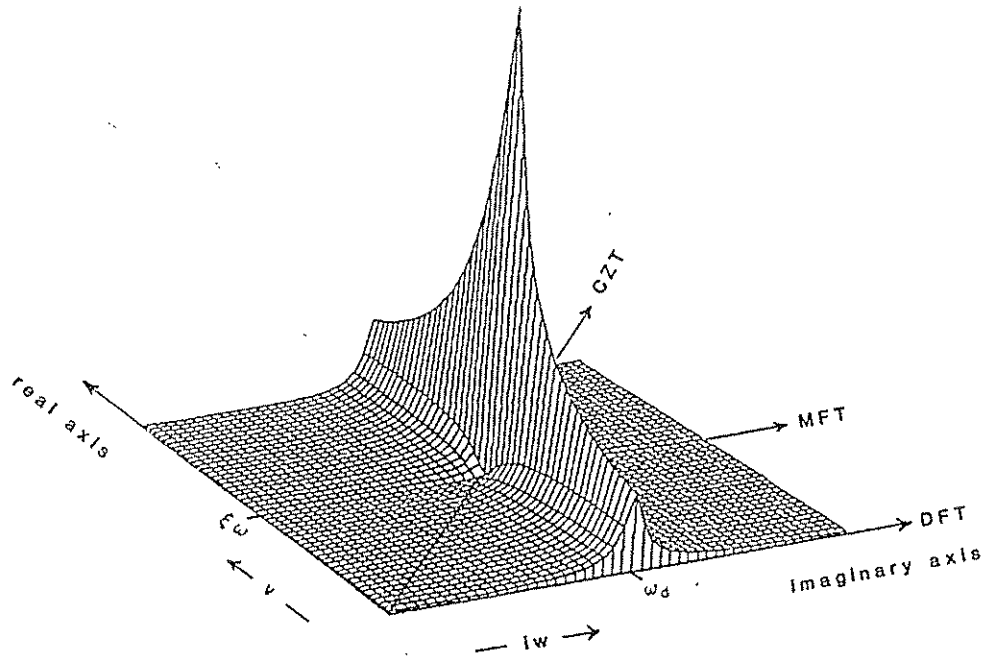


Figure 4-2 One quadrant of the surface formed by the real and imaginary components of the Laplace Transform of a damped simple oscillator.

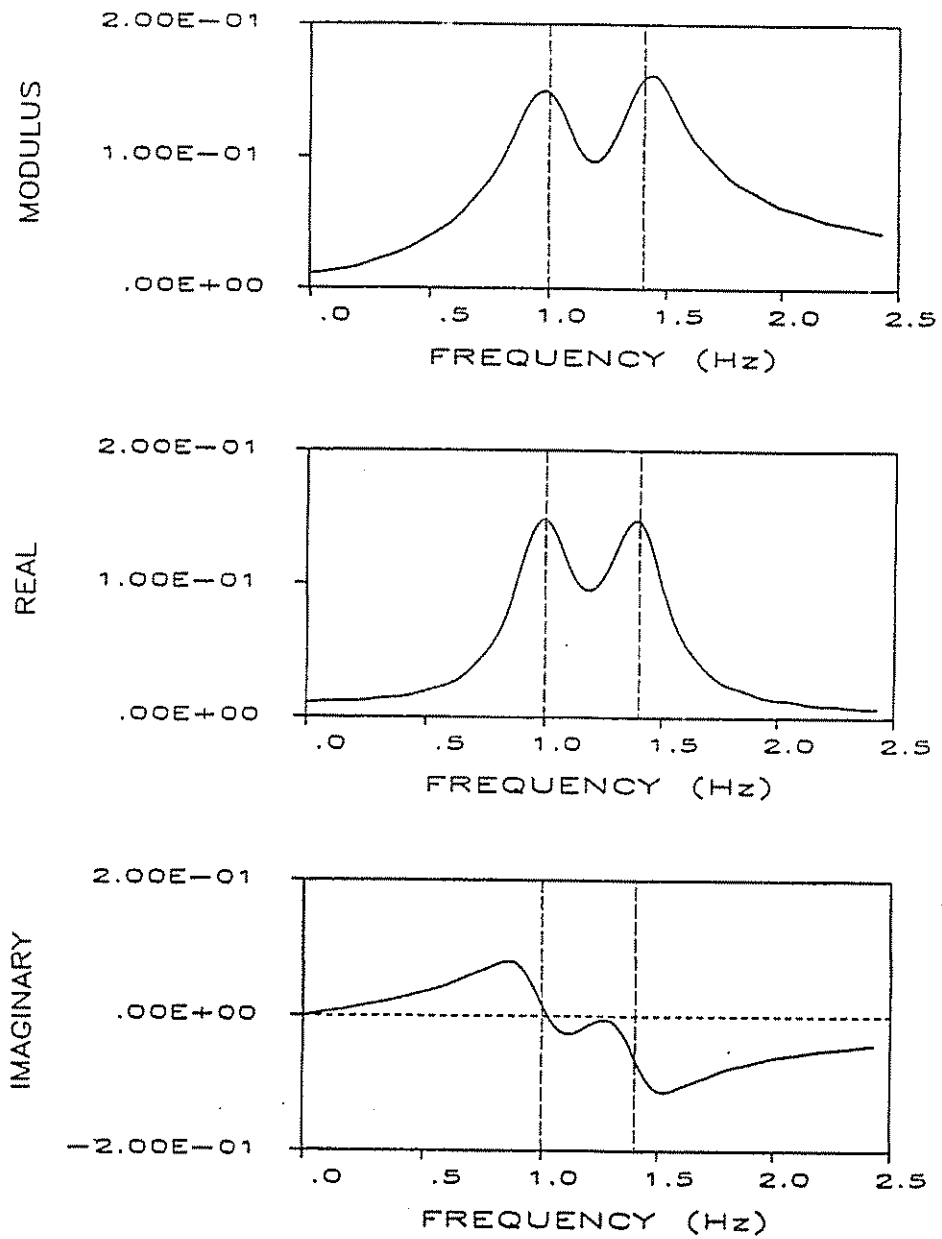


Figure 4-4 The modulus, real component and imaginary component of the frequency response of two oscillators closely spaced in frequency.

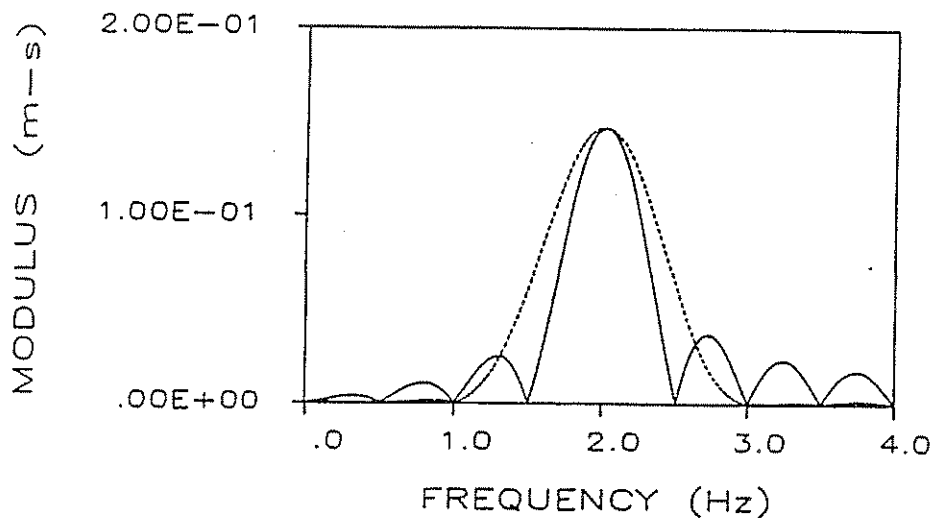


Figure 4-6 FFT modulus of an unsmoothed time history (solid line) and of an identical but smoothed time history (dashed line).

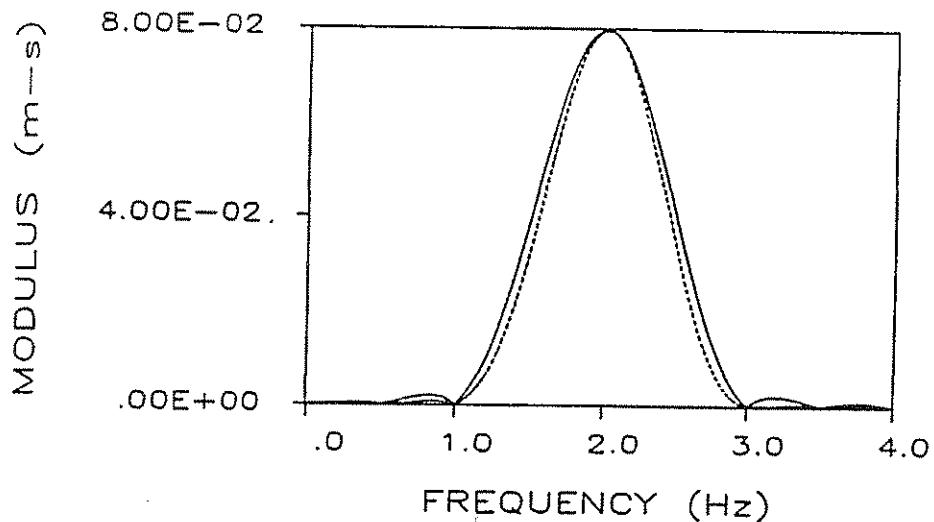


Figure 4-7 Hamming smoothing window (solid line) vs. Hanning smoothing window (dashed line).

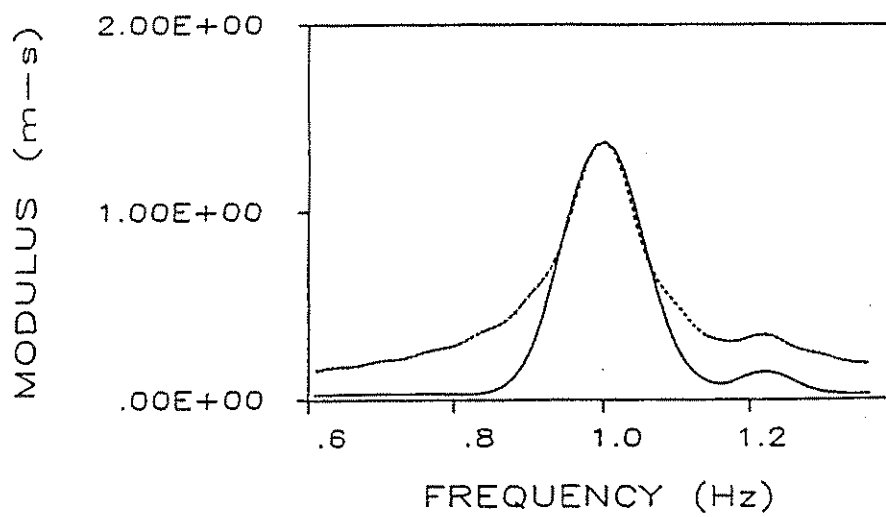


Figure 4-10 FFT modulus of smoothed (solid) and unsmoothed (dashed) free vibration time history with relatively high damping.

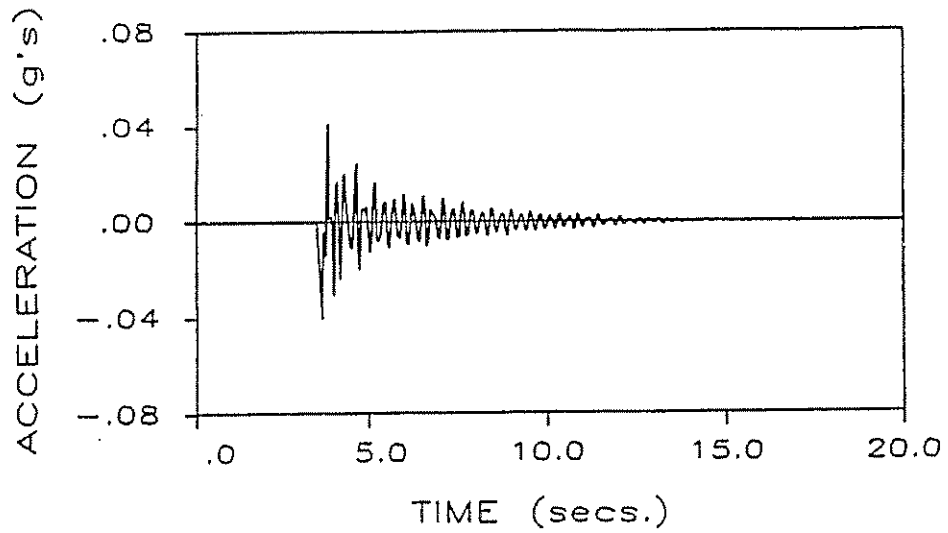


Figure 4-13 Typical vertical response time history, (measurement station 28).

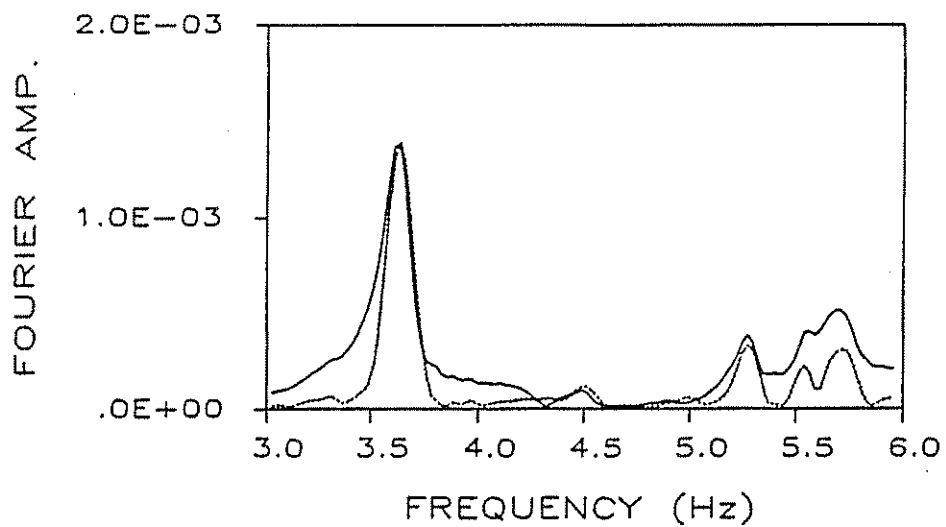


Figure 4-14 FFT modulus of smoothed (dashed) and unsmoothed (solid) of time history of Figure 4-13.

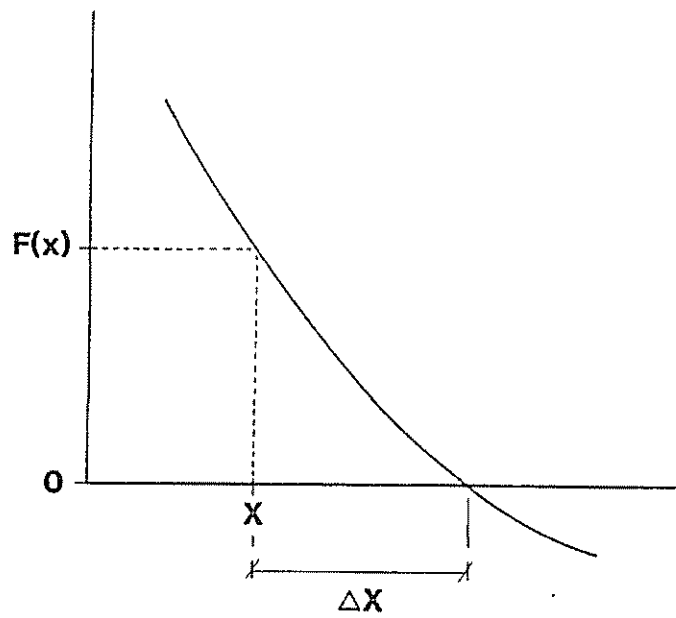


Figure 4-16 Demonstration of Newton's Method for finding root of  $F(x)$ .

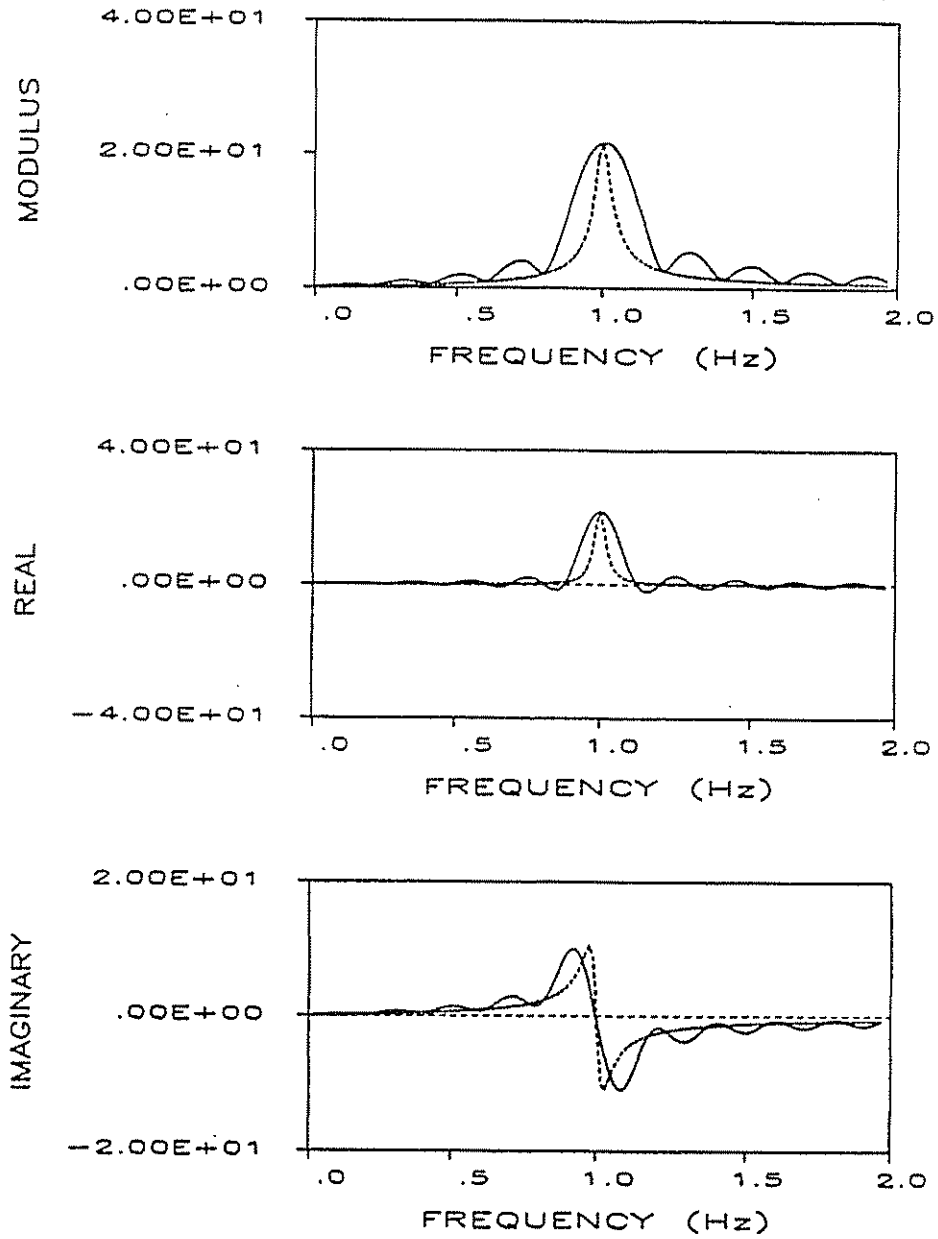


Figure 4-18 Comparison of FFT (solid) and Method C (dashed) frequency responses for low damped free vibration time history.

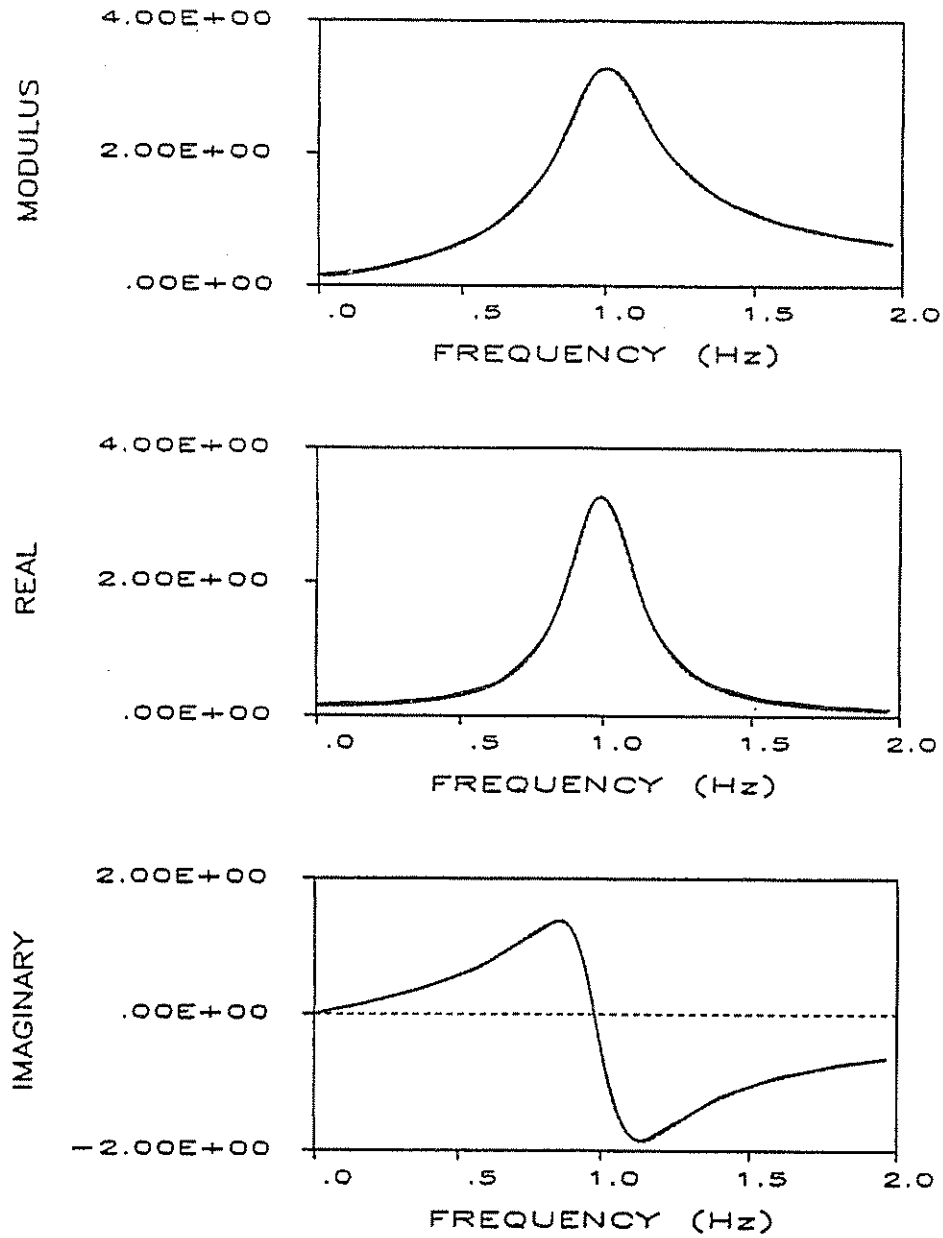


Figure 4-20 Comparison of FFT (solid) and Method C (dashed) frequency responses for highly damped free vibration time history.

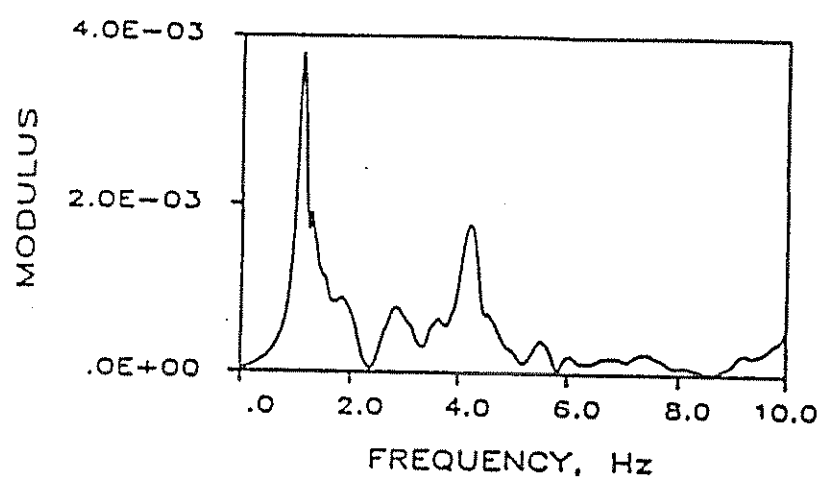


Figure 4-22 FFT modulus of a typical radial response time history.

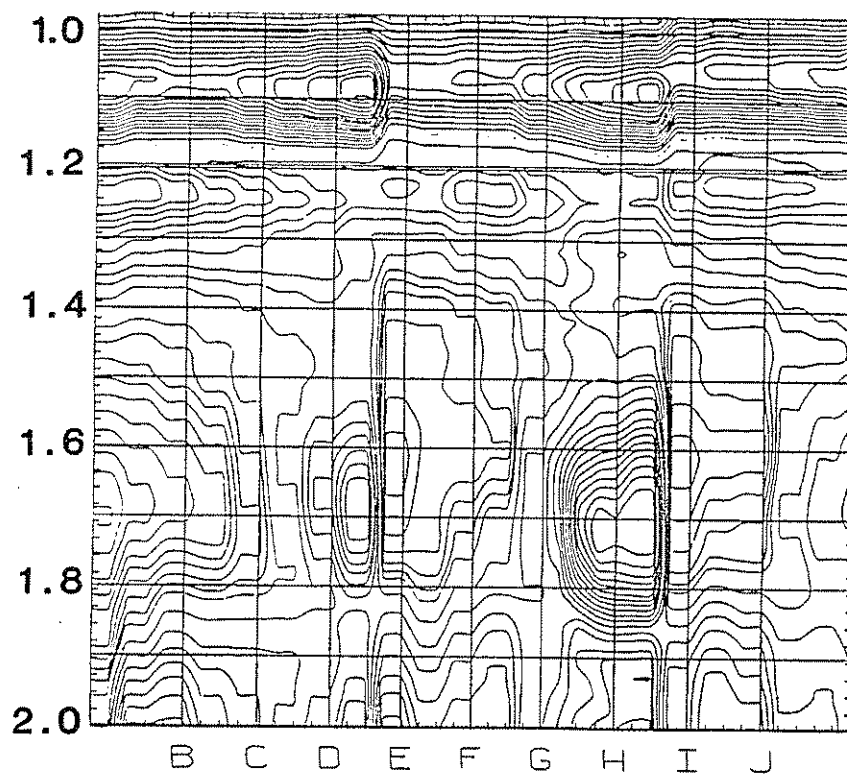


Figure 4-24 Power spectral density contour plot of radial response reference accelerometer between 1.0 and 2.0 Hz.

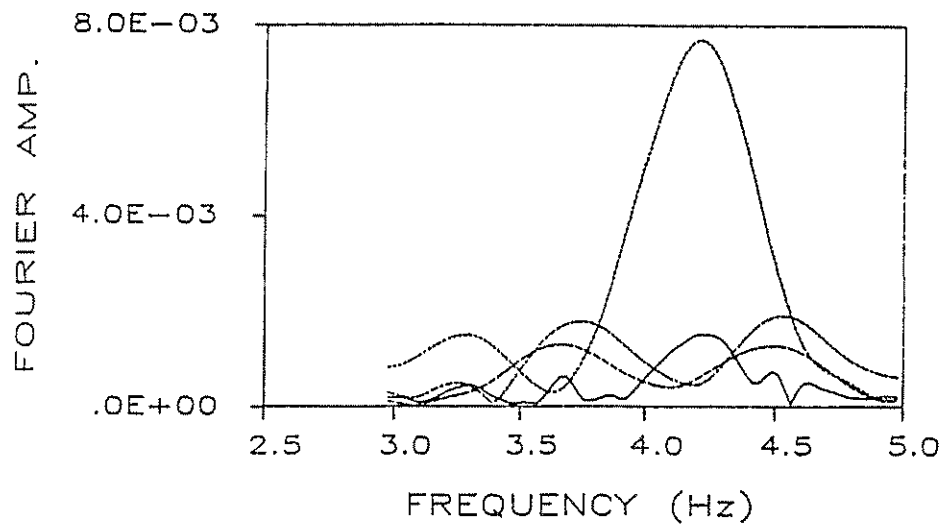


Figure 4-27 Magnified view of 3.0 to 5.0 Hz region of Figure 4-25.

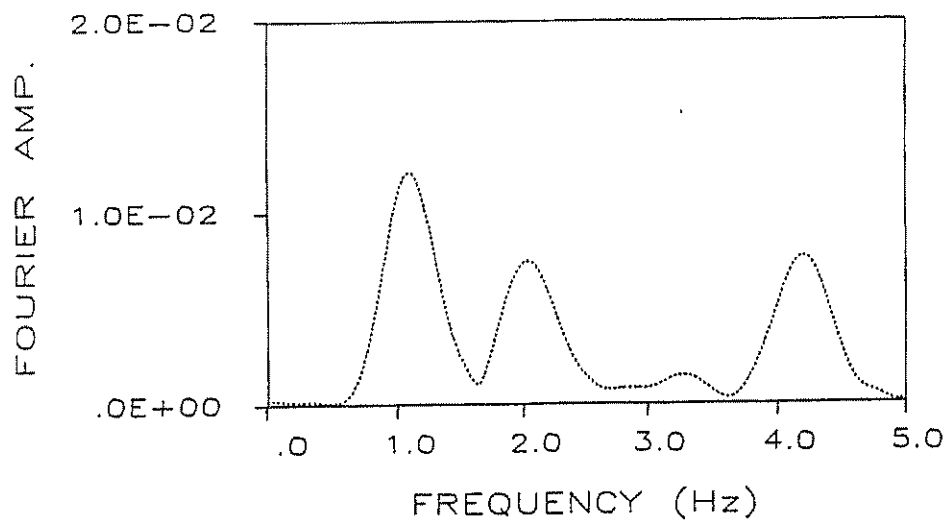


Figure 4-28 FFT modulus of the initial four seconds of bridge response at the beginning of the day.

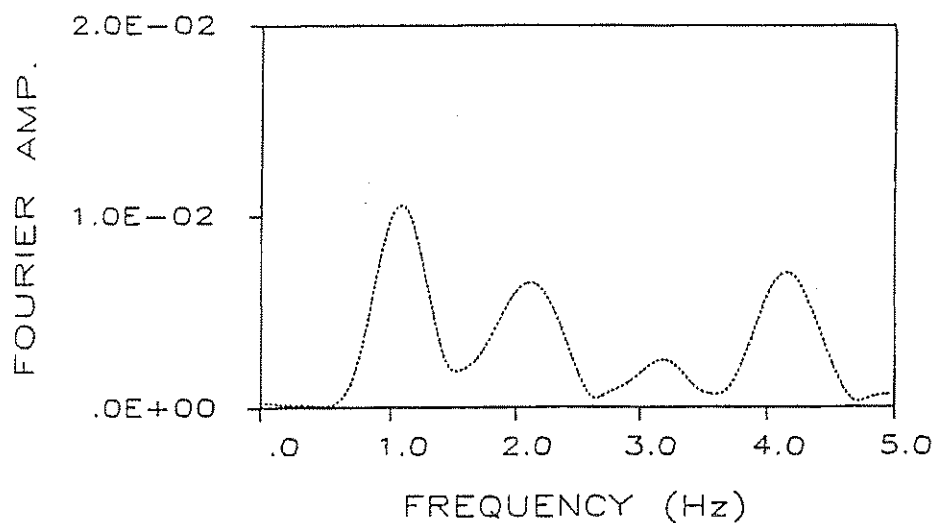


Figure 4-31 FFT modulus of the initial four seconds of bridge response at the beginning of the next day.

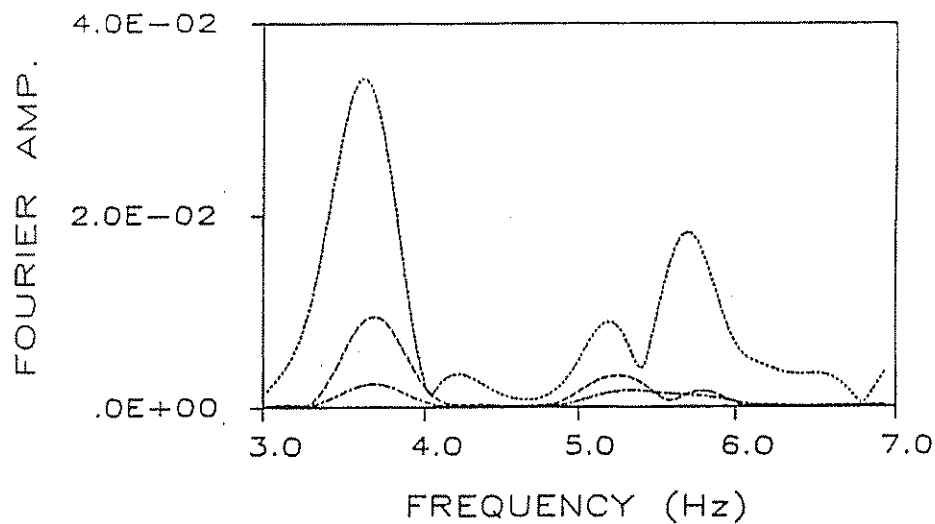


Figure 4-32 FFT moduli of first four-second segment (dotted), second four-second segment (dashed) and third four-second segment (dot-dashed) of vertical reference accelerometer time history.

## 5. ESTIMATION OF FOUNDATION STIFFNESSES

This chapter outlines the procedure by which the lateral and rotational stiffnesses of the pile foundations of the Dominion Road bridge were estimated. Geotechnical methods developed by Dr. Gary Norris [1,2,3,4,5] were used on available soil property data from the bridge site to estimate the foundation stiffnesses. The foundation stiffness values from this procedure were substituted for the boundary element spring rates of the analytical bridge response model developed in Chapter Six.

Norris has used his methods to successfully predict foundation stiffness values measured during the Rose Creek bridge test [1]. His methods are unique in that they take into account the magnitude of the foundation soil strains associated with a bridge test, which are considerably smaller than those due to a design level earthquake.

This chapter begins by describing the foundation configuration and soil conditions. Next, an overview of Norris's method for computing lateral pile group stiffness is presented and the lateral foundation stiffnesses are calculated following his method. In the next section, an overview of Norris's method for computing pile group rotational stiffness is presented and the rotational

appears that the piles were designed to be end bearing as most of the soil samples were taken at elevations near the elevation of the pile tip. The lack of soil property data for the upper 10 to 20 feet of the pile groups is unfortunate since it is the soil in this region which contributes the majority of the resistance to lateral pile movement. The unconfined compressive strength ( $q_u$ ) values from boring logs near foundations B, C, D, F, G, I and J are tabulated in Tables 5-2a, 5-2b and 5-2c. The depth values in the tables refer to depth below the top of the pile. No borings were located near foundations E and H.

Pile group stiffness values were not calculated for every pile group. Rather, the soil properties at each location were ranked from softest to stiffest and pile group stiffnesses were calculated for the extreme conditions. This was done for both pile lateral resistance (soil strength in the upper 10 to 20 feet) and for pile rotational resistance (soil strength at the pile tip elevation). The soils at the following locations are ranked from softest to stiffest against lateral pile deformation:

Softest

Stiffest

D - F - I - B - J - G - C

## 5.2 LATERAL FOUNDATION STIFFNESSES

Norris assumes the behavior of long slender piles arranged in a group and fastened together at their heads by a rigid cap is such that a lateral force applied at the cap will cause only lateral translation of the cap, no rotation; and a moment about a lateral axis will cause only rotation about that axis and no translation. The lateral and the rotation responses are said to be decoupled.

The method developed by Norris and used for this chapter assumes that the lateral and rotation responses are decoupled. Therefore, the method yields pile group stiffness values directly comparable with analytical model boundary element spring stiffness values. The configuration of the pile groups of the Dominion Road bridge is such that the above assumption is true for all but the three-pile pile groups in the longitudinal direction. For these pile groups, the longitudinal translation and rotation about the radial axis are coupled responses. This is discussed in a later section of this chapter.

An overview and a detailed explanation of Norris's method of computing lateral pile group stiffness is given in [1] and [2,3,4], respectively. The procedure used in this dissertation for calculating the lateral stiffness of a

Coefficient  $A_{\Delta}$  or  $C_{\Delta}$  is used for free pile head or fixed pile head conditions, respectively. The fixed pile head condition was assumed for the Dominion Road bridge foundations.

Other features of this procedure include consideration of the pile group and the cyclic load effects and inclusion of the additional resistance provided by the embedded portion of the pile cap. The pile group effect factor,  $e_g$ , accounts for the interference between the developing passive soil wedges of adjacent piles. The stiffness contribution of a pile that is part of a closely spaced group is less than if the piles were widely spaced; therefore the stiffness of the individual pile is reduced by the factor  $e_g$ . Also, for a given pile top displacement, a pile in a group causes less strain to the soil immediately adjacent to it than an individual pile would cause. Therefore, for a given pile group top displacement,  $\Delta_g$ , the nonlinear stiffness of an individual pile,  $K_p$ , is calculated based on a reduced pile top displacement,  $e_g \Delta_g$ . To summarize, the net stiffness of a pile group,  $K_g$ , composed of  $n$  piles is:

$$K_g = e_g n K_p \quad (5.4)$$

and  $K_p = \text{function}(e_g \Delta_g)$

above assumptions is that the rotational response is decoupled from the lateral response.

Norris examines the rotational response of a pile group as it progresses cycle by cycle. His analysis reveals that although the initial response of the pile group is complicated, the "steady-state" response is much simpler and can be effectively modeled with linear springs for a specified displacement range.

In the initial cycle of rotation, the piles on opposite sides of the axis of rotation experience unequal resistance. The unequal resistance of downward vs. upward moving piles is due to their very different load-displacement paths. Both piles start at the same point on a graph of pile load vs. pile displacement, (Point 1 in Figure 5-2). Point 1 represents the dead load on the pile and the corresponding deflection due to the dead load.

As a moment is applied to the pile cap, (due to an earthquake for example), the pile cap rotates. The downward moving pile moves to Point 3 in Figure 5-2 and the upward moving pile follows an unload load-displacement path to Point 2 in the figure. The soil resistance to the piles' displacement can be characterized by stiffness values computed from the slope of the lines joining Point 1 to

computed as the sum of the vertical stiffness times the moment arm squared for each member pile. Because the pile load-displacement relationship is nonlinear, the pile vertical stiffness was calculated for a specific "design" vertical displacement.

The design displacement was the maximum vertical movement (plus to minus) of the pile during the bridge test. This displacement was estimated as follows. The mode one foundation displacements were scaled to the measured static foundation displacements at release. The mode one foundation rotations were then divided by this scale factor to obtain an estimate of the static release rotations. This estimated release rotation was multiplied by the distance from the pile cap center to the center of the pile, and then multiplied by two to yield the total plus to minus pile vertical movement during a cycle of rotation, termed the design vertical displacement.

The vertical pile stiffness at the design vertical displacement was picked off the pile stiffness-displacement curve constructed for each foundation. Each point of this curve was calculated as follows. First, a pile tip displacement was arbitrarily chosen. The resistance of the soil at the pile tip to this displacement was then calculated. The pile side shear resistance depends on the

foundation flexibilities in the bridge response model (described in Chapter Six) can accurately model only uncoupled foundation flexibilities. This is because the structural analysis program SAPIV [8] used for the model does not compute boundary element stiffnesses which couple translation and rotation.

It was anticipated that the longitudinal foundation response would not affect the overall bridge response nearly as much as the radial foundation response, however. Therefore, this deficiency in the bridge model was not expected to have a significant effect on the system identification results presented in the next chapter.

Location	Pile Dimensions (ft)		
	Length	Diameter of Shaft	Diameter of Base
Foundation B	65.4	2.0	5.0
Foundation C	34.5	2.0	5.0
Foundation D	27.8	2.0	5.0
Foundation E	25.6	2.0	5.0
Foundation F	30.3	3.0	5.5
Foundation G	43.0	3.0	5.5
Foundation H	31.5	2.5	5.5
Foundation I	26.4	2.5	5.5
Foundation J	26.9	2.0	5.0

Table 5-1 Summary of pile dimensions.

Foundation F		Foundation G		Foundation I	
Depth, ft.	$q_u$ , ksf	Depth, ft.	$q_u$ , ksf	Depth, ft.	$q_u$ , ksf
10	0.9	2	2.4	2	1.0
13	1.3	5	2.0	6	0.8
15	0.9	9	1.6	10	3.6
16	2.5	14	1.0	13	1.5
18	3.4	20	2.1	16	3.4
22	11.5	24	3.6	20	6.4
23	7.6	28	10.5	25	2.2
30	13.8	30	11.9	26	14.5
35	34.2	31	4.2	28	12.2
37	32.2	33	5.5	29	4.4
39	9.5	36	2.8	33	19.5
		41	3.9	37	21.4
		45	29.6		
		48	16.5		
		50	13.3		
		54	16.1		

Table 5-2b Unconfined compressive strength vs. depth below top of pile for Foundations F, G & I.

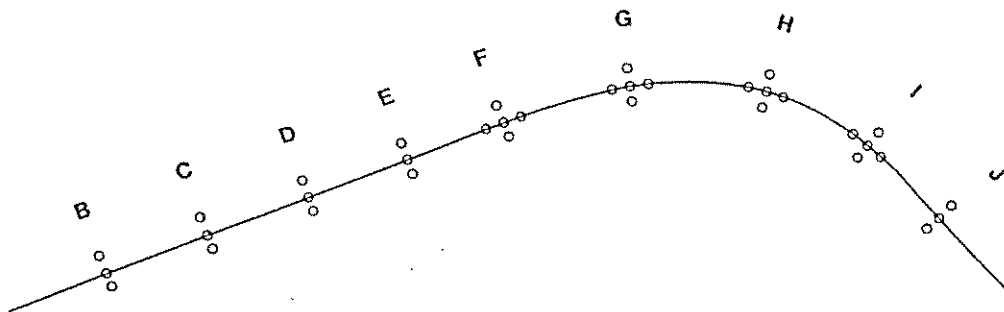


Figure 5-1 Plan of pile layout.

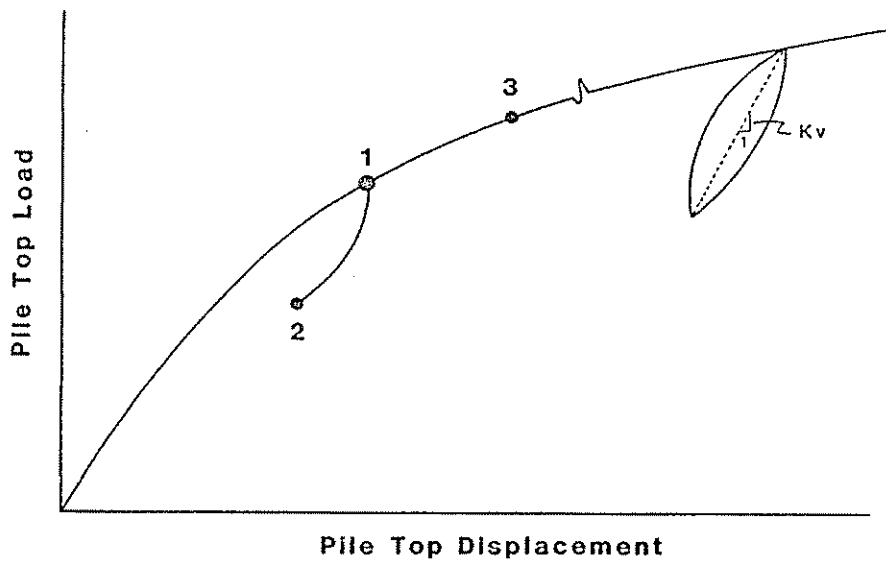


Figure 5-2 Schematic of vertical pile top load vs. pile top displacement.

dynamic loads. The subsection below describes the components of the model.

#### **6.1.1 Node and Element Layout**

Each span of the ten span bridge was divided into four beam elements and each column was divided into two beam elements. The elastomeric pads between the deck and column tops were modeled with a beam element and the space from the bottom of the box girder to its center of gravity was modeled with a massless rigid link. A set of four boundary element springs was placed at each abutment and at the base of each column. Masses were lumped by the program at each node according to its tributary area.

#### **6.1.2 Material and Element Properties**

The material and cross section properties of the deck, elastomeric pad and column elements are summarized in Table 6-1. The units used for all tables in this chapter are kips and feet. The subsections below explain how the values in Table 6-1 were calculated.

shear. Unfortunately the SAP4 element library does not include a shear element. The bearing pads at the column tops were modeled with beam elements. This presents a problem in that the shear and bending responses are coupled in a beam element whereas in the real pad they are not. The magnitude of the error in modelling the elastomeric pads at the column tops with beam elements was judged to be small, however, by the following calculation.

The two degree of freedom flexibility matrix,  $f$ , for a cantilever beam was calculated from the following standard equation

$$f = \begin{bmatrix} \frac{L^3}{3EI} + \frac{L}{A_s G} & \frac{L^2}{2EI} \\ \frac{L^2}{2EI} & \frac{L}{EI} \end{bmatrix} \quad (6.2)$$

where  $L$  equals the length of the beam,  $E$  represents its modulus of elasticity,  $G$  represents its shear modulus,  $I$  equals its moment of inertia about its centroid and  $A_s$  represents its shear area. Figure 6-1 indicates the assignment of the two degrees of freedom. Inserting values from Table 6-1 into equation 6.2,  $f$  becomes

$$f = \begin{bmatrix} 1.58 \text{ E-03} & 6.11 \text{ E-08} \\ 6.11 \text{ E-08} & 1.16 \text{ E-06} \end{bmatrix} \quad (6.3)$$

The modulus of elasticity in compression for the pads,  $E_c$ , was calculated following the procedure outlined in a Natural Rubber Producers Research Association publication [3]. A durometer hardness of 55 was assumed for the rubber of the pads. This modulus,  $E_c$ , was input as Young's modulus,  $E$ , into the computer model. The computer program SAPIV calculates the shear modulus,  $G$ , from the values of  $E$  and  $\nu$ , (Poisson's ratio) input using the following familiar equation:

$$G = \frac{E}{2(1 + \nu)}$$

However, the actual shear modulus of the pads (115 ksi) was much lower than the value computed by the program using the above equation. To compensate for this, the properties of the elastomeric pads involving shear deformation (shear areas and torsional constant) were multiplied by the following factor:

$$\text{reduction factor} = \frac{.115 \text{ ksi}}{\frac{E_c}{2(1 + \nu)}} \quad (6.4)$$

### 6.1.2.3 Column Properties

The modulus of elasticity of the columns was calculated from Equation 6.1 using a 28-day compressive strength,  $f'_c$ , equal

## 6.2 PRELIMINARY PARAMETER IDENTIFICATION

A streamlined analytical model was constructed for computing the mode one response only of the Dominion Road bridge. Results of the eigenanalysis were displayed graphically on a high resolution computer monitor for visual comparison with a similar plot of the experimentally measured mode one response. The eigenanalysis and plot construction required very little computation time and allowed the results to be displayed very quickly (less than two minutes.) Engineering judgement was used to adjust the calculated model parameter values listed in Tables 6-1 and 6-2 in order to bring the model response into better agreement with the experimental response.

The first step in the preliminary parameter identification was to adjust the modulus of elasticity of the deck in the "full" bridge model so that the frequency of the model and experimental first vertical modes agreed. It was anticipated that the response of the bridge superstructure in the first vertical mode would be almost solely influenced by the bending stiffness of the box girder,  $EI$ . Since the moment of inertia,  $I$ , of the prestressed box girder could be calculated reliably, the  $E$  value resulting from this adjustment was considered to be an accurate estimate of the actual modulus of the box girder. It was necessary to

figure by the solid line, the ovals and the rectangles, respectively. The maximum amplitude of each frame, from centerline to top of the frame, is indicated at the left of each frame. The number in parentheses represents the foundation maximum amplitude for that frame.

The preliminary parameter identification provided a good starting base for the more rigorous parameter identification described in the next section. It not only yielded better initial estimates of the parameter values, it also indicated which parameters most affect the model response.

### 6.3 PARAMETER IDENTIFICATION METHOD

A computer algorithm was used to systematically adjust the input parameters of a bridge response model until the frequencies and mode shapes of the model matched the measured frequencies and mode shapes of the bridge. The methodology for this procedure is termed "system identification".

System identification techniques have been developed by a number of investigators for identifying structural parameters from dynamic response measurements of civil engineering structures. Wilson [4] used the system identification method developed by Beck [5] to identify the

reference [11] is reproduced in Appendix D of this dissertation. Features of the system identification algorithm are described below.

### *6.3.1 Overview of System Identification Algorithm*

The algorithm was designed to be a practical tool to identify model parameter values and to give information on the sensitivity of the model to those model parameters.

A practical feature of the algorithm was that it ran to final convergence without operator intervention. Also, provisions were included in the algorithm to ensure that steady progress toward a solution was maintained and to protect against "crashes" of the algorithm caused by divergence of the optimization routine.

Information regarding the behavior of the error function was output periodically so that the reliability of the solution could be evaluated. The relative sensitivity of the error function, (and hence of the response model), to each model input parameter was assessed at the end of the system identification procedure.

The original error function (Equation 6.5) was modified after the algorithm was implemented on Dominion Road data. Two observations of the algorithm's behavior led to a modification of the error function.

The first observation was that the error between measured and modeled frequencies was overshadowed by the error between measured and modeled mode shapes. This was because there was only one frequency error value to nearly 155 mode shape error values in the sum of Equation 6.5. The frequency error value was therefore weighted. The value of the weight factor was chosen by the following reasoning.

Each experimental measurement of the mode one response of the Dominion Road bridge consisted of a frequency value and an amplitude value. Assume the frequency value and amplitude value are equally reliable. Now for illustrative purposes, assume the following definition for the error function, in which all variables represent positive quantities,

$$\epsilon = \sum_{i=1}^m ( f_i - F_i + a_i - A_i ) \quad (6.6)$$

$\epsilon$  represents the error between a set of  $m$  frequency and amplitude measurements,  $f_i$  and  $a_i$ , and a set of  $m$  frequency and amplitude model responses,  $F_i$  and  $A_i$ . Equation 6.6 can

$W_i$  depended on the distance separating the accelerometers and/or the gain setting of each measurement. Table 6-5 lists the weight factor used for each type of measurement.

The final form of the error function is given below:

$$\epsilon = \sum_{i=1}^M (W_i(E_i - F_i))^2 \quad (6.11)$$

### 6.3.3 Optimization Routine

The optimization routine solved the following numerical problem: given an error function of  $N$  dependent parameters, determine the values of those parameters which minimize the error function.

The optimization routine EO4FCF from Numerical Algorithms Group [12] was used initially to determine the  $N$  model parameters which minimized the error function. A problem was encountered, however. The optimization routine estimated the derivatives of the error function by the method of finite differences. The magnitudes of the model parameter differences from the NAG routine were much smaller than could be represented by the four significant figures (minimum) in the SAPIV input file. Rather than circumvent this problem, however, a "homemade" optimization algorithm was constructed. Though less computationally efficient, the

The system identification algorithm therefore checked each model parameter before an optimization iteration. The parameter checking routine in the algorithm insured that a parameter did indeed affect the error function. If a parameter did not affect the error function, it was not included in the current iteration of optimization.

The algorithm used the following procedure to check whether a particular parameter had an effect on the error function. All model parameters were set to their initial or base values. The value of the parameter was then increased by a factor and the error function was computed. If the error function did not exceed a minimum value, (110% of the base error was the usual minimum), the parameter value was increased by a larger factor and the value of the error function was recomputed. This process was repeated until the error function exceeded the minimum error. If the error function did not exceed the minimum value after four iterations, the parameter was considered to have no upper bound.

The existence of a lower bound for the parameter was checked in a similar manner by dividing the parameter value by the same series of factors. Only parameters with a lower and an upper bound were included for optimization. The model response parameters (frequencies and mode shapes) from each

And the Hessian matrix is the matrix of second derivatives of the error function with respect to the model parameters

$$H_{ij} = \frac{\delta^2 \epsilon}{\delta x_i \delta x_j}, \quad \begin{matrix} i = 1, 2, \dots, N \\ j = 1, 2, \dots, N \end{matrix} \quad (6.15)$$

The search direction is defined as the line in "parameter space" connecting  $x$  and  $x_{\text{new}}$ .

The first and second derivatives of the error function were determined following a method developed by Douglas and Reid [7]. Each model response,  $F_i$ , was represented by a quadratic function of the  $N$  model parameters,  $x$ .

$$F_i = \sum_{j=1}^N (a_{ij} + b_{ij}x_j + c_{ij}x_j^2) \quad (6.16)$$

The values of the polynomial coefficients  $a_{ij}$ ,  $b_{ij}$  and  $c_{ij}$  were determined from a minimum of three pairs of  $F_i$ ,  $x_j$  values. These values were stored from the parameter check portion of the algorithm so they did not need to be recomputed. If there were more than three pairs of  $F_i$ ,  $x_j$  values from the parameter check, then the polynomial coefficients were determined in the least squares sense.

#### 6.3.4 Evaluation of Reliability

The optimization algorithm output information concerning the behavior of the error function as it progressed toward its minimum. The gradient vector and Hessian matrix were output after each computation of the search direction. Also, the values of the error function and the model parameters were output at each step along the line search. This information was used to assess the overall reliability of the solution from the optimization algorithm.

A reliable final solution was indicated by the following characteristics: a steady decrease in the gradient vector and a final Hessian matrix with large diagonal terms and small off-diagonal terms [11].

#### 6.4 RESULTS OF PARAMETER IDENTIFICATION

The values of eight model parameters were identified from the parameter identification procedure. These eight parameters were determined to have the largest effect on the error function. The criteria used to judge a parameter's effect on the error function were the normalized curvature of the error function with respect to the particular model parameter. Because the normalized curvatures at the

This large list of possible parameters was trimmed in four steps as follows.

The first cut of model parameters was made using engineering judgement. For example, deck bending stiffness is controlled by the product  $EI$  (modulus of elasticity and moment of inertia). Since it was not possible to separate the values of these two parameters, the value of  $E$  was frozen, (after the simple initial adjustment mentioned earlier), and the value of  $I$  alone was optimized.

The second cut of the list of possible model parameters was made during the preliminary system identification process. Parameters which repeatedly had no effect on the model response, (e.g. shear area of the columns), were cut from the list.

The third step in reducing the list of possible parameters was to "slave" parameters in the system identification program. A group of parameters was "slaved" to a "master" parameter so that whenever the master parameter value was changed in the model, the slaved parameters' values were changed also. The ratio of a slaved parameter to the master parameter was constant throughout a particular system identification run.

first column of Table 6-7. The parameters are listed in order of decreasing effect on the error function. The measure of effect on the error function was the normalized curvature, listed in the fifth column of the table. The normalized curvature for the model parameter  $x_i$  was computed by multiplying the diagonal term in the Hessian matrix,  $H_{ii}$ , by  $x_i^2$ .

#### 6.4.2 *Optimized Parameter Values*

The final optimized parameter values from the system identification program are listed in the fourth column of Table 6-7. The second and third columns of this table list the values of the parameters from the initial calculations and the preliminary parameter identification, respectively, for comparison. More confidence should be placed in the optimized parameter values near the top of the table. Each of the eight parameter values are discussed below.

The shear stiffness of the column top bearing pads had the most effect on the error function. The optimized value for the shear area of the pad is nearly twice the initial calculated value. Examination of the connection between the box girder and the column top (Figure 2-3) reveals that additional resistance to the movement of the box girder on

optimized transverse foundation stiffness is greater than the calculated stiffness by a factor of five, however. The lack of soil property information in the upper regions of the piles seriously hampered the lateral foundation stiffness calculations since it is the soil near the top of the piles which most affects its lateral resistance. Also, the methods of Norris used to calculate the lateral foundation stiffnesses are appropriate for long, slender piles. Methods for calculating the lateral stiffness of pier foundations may have been more appropriate. Such methods, (including one by Norris), include the additional resistance to lateral response due to side shear, end bearing and end moment.

The least dominant model parameter which was optimized was the torsional stiffness of the box girder. The optimized torsional stiffness was 28% greater than the calculated value, but very little confidence should be placed in the optimized value because of the very small effect of this parameter on the error function.

The final optimized mode one response of the model is presented in Figures 6-3a, 6-3b and 6-3c. The measured deck, column top and foundation responses are represented by the solid line, the circle and the square, respectively. The model deck, column top and foundation responses are

The predicted dynamic radial responses also agreed quite well with the corresponding experimental responses. Figures 6-5 and 6-6 show this comparison for experimental modes four and six, respectively. The solid line in the figures represent the predicted response and the solid triangles represent the measured response. The predicted vs. measured frequencies were 2.8 vs. 2.9 Hz for experimental mode four, and 3.8 vs. 4.2 Hz for experimental mode six.

10. Douglas, B.D., et al., "Behavior of the Meloland Road Overcrossing during the 1979-Imperial Valley Earthquake", Seismic Research for Highway Bridges, (U.S.-Japan Program), 1984, University of Pittsburgh, PA, pp 339-365.
11. Buckle, I.G., Richardson, J.A. and Sveinsson, B.J., "System Identification Studies of a Curved Box Girder Bridge under Dynamic Lateral Loads," Computech Engineering Services Report No. 5512.1, Berkeley, 1988.
12. Numerical Algorithms Group, Inc., Downers Grove, Illinois.
13. Gill, P.E., Murray, W. and Wright, M.H., Practical Optimization, Academic Press, New York, 1981.

Location	X-axis transl. (k/ft)	Y-axis transl. (k/ft)	Z-axis transl. (k/ft)	X-axis rotation (k-ft)	Y-axis rotation (k-ft)	Z-axis rotation (k-ft)
Abut. A	263	263	fixed	5,500,000	free	60
Fnd. B	5,300	5,000	fixed	2,900,000	170,000	free
Fnd. C	8,500	14,000	fixed	4,300,000	177,000	free
Fnd. D	2,500	14,000	fixed	2,700,000	129,000	free
Fnd. E	5,300	5,000	fixed	2,900,000	170,000	free
Fnd. F	14,500	14,500	fixed	6,600,000	6,600,000	free
Fnd. G	14,500	14,500	fixed	6,600,000	6,600,000	free
Fnd. H	11,000	11,000	fixed	5,000,000	5,000,000	free
Fnd. I	11,000	11,000	fixed	5,000,000	5,000,000	free
Fnd. J	5,300	5,000	fixed	2,900,000	170,000	free
Abut. K	263	263	fixed	5,500,000	free	60

Table 6-2 Summary of bridge model boundary element spring rates.

Location	X-axis transl. (k/ft)	Y-axis transl. (k/ft)	Z-axis transl. (k/ft)	X-axis rotation (k-ft)	Y-axis rotation (k-ft)	Z-axis rotation (k-ft)
Abut. A	(263) 10,000	(263) 10,000	fixed	(776,600) 4,000,000	free	(2,550) 2,550
Fnd. B	(5,300) 7,500	(5,000) 20,000	fixed	(2,900,000) 4,000,000	(170,000) 100,000	free
Fnd. C	(8,500) 12,000	(14,000) 32,000	fixed	(4,300,000) 8,000,000	(177,000) 200,000	free
Fnd. D	(2,500) 2,000	(14,000) 16,000	fixed	(2,700,000) 5,000,000	(129,000) 100,000	free
Fnd. E	(5,300) 11,200	(5,000) 30,000	fixed	(2,900,000) 10,000,000	(170,000) 200,000	free
Fnd. F	(14,500) 40,000	(14,500) 40,000	fixed	(6,600,000) 12,000,000	(6,600,000) 12,000,000	free
Fnd. G	(14,500) 120,000	(14,500) 120,000	fixed	(6,600,000) 48,000,000	(6,600,000) 48,000,000	free
Fnd. H	(11,000) 120,000	(11,000) 120,000	fixed	(5,000,000) 48,000,000	(5,000,000) 48,000,000	free
Fnd. I	(11,000) 120,000	(11,000) 120,000	fixed	(5,000,000) 12,000,000	(5,000,000) 12,000,000	free
Fnd. J	(5,300) 3,000	(5,000) 16,000	fixed	(2,900,000) 3,000,000	(170,000) 500,000	free
Abut. K	(263) 4,500	(263) 1,500	fixed	(776,600) 600,000	free	(2,550) 2,550

Table 6-4 Summary of boundary element spring rates from preliminary parameter identification. (Original values are in parentheses.)

Parameter	Parameter Value			Norm. Curv.
	Calculated	Preliminary Identification	System Identification	
Shear Area of Bearing Pads atgp all Columns (ft <sup>2</sup> )	0.022	0.040	0.041	2185.
Moment of Inertia about Vertical Axis of Box Girder (ft <sup>4</sup> )	2146.0	2146.0	2775.0	244.
Moment of Inertia of All Columns (ft <sup>4</sup> )	30.68	30.68	39.10	242.
Longitudinal Stiffness of Bearing Pads at Abutment A (k/ft)	263.0	10,000.0	8,300.0	3.7
Longitudinal Stiffness of Bearing Pads at Abutment K (k/ft)	263.0	4,500.0	7,300.0	0.94
Rotational Stiffness about Long. Axis of Foundation B (k-ft)	2,900,000.	4,000,000.	3,940,000.	0.27
Transverse Stiffness in Radial Direction of Foundation B (k/ft)	5,000.0	20,000.0	24,000.0	0.18
Torsional Constant of Box Girder (ft <sup>4</sup> )	204.5	204.5	262.0	0.07

Table 6-7 Summary of the results for the eight bridge model parameters optimized in the system identification procedure.

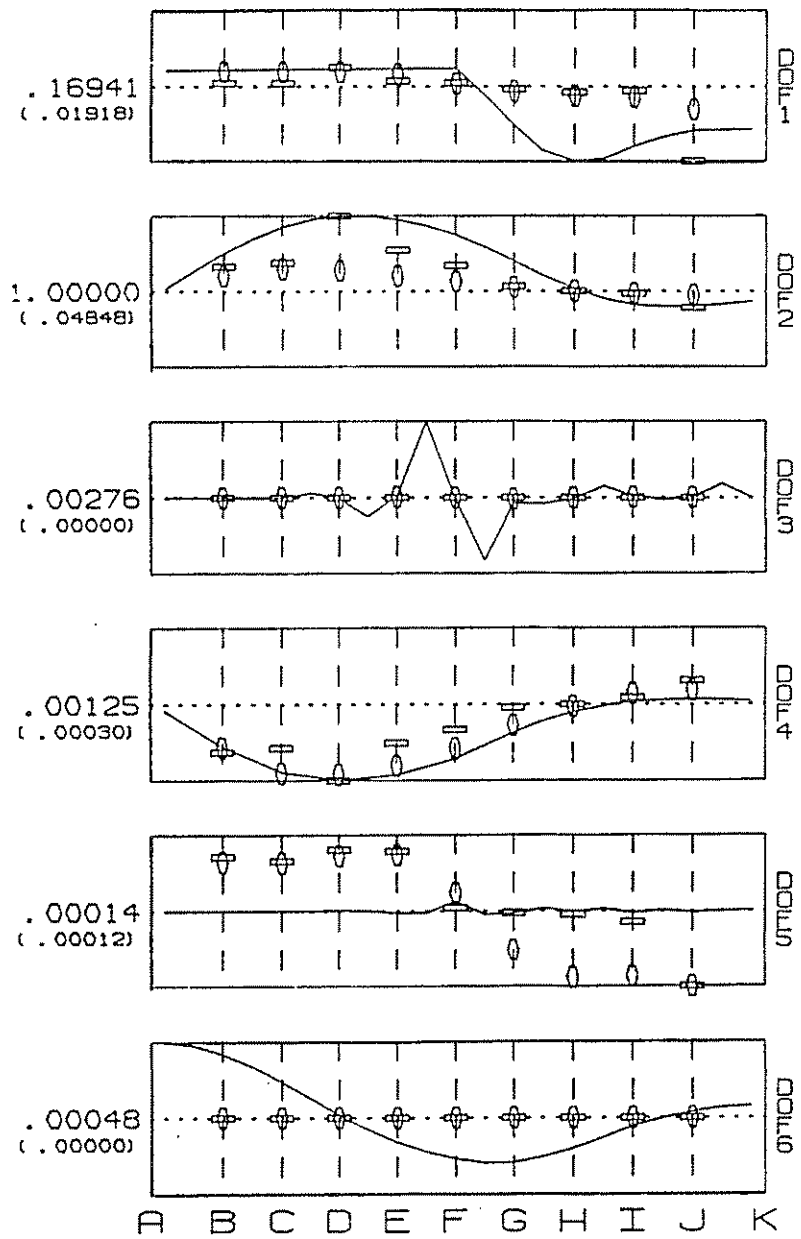


Figure 6-2 Mode one of bridge model after the preliminary parameter identification.

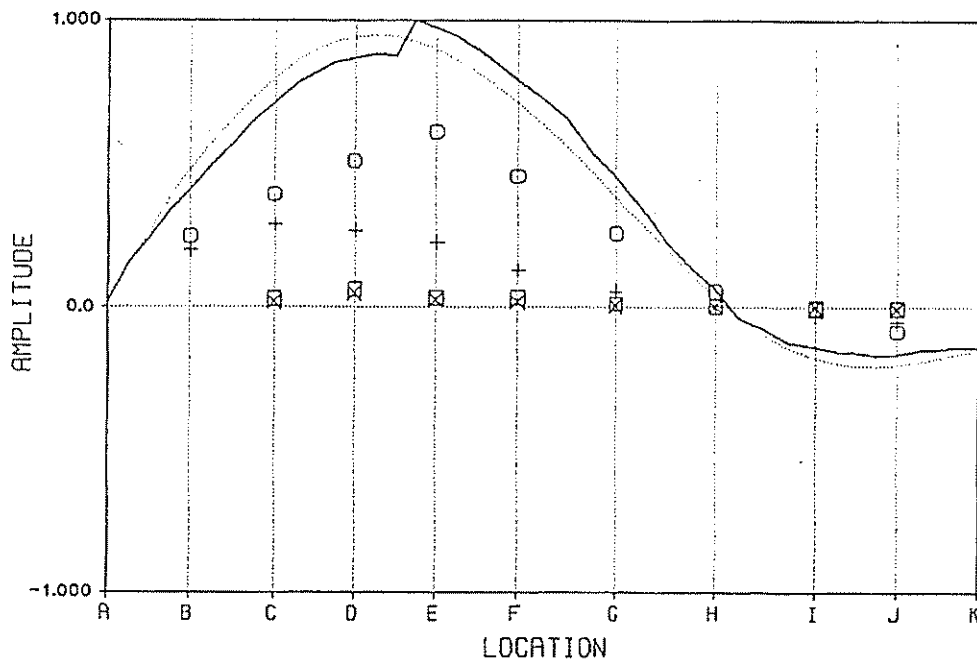


Figure 6-3b Radial (DOF 2) mode one response of optimized bridge model after system identification.

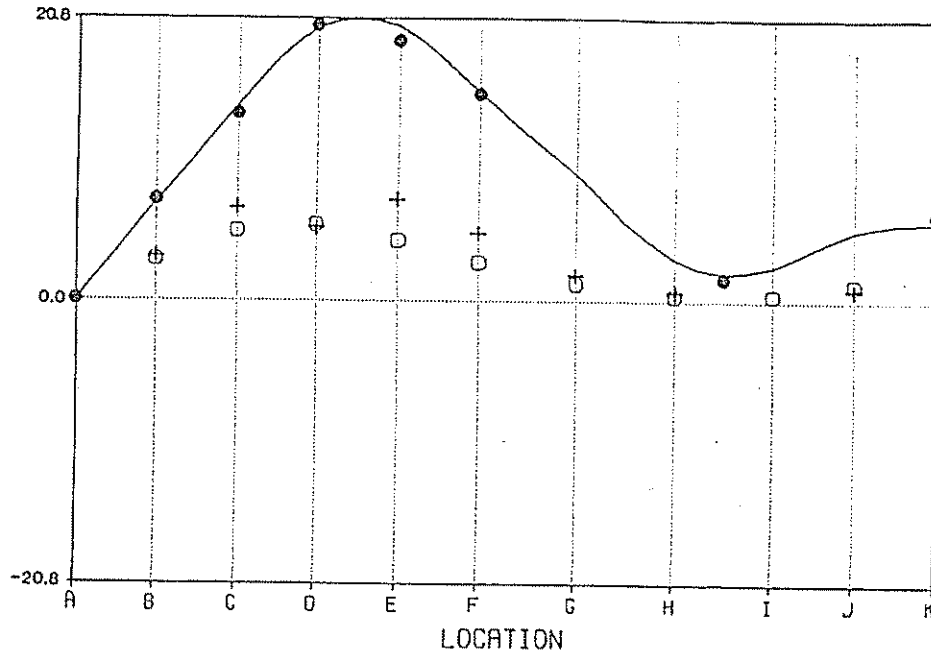


Figure 6-4a Predicted vs. measured static deck and column top deflections (in mm) in radial direction for Load Pattern One.

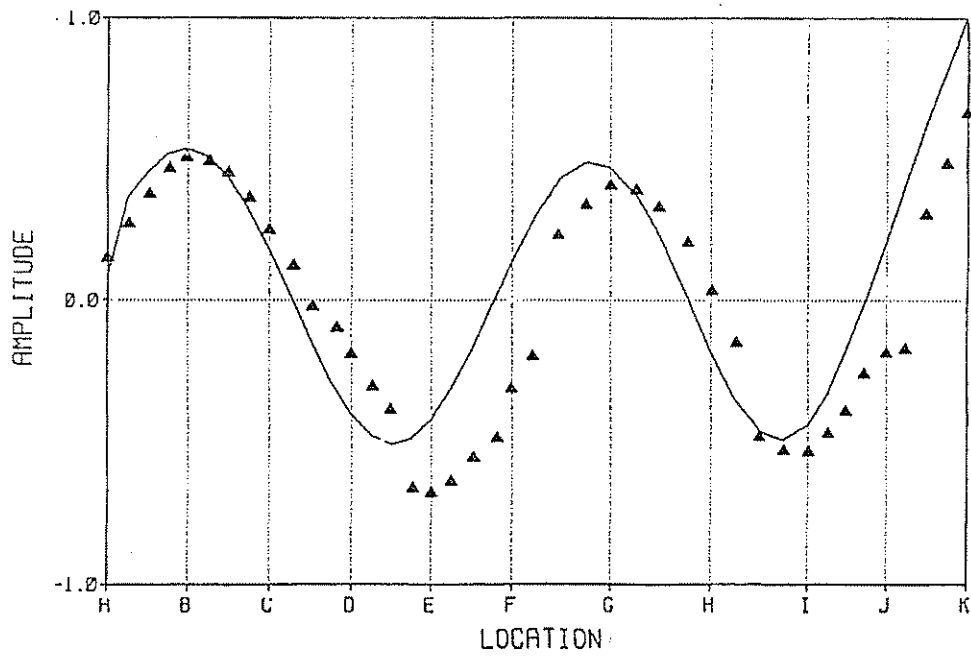


Figure 6-5 Predicted (solid line) vs. measured (triangles) radial direction mode shape component for mode four.

## 7. SUMMARY AND CONCLUSIONS

This study analyzed the three-dimensional dynamic response of an existing highway overpass to large-amplitude lateral loads. The work is based on the data collected from the full-scale test of the Dominion Road bridge, in Auckland, New Zealand.

The snap-back and quick-release method, used previously by Douglas [1,2], was used to excite the free vibration response of the bridge. Important features of the bridge test include the large amplitude of the bridge response, the complexity of the bridge and the extensiveness of the response measurements. The measured bridge response was the same order magnitude as the response expected due to a moderate magnitude earthquake. Accelerations exceeding 25% of gravity were recorded on the superstructure in the lateral direction.

Unique methods were used to extract the natural frequencies and three-dimensional mode shapes of the bridge from the free vibration measurements. An improved system identification procedure was used to fit a computer model of the bridge to the experimental mode one response.

computer model to the experimental mode one frequency and mode shape. The eight model parameters which had the largest effect on the error between the model-predicted and the experimental frequencies and mode shapes were optimized. The final computer model accurately predicted both the measured static responses and the next two lateral response modes.

Results from the system identification work include:

- 1) The modulus of the bridge superstructure from system identification was approximately 1.4 times higher than the modulus calculated from the familiar ACI formula,

$$E = 57,000 [ f_c ]^{1/2}$$

- 2) The lateral movement of the box girder across the column tops was resisted by more than the bearing pads alone; the flexcell packing material surrounding the shear key is the likely source of this additional resistance.
- 3) The rotational stiffness of the foundations was fairly accurately predicted, considering the quality of the available soil data.

The model response computed with the parameter values determined from the system identification procedure fit the measured mode one response quite well. The model also accurately predicted four responses not included in the system identification procedure. The model-predicted static deflections due to load patterns one and two agreed very well with the deflections measured immediately before release of the bridge. Also, the model-predicted

## CHAPTER REFERENCES

1. Douglas, B.M. and Reid, W.H., "Dynamic Tests and System Identification of Bridges," Journal of the Structural Division, ASCE, Vol. 108, ST10, Oct. 1982, pp.2295-2312.
2. Douglas, B.M. and Richardson, J.A., "Maximum Amplitude Dynamic Response of a Highway Bridge," Proceedings of the Eighth World Conference on Earthquake Engineering, Vol. II, San Francisco, 1984, pp. 889-896.
3. Norris, G.M., "Foundation Stiffness Evaluation for Seismic Analysis of Highway Bridges", Proceedings, 23rd Symposium on Engineering Geology and Soils Engineering, Logan, Utah, April 1987, pp. 375-394.

tabulated in the sixth column of the tables. No deflection values are entered in Table A-1a for the deck measurement station at Pier D for Load Pattern One because the tare for this series of measurements was not recorded. Also no values appear in Table A-1a and A-1b for the deck measurement station at Pier F except for the 100 kip load increment because the dial gage was installed after the dynamic series of bridge releases had begun.

All measurements represented in the tables were made with dial gages except for the measurements at Abutments A and K and midspan H-I. These measurements were made with the electrical displacement gages described in Chapter 2.

The deflection values in the tables indicate the bridge was mildly nonlinear over the range of loading. A comparison of the deflection values in the two tables indicate the bridge deflected more after the dynamic series than before at all deck locations. The foundation deflections do not reflect a consistent trend. The large increase in the deflection of Foundation D from pre to post dynamic series is notable, especially the large increase in the unload value for Load Pattern One.

The bridge deflections due to the 100 kip load applied in Load Patterns One and Two are plotted in Figures A-1 and A-

displacement was computed as the difference between the deflection prior to release and the deflection value at the end of the time history after all motion has stopped. The relative release displacements (in mm) are tabulated for locations A through K in Tables A-3a, through A-3f. While the relative displacements are fairly constant from release to release at the majority of measurement locations, the relative displacements at Abutment A decrease in amplitude dramatically with each consecutive release and appear to be converging to a value of approximately -0.10 mm.

Location	Load Level				
	25 kip	50 kip	75 kip	100 kip	unload
Deck @ A	0.02	0.06	0.10	0.15	0.03
Deck @ B	1.55	3.45	5.25	6.94	0.27
Deck @ C	2.86	6.46	9.79	12.94	0.15
Deck @ D	4.06	9.12	13.77	18.30	0.09
Deck @ E	4.23	9.73	14.53	19.15	-0.05
Deck @ F	- -	- -	- -	17.10	-0.15
Deck @ H-I	-1.00	-1.54	-2.09	-2.62	0.84
Deck @ K	-0.02	1.60	2.88	3.72	- -
Foundation @ C	0.00	0.06	0.14	0.22	-0.07
Foundation @ D	0.11	0.50	0.83	1.20	-0.06
Foundation @ E	0.08	0.28	0.46	0.82	-0.07
Foundation @ F	0.10	0.34	0.62	0.89	-0.02

Table A-1b Summary of release displacements (in mm) taken before the dynamic series of measurements, Load Pattern Two.

Location	Load Level				
	25 kip	50 kip	75 kip	100 kip	unload
Deck @ A	0.01	0.03	0.05	0.07	-0.02
Deck @ B	1.61	3.78	5.75	7.51	-0.20
Deck @ C	3.13	7.26	10.95	14.38	-0.20
Deck @ D	4.28	9.76	15.25	19.87	0.42
Deck @ E	4.41	10.11	15.93	20.60	-0.74
Deck @ F	3.59	8.10	12.83	16.49	-0.44
Deck @ H-I	-0.69	-2.05	-3.02	-3.80	-0.88
Deck @ K	-0.06	0.02	3.59	5.73	5.53
Foundation @ C	0.04	0.11	0.17	0.21	-0.07
Foundation @ D	0.18	0.52	0.84	1.18	-0.16
Foundation @ E	0.16	0.33	0.52	0.82	-0.09
Foundation @ F	0.13	0.29	0.49	0.69	-0.09

Table A-2b Summary of release displacements (in mm) taken after the dynamic series of measurements, Load Pattern Two.

Release	Pier C		Pier D	
	Load Pattern		Load Pattern	
	One	Two	One	Two
1	7.27		10.7	
2		7.29		11.0
3		7.29		10.9
4	7.44		10.9	
5	7.43		10.9	
6		7.35		11.1
7		7.36		11.0
8	7.63		11.2	
9	7.35		10.8	
10		7.38		11.1
11		7.37		11.1

Table A-3b Relative release displacements (in mm) at Piers C and D.

Release	Pier G		Pier H	
	Load Pattern		Load Pattern	
	One	Two	One	Two
1	6.75		2.65	
2	6.58		2.61	
3		8.23		1.24
4		7.80		1.03
5	6.72		2.25	
6	6.45		2.32	
7		8.01		0.67
8		7.55		0.44

Table A-3d Relative release displacements (in mm) at Piers G and H.

Pier K		
Release	Load Pattern	
	1	2
1	5.36	
2	7.50	
3		-6.59
4		-6.87
5	4.00	
6	8.63	
7		-5.37
8		-5.94

Table A-3f Relative release displacements (in mm) at Abutment K.

APPENDIX B. EXPERIMENTAL MODE SHAPES

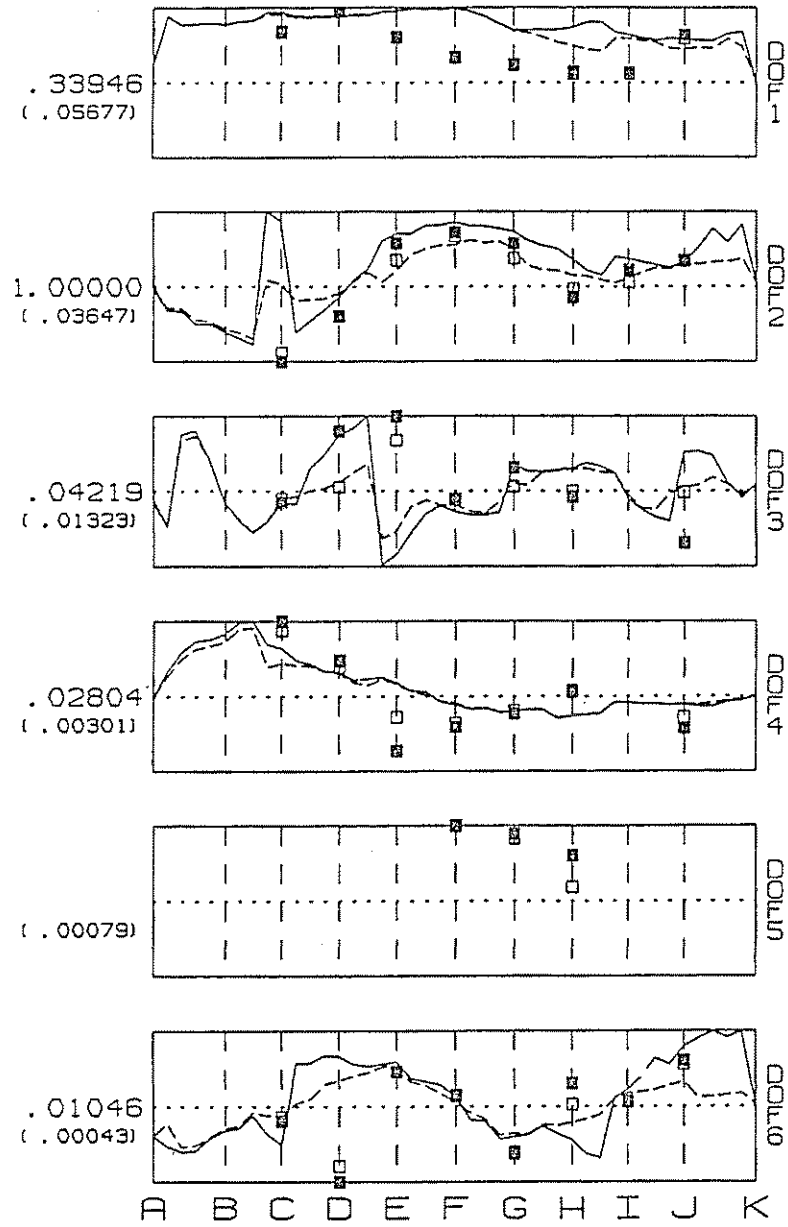


Figure B-2 Experimental mode three, 2.20 Hz.

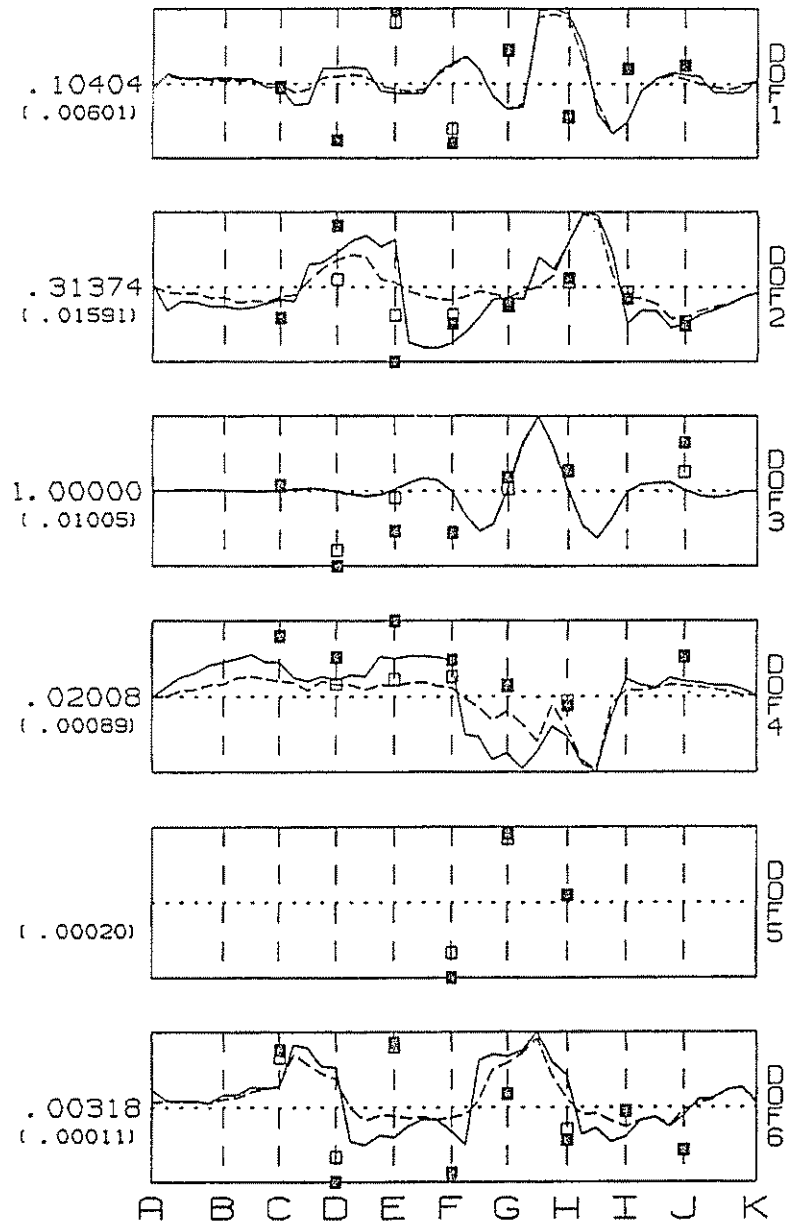


Figure B-4 Experimental mode five, 3.65 Hz.

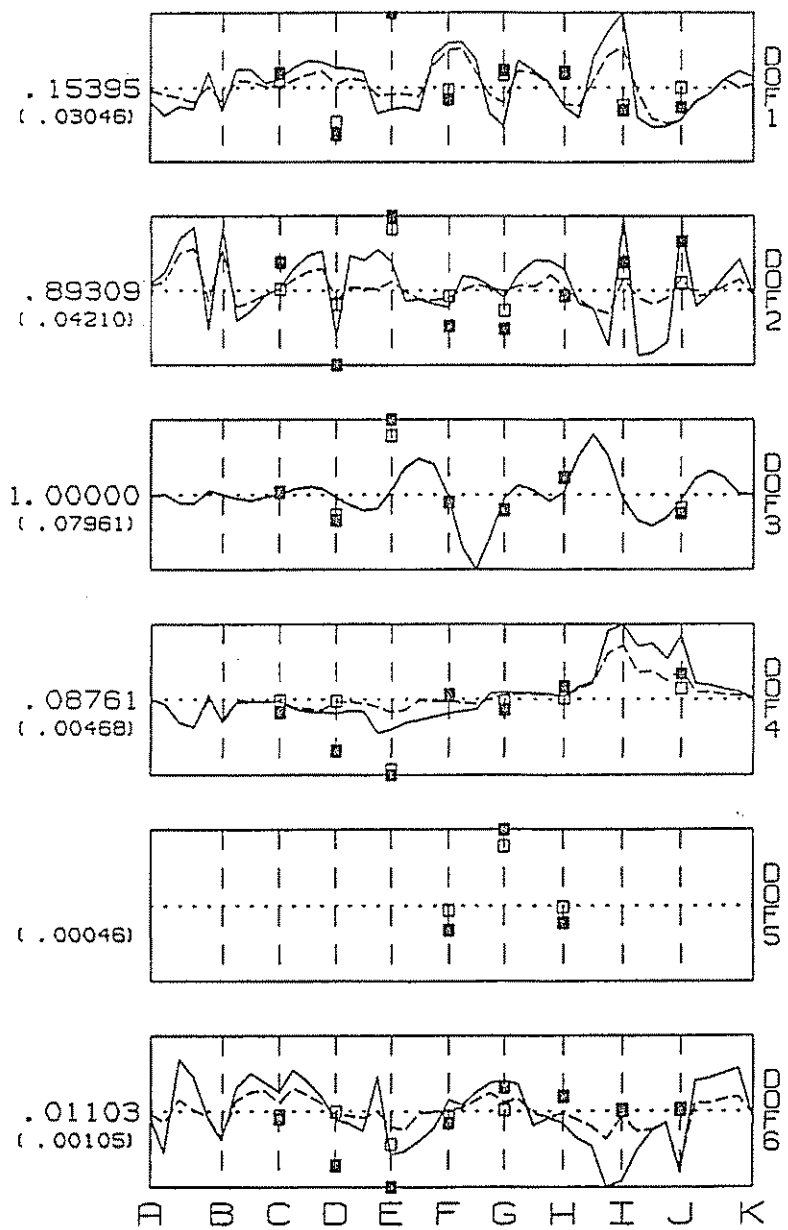


Figure B-6 Experimental mode seven, 4.50 Hz.

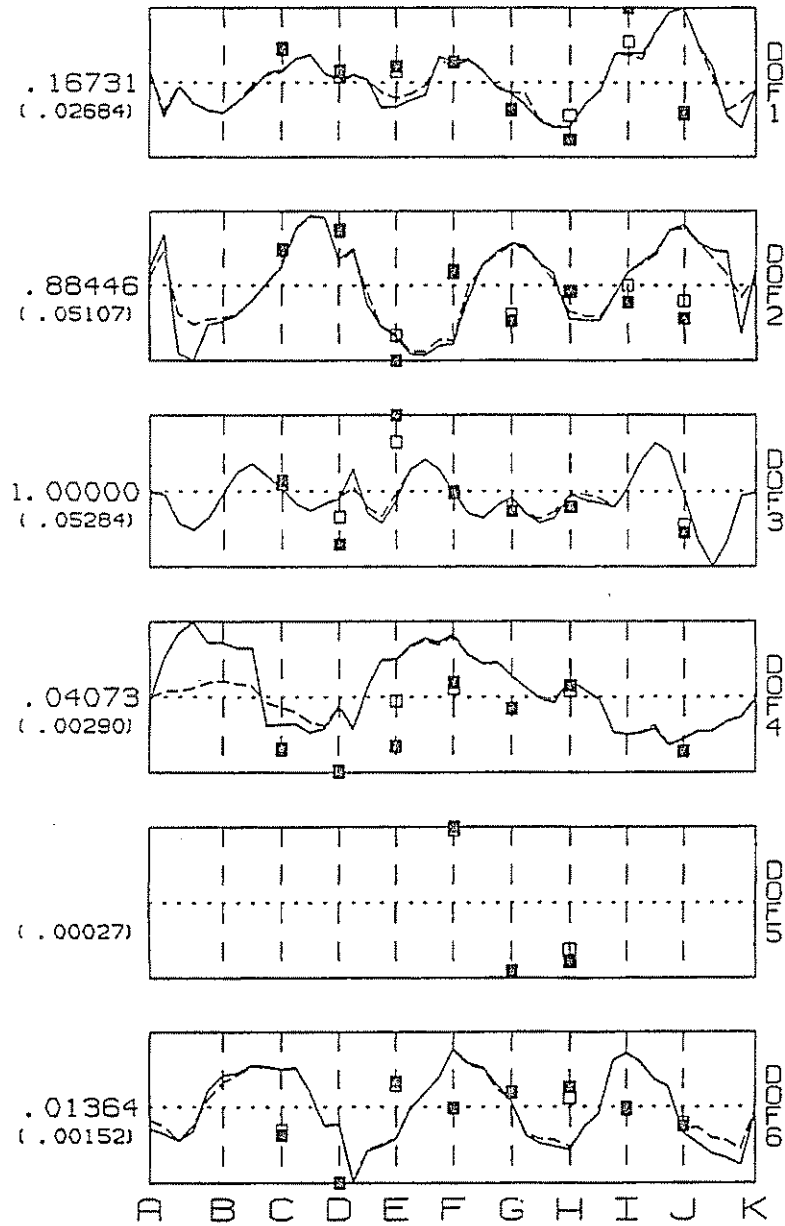


Figure B-8 Experimental mode nine, 5.30 Hz.

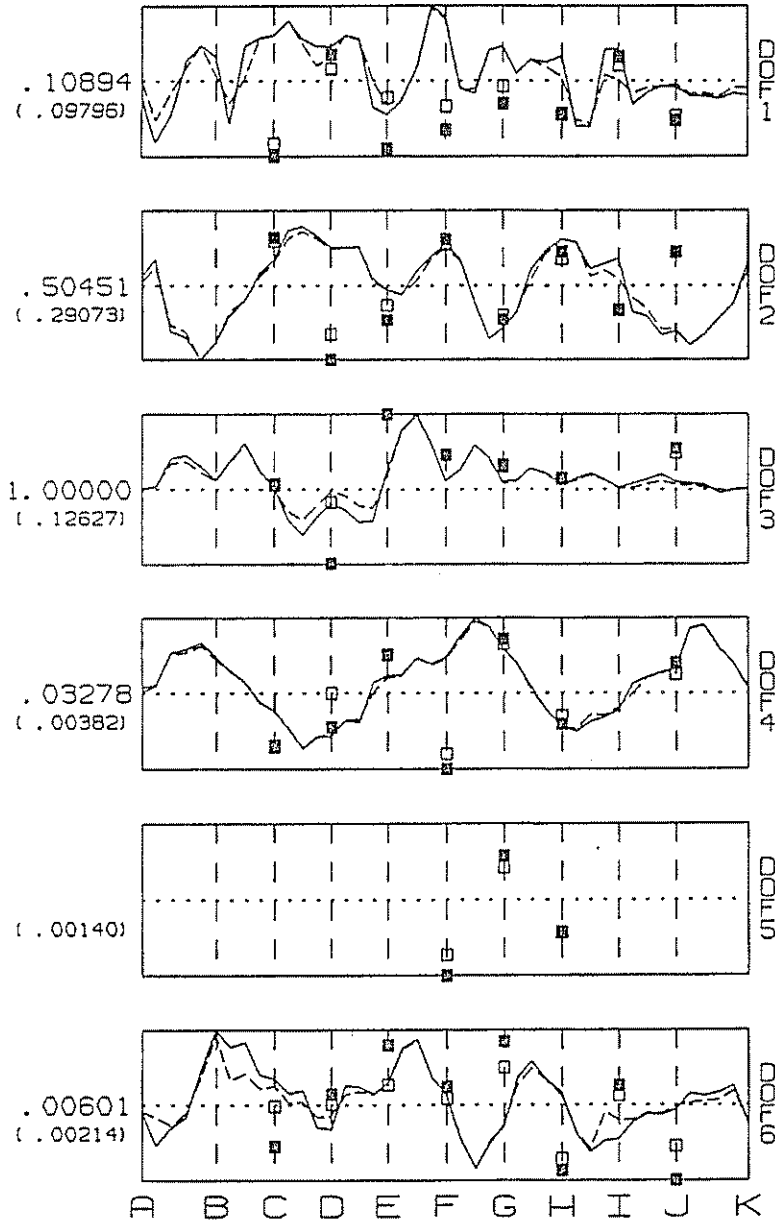


Figure B-10 Experimental mode 11, 6.50 Hz.

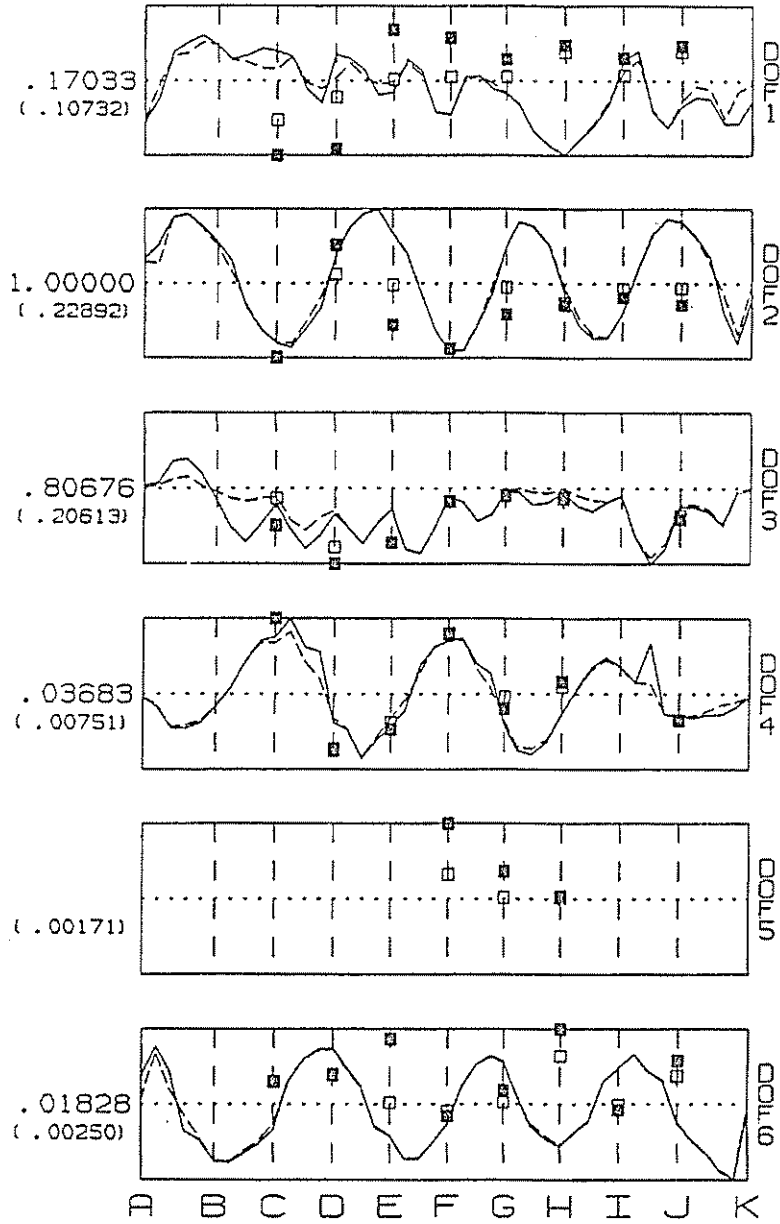


Figure B-12 Experimental mode 13, 7.30 Hz.

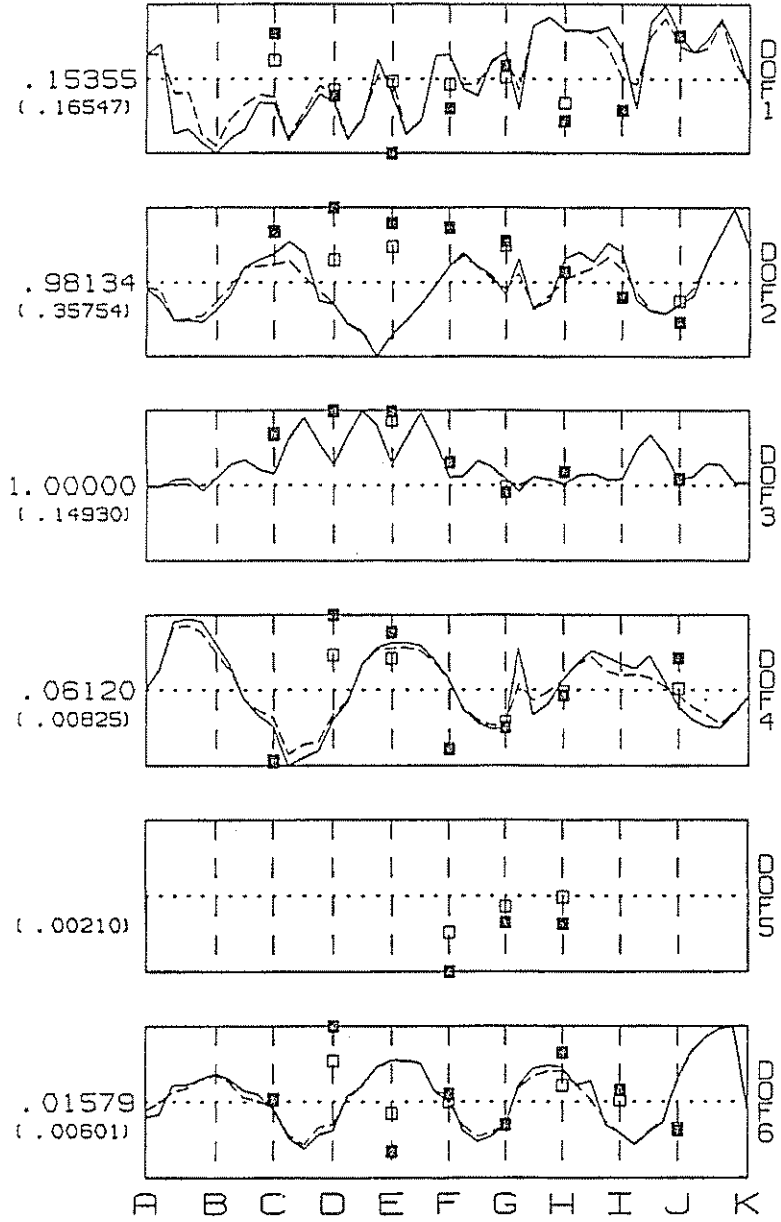


Figure B-14 Experimental mode 15, 7.70 Hz.

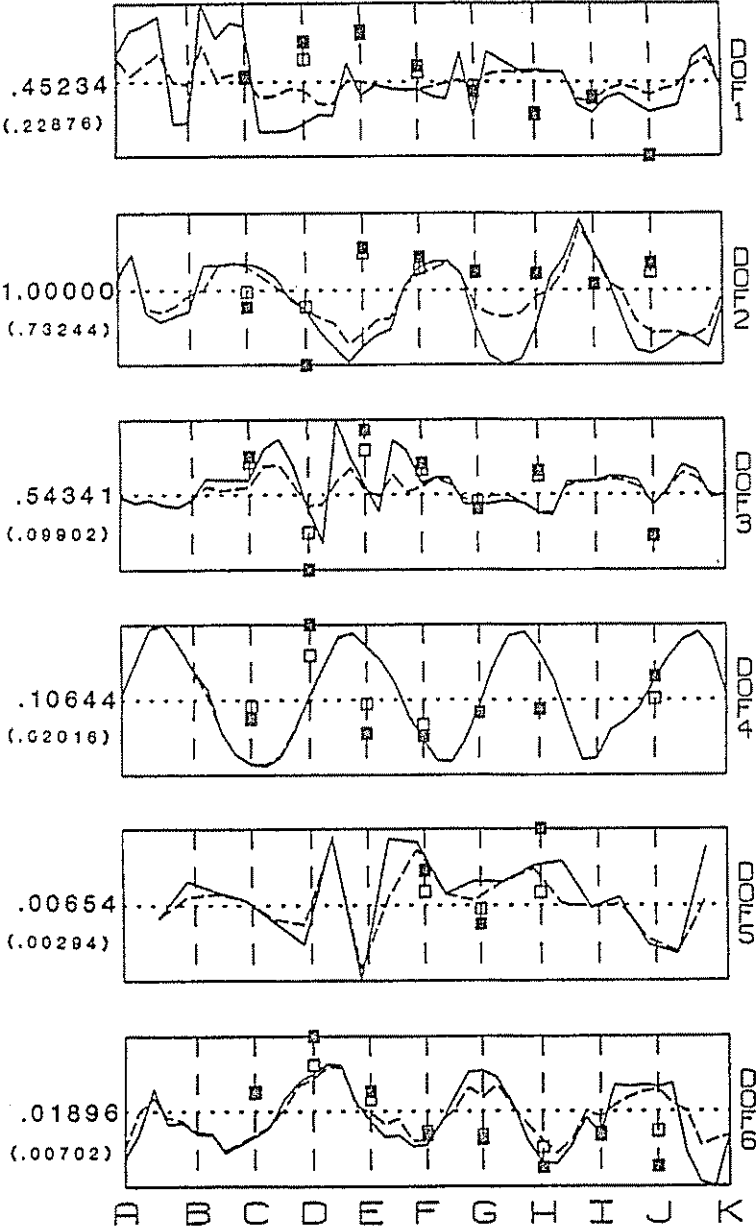


Figure B-16 Experimental mode 17, 8.55 Hz.

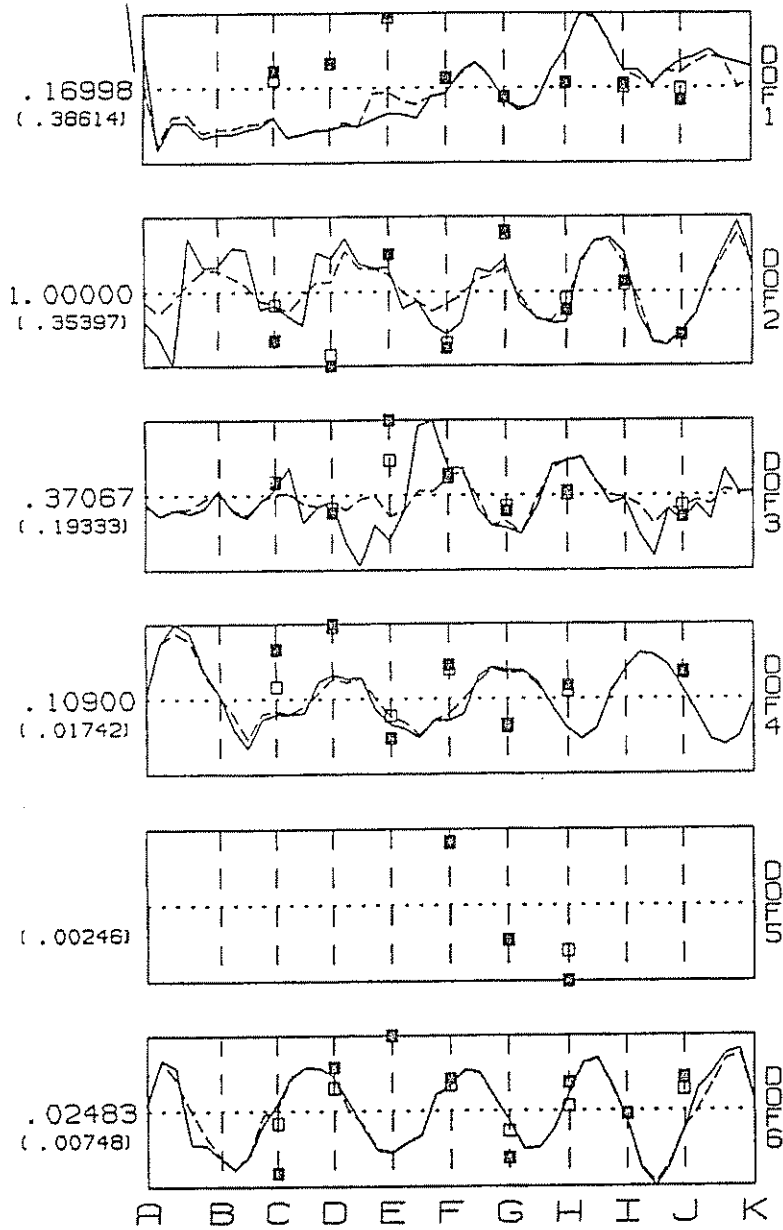


Figure B-18 Experimental mode 19, 9.60 Hz.

```

PROGRAM SEPNEWZ( SEPCI,SEPL0G,PFILE,INPUT,OUTPUT,ACC13,ACC15,
* ACC16,ACC20,ACC21,TAPE1=SEPCI,TAPE2=SEPL0G,TAPE3=PFILE,
* TAPE5=INPUT,TAPE6=OUTPUT,TAPE13=ACC13,TAPE15=ACC15,
* TAPE16=ACC16,TAPE20=ACC20,TAPE21=ACC21 )
*
INTEGER DYDOFUN(2,6),DYREC(22),DYUN(5),IW(10)
REAL F(5),ZT(5),X(10),FVEC(400),FJAC(400,10),S(10),V(10,10),
* WS(4905),KR(200,10),KI(200,10)
* LWS = 6*NSP + NFP*NSP + 2*NFP + NSP*(NSP-1)/2
CHARACTER TITLE*50,SMFLG*10,LMFLG*10,METHFLG*10
COMMON /CO6/ CO6WORK(8192)
COMMON /READ/ E(8192),F,ZT,NM
COMMON /FUNCT/ ER(200),EI(200),C(10),IW1,DW,HPREC,DT,NPT
COMMON /FLGS/ SMFLG,LMFLG,METHFLG
COMMON /KRKI/ KR,KI
EXTERNAL LSQFUH,LSQMON
*
*
***** INITIALIZE *****
*
DATA DYDOFUN / 13,21,
* 15,15,
* 16,20,
* 16,20,
* 0, 0,
* 13,21 /
DATA DYUN / 13,15,16,20,21 /
DATA LJ,LV,LIW,LWS / 400,10,10,4905 /
NPT = 8192
PI = 4. * ATAN(1.0)
*
*
***** READ IN AND WRITE OUT CONTROL INFO. *****
*
READ(1,12) TITLE
12 FORMAT(A50)
READ(1,*) IDOF
READ(1,*) NREC,(DYREC(I),I=1,NREC)
READ(1,*) NM
READ(1,*) (F(I),I=1,NM)
READ(1,*) (ZT(I),I=1,NM)
READ(1,*) F1,F2
READ(1,13)LMFLG,SMFLG,METHFLG
13 FORMAT(A10)
*
WRITE(2,1)TITLE, IDOF
1 FORMAT(/1X,72(1H*)//1X,A50//1X,72(1H*)// ' DOF ',I1)
WRITE(2,2)NM,NPT
2 FORMAT(/' NO. MODES = ',I1,/' NO. POINTS IN TRANSFORM = ',
* I5)

```

```

                END IF
*
                J1 = 0
                NPTP2 = NPT + 2
                DO 22 J = IW1,IW2
                    J1 = J1 + 1
                    ER(J1) = E(J)
                    EI(J1) = E(NPTP2-J)
22             CONTINUE
*
*
***** PROVIDE STARTING ESTIMATES OF W,ZT *****
*
                DO 30 I = 1,NM
                    X(I*2-1) = F(I) * 2.*PI
                    X(I*2) = ZT(I)
30             CONTINUE
*
* CALL VTRAN( X,NSP,'IN' )
*
***** CALL NAG OPTIMIZATION ROUTINE *****
*
                IFAIL = 1
                IPRINT = 5
                MAXCAL = 50 * NSP
                ETA = 0.1
                XTOL = .001
                STEPMX = 1.
*
32             CALL E04FCF( NFP,NSP,LSQFUN,LSQMON,IPRINT,MAXCAL,ETA,
*             XTOL,STPEMX,X,FSUMSQ,FVEC,FJAC,LJ,S,V,LV,NITER,NF,IW,LIW,
*             WS,LWS,IFAIL )
*
                IF( IFAIL .EQ. -5 ) THEN
                    NSP = NSP - 2
                    NM = NM - 1
                    IFAIL = 1
                    GO TO 32
                END IF
*
                WRITE(2,34)IFAIL
34             FORMAT(/// ***** IFAIL = ',I1,' FROM E04FCF *****// )
*
                WRITE(2,36)
36             FORMAT(///1X,46(1H*),2(// '**,44X,***'),// * MODE FRQ ZT'
*             , 6X,'AMP',6X,'PHASE **// '**,44X,***')
*
* CALL VTRAN( X,NSP,'OUT' )
*
                DO 40 I = 1,NM
                    II = I + NM
                    I2 = I*2

```

```

*
***** COMBINE RECORDS *****
*
      DO 14 IU = 1,2
          ISUM = 0
          DO 12 J = 1,NS
              ISUM = ISUM + ACC(J,IU)
          12 CONTINUE
          AVE(IU) = FLOAT(ISUM) / FLOAT(NS)
      14 CONTINUE
*
      SF(1) = SF(1) * FACL(IDOF)
      SF(2) = SF(2) * FACR(IDOF)
      DO 16 J = 1,NS
          E(J) = ( FLOAT(ACC(J,1)) - AVE(1) ) * SF(1)
          *      + ( FLOAT(ACC(J,2)) - AVE(2) ) * SF(2)
      16 CONTINUE
*
      TITLE2 = ACCTIT(1)(13:36)//', '//ACCTIT(2)(13:36)
*
***** LOCATE JFIRST *****
*
      AMAX = 0.
      DO 20 J = 1,NS
          IF( ABS( E(J) ) .GT. AMAX ) THEN
              AMAX = ABS( E(J) )
              JMAX = J
          END IF
      20 CONTINUE
      AMAX = AMAX * .10
*
      DO 22 J = 1,JMAX
          IF( ABS( E(J) ) .GT. AMAX ) THEN
              JSTRT = J
              GO TO 24
          END IF
      22 CONTINUE
*
      24 JSIGN = E(JSTRT) / ABS( E(JSTRT) )
      DO 26 J = JSTRT,1,-1
          IF( E(J) * JSIGN .LT. 0. ) THEN
              JFRST = J
              GO TO 28
          END IF
      26 CONTINUE
*
      28 READ(1,*) JCI1,JCI2
          JFRST = JFRST + JCI1
          IF( JCI2 .EQ. 0 ) THEN
              JLST = NS
          ELSE
              JLST = JFRST + JCI2 - 1

```

```

*
*****
*
SUBROUTINE LSQFUN( IFLAG,NFP,NSP,XC,FVECC,IWS,LIW,WNAG,LWNAG )
*
INTEGER IWS(LIW)
REAL XC(NSP),FVECC(NFP),WNAG(LWNAG)
REAL KR(200,10),KI(200,10),VEC(10),MAT(10,10),WKS1(10),WKS2(10),
* AA(10,10),X(10)
CHARACTER SMFLG*10,LMFLG*10,METHFLG*10
COMMON /FLGS/ SMFLG,LMFLG,METHFLG
COMMON /FUNCT/ ER(200),EI(200),C(10),IW1,DW,NPREC,DT,NPT
COMMON /KRKI/ KR,KI
*
NM = NSP/2
NW = NFP/2
*
DO 1 I = 1,NSP
    X(I) = XC(I)
1 CONTINUE
* CALL VTRAN( X,NSP,'OUT' )
*
***** FORM BUILDING BLOCK VECTORS, KR AND KI *****
*
WHERE
*
* A = DENOM.
* K = FIRST DERIV. OF F W.R.T. COEFFICIENTS
* R,I = REAL, IMAG. COMPONENTS
* C = COEFFICIENTS
*
IF( METHFLG(1:2) .EQ. 'EX' ) THEN
    INCEX = 1
    NPTEX = NPT / INCEX
    DTEX = DT * INCEX
    CALL EXPTRAN( NPTEX,NM,X,NSP,NPREC,DTEX,NW,IW1 )
ELSE IF( METHFLG(1:2) .EQ. 'AN' ) THEN
    IF( LMFLG(1:2) .EQ. 'IN' ) THEN
        CALL ANTRANI( LMFLG,NPREC,DT,NM,X,NSP,NW,DW,IW1 )
    ELSE IF( LMFLG(1:2) .EQ. 'FI' ) THEN
        CALL ANTRANF( LMFLG,NPREC,DT,NM,X,NSP,NW,DW,IW1 )
    END IF
END IF
*
***** FORM MATRIX AND VECTOR TO SOLVE FOR COEFFICIENTS,C *****
*
DO 20 I = 1,NSP
    VEC(I) = RMULT( ER(1),KR(1,I),NW ) + RMULT( EI(1),KI(1,I),NW )
    DO 20 J = 1,NSP
        MAT(I,J) = RMULT( KR(1,J),KR(1,I),NW ) + RMULT( KI(1,J),
* KI(1,I),NW )
20 CONTINUE
DO 21 I = 2,NSP

```

```

      RETURN
      END
*
*
*****
*
      FUNCTION RMULTBW( A, IDIM, B, N )
*
      REAL A( IDIM, N ), B( N )
*
      RMULTBW = 0.
      DO 10 J = 1, N
          RMULTBW = RMULTBW + A( 1, J ) * B( J )
      10 CONTINUE
*
      RETURN
      END
*
*
*****
      SUBROUTINE LSQMON( NFP, NSP, XC, FVECC, FJACC, LJC, S, IGRADE, NITER,
* NF, IW, LIW, W, LW )
*
      INTEGER IW( LIW )
      REAL XC( NSP ), FVECC( NFP ), FJACC( LJC, NSP ), S( NSP ), W( LW ), G( 171 ), X( 10 ),
* C( 10 )
*
      PI = 4. * ATAN( 1.0 )
      FSUMSQ = F01DEF( FVECC, FVECC, NFP )
      CALL LSQGRD( NFP, NSP, FVECC, FJACC, LJC, G )
      GTG = F01DEF( G, G, NSP )
*
      WRITE( 2, 10 ) NITER, NF, FSUMSQ, GTG, IGRADE
      10 FORMAT( // ' 1TNS', 4X, ' F EVALS', 10X, ' SUMSQ', 13X, ' GTG', 8X,
* ' GRADE' // ' ', 14, 6X, 15, 6X, 1PE13.5, 6X, 1PE9.1, 6X, 13 )
      WRITE( 2, 12 )
      12 FORMAT( / 8X, ' X', 20X, ' G', 16X, ' COEFFICIENTS' )
*
***** CONVERT FROM W TO F *****
*
      DO 30 I = 1, NSP
          X( I ) = XC( I )
      30 CONTINUE
*
      CALL VTRAN( X, NSP, 'OUT' )
*
      CALL LSQFUNH( NFP, NSP, X, C )
*
      DO 18 I = 1, NSP, 2
          X( I ) = X( I ) / ( 2. * PI )
      18 CONTINUE
*

```

```

      C1 = 2./62.83
      C2 = 2./10
      DO 10 I = 1,NSP,2
        X(I) = X(I) * C1 - 1.
        X(I+1) = X(I+1) * C2 - 1.
10    CONTINUE
      ELSE IF( FLG(1:3) .EQ. 'OUT' ) THEN
        C1 = 62.83/2.
        C2 = .10/2.
        DO 20 I = 1,NSP,2
          X(I) = X(I) * C1 + C1
          X(I+1) = X(I+1) * C2 + C2
20    CONTINUE
      ELSE
        WRITE(2,*)' ERROR IN VTRAN, FLG = ',FLG
        STOP
      END IF

      RETURN
      END

*
*
*****
*
      SUBROUTINE CONV(L F,N )
      COMPLEX F(N),TM(200),A0,A1

*
      A0 = CMPLX( 25./46.,0. )
      A1 = CMPLX( -(1. - 25./46.),0. )

*
      DO 1 K = 1,N
        TM(K) = F(K)
1    CONTINUE

*
      DO 10 K = 2,N-1
        F(K) = A0 * TM(K) + A1 * (TM(K-1) + TM(K+1))
10   CONTINUE

*
      RETURN
      END

*
*
*****
*
      SUBROUTINE EXPTRAN( NPT,NM,X,NSP,NPREC,DT,NW,IW1 )
      REAL X(NSP),KR(200,10),KI(200,10),F(8192,2)
      COMMON /KRKI/ KR,KI
      COMMON /CO6/ CO6WORK(8192)

*
      NPTP2 = NPT + 2
      DO 5 I = 1,NM
        II = I + NM

```

```

*
* IF( LMFLG(1:2) .EQ. 'IN' ) THEN
*   PINFIN = CMPLX( 0.,0. )
* ELSE
*   PINFIN = CMPLX( 1.,0. )
* END IF
*
*
* T = (NPREC - 1) * DT
* TPT = 8.*ATAN(1.0) / T
* DO 10 I = 1,NM
*   II = I+NM
*   WC = X(I*2-1)
*   Z = X(I*2)
*
*   RAD = 1. - Z*Z
*   IF( RAD .LT. 0. ) RAD = 0.
*   WD = WC * SQRT( RAD )
*
*   WDM = WD - TPT
*   WDP = WD + TPT
*
*   SI = SIN( WD*T )
*   CO = COS( WD*T )
*
*
*   WCZ=WC*Z
*
*   WCZT = WCZ*T
*   IF( WCZT .GT. 675. ) THEN
*     WCZT = 675.
*   ELSE IF( WCZT .LT. -741. ) THEN
*     WCZT = -741.
*   END IF
*
*   W = (IW1 - 1) * DW - DW
*   DO 10 K = 1,NW
*     W = W + DW
*     B = CMPLX( -WCZ, -W )
*     BB = B * B
*     A = 1./ ( BB + WD*WD )
*
*   A1 = 1./ ( 2. * ( BB + WDM*WDM ) )
*   A2 = 1./ ( 2. * ( BB + WDP*WDP ) )
*   E = EXP( CMPLX( -WCZT, -W*T ) ) * PINFIN
*
*   DFA = A * WD
*   * *
*   * * - P46 * ( A1 * ( E*( B*SI - WDM*CO ) + WDM )
*   * *       + A2 * ( E*( B*SI - WDP*CO ) + WDP ) )
*
*   DFB = A * (- B )
*   * *
*   * * - P46 * ( A1 * ( E*( WDM*SI + B*CO ) - B )
*   * *       + A2 * ( E*( WDP*SI + B*CO ) - B ) )
*
*
*   KR(K,I) = REAL( DFA )
*   KI(K,I) = AIMAG( DFA )

```

```

      WCZT = -741.
      END IF
*
      W = (IW1 - 1) * DW - DW
      DO 10 K = 1,NW
        W = W + DW
        B = CMPLX( -WCZ, -W )
        BB = B * B
        A = 1./ ( BB + WD*WD )
*      A1 = 1./ ( 2. * ( BB + WDM*WDM ) )
*      A2 = 1./ ( 2. * ( BB + WDP*WDP ) )
        E = EXP( CMPLX( -WCZT, -W*T ) )
*
        DFA = A * ( E * ( B*SI - WD*CO ) + WD )
*      - P46 * ( A1 * ( E*( B*SI - WDM*CO ) + WDM )
*      + A2 * ( E*( B*SI - WDP*CO ) + WDP ) )
*
        DFB = A * ( E * ( B*CO + WD*SI ) - B )
*      - P46 * ( A1 * ( E*( WDM*SI + B*CO ) - B )
*      + A2 * ( E*( WDP*SI + B*CO ) - B ) )
*
        KR(K,I) = REAL( DFA )
        KI(K,I) = AIMAG( DFA )
        KR(K,II) = REAL( DFB )
        KI(K,II) = AIMAG( DFB )
      10 CONTINUE
*
*
      RETURN
      END
*
*
*****
*
      SUBROUTINE LSQFUNM( NFP,NSP,XC,CMON )
*
      REAL XC(NSP),CMON(NSP)
      REAL KR(200,10),KI(200,10),VEC(10),MAT(10,10),WKS1(10),WKS2(10),
* AA(10,10),X(10)
      CHARACTER*10 SMFLG,LMFLG,METHFLG
      COMMON /FLGS/ SMFLG,LMFLG,METHFLG
      COMMON /FUNCT/ ER(200),EI(200),C(10),IW1,DW,NPREC,DT,NPT
      COMMON /KRKI/ KR,KI
*
      NM = NSP/2
      NW = NFP/2.
*
      DO 1 I = 1,NSP
        X(I) = XC(I)
      1 CONTINUE
*      CALL VTRAN( X,NSP,'OUT' )
*

```

APPENDIX D. SOURCE CODE OF SYSTEM IDENTIFICATION PROGRAM

```

*
      CALL RDCI( NP,FALPHA,XALPHA,ISDEC,ITERHX,DELFMN )
*
* FORM SAP STA DIRECTORY
*
      M = 0
      DO 20 I = 1,NM
        M = M + 1
        DO 20 J=1,DMOD(I,2)
          DSTASP(I,J,1) = DSTA(I,J,1)
          M = M + DSTA(I,J,1)
          DO 20 K = 1,DSTA(I,J,1)
            DSTASP(I,J,K+1) = DSTACV( DSTA(I,J,K+1) )
        20 CONTINUE
*
      WRITE(35,21) M
      21 FORMAT(/// No. of Measurements (M) = ',15)
*
* INITIALIZE PARAMETER DIRECTORY MATRICES
*
      DO 22 I = 1,NP
        DP(I) = I
      22 CONTINUE
      CALL DIRGEN
*
* READ IN BASE VALUES OF XB FROM EXISTING SAP INPUT FILE
*
      CALL RDSAPIN( XB,NP,NMT )
*
* READ THE EXPERIMENTAL FREQUENCIES AND MODE SHAPES
*
      CALL RDEXPD
*
* GENERATE ARTIFICIAL EXPERIMENTAL DATA FILE IF NECESSARY
*
      IF( LARTGH ) THEN
        CALL SAPFUNC( XB,NP,FC,FVEC,M )
        WRITE(35,30) FC
      30  FORMAT( ///' ARTIFICIAL DATA GENERATION RUN'//
*          '   FC = ',E10.3 )
        CALL DELTAP
        STOP
      END IF
*
***** CALL SEARCH ROUTINE *****
*
      CALL SRCH( XB,NP,FALPHA,XALPHA,ISDEC,ITERMX,DELFMN,NPN,FVEC,M )
*
      STOP
      END
*****

```

12 CONTINUE

\*

```

read(32,4) ajunk, ajunk
READ(32,*) FALPHA, XALPHA, ISDEC, ITERMX, DELFMN
read(32,4) ajunk, ajunk
READ(32,*) (DEL(I),I=1,4)
DO 13 I = 1,4
    DEL(-1) = 1. / DEL(I)

```

13 CONTINUE

\*

```

read(32,4) ajunk, ajunk
READ(32,*) NSKP(1), NSKP(2), NNDSPRD, LARTGN

```

\*

```

read(32,4) ajunk, ajunk
READ(32,*) NM, WTF, WTMS
read(32,4) ajunk, ajunk
DO 15 I = 1,NM
    READ(32,*) (DMOD(I,J),J=0,2),(DMOD(I,J),J=3,DMOD(I,2)+2)

```

15 CONTINUE

```

NMT = DMOD(NM,0)
read(32,4) ajunk, ajunk
DO 17 I = 1,NM
    DO 17 J = 1,DMOD(I,2)
        READ(32,16) DSTA(I,J,1),(DSTA(I,J,K+1),K=1,DSTA(I,J,1))

```

16 FORMAT( 1X,12, 20(1X,12) )

17 CONTINUE

\*

```

RETURN
END

```

```
ERVEC(I1) = (FU(I) - FR(I)) * WT(I1)
FC = FC + ERVEC(I1) * ERVEC(I1)
*
DO 50 J = 1,DNOD(I,2)
  DO 50 K = 1,DSTA(I,J,1)
    I1 = I1 + 1
    FVEC(I1) = FAC(I) * MSR(K,J,I)
    ERVEC(I1) = (MS(K,J,I) - FVEC(I1)) * WT(I1)
    FC = FC + ERVEC(I1) * ERVEC(I1)
  50 CONTINUE
*
*
  RETURN
  END
*=====
```

```
*
      READ(33,992) (A(1),I=1,NBEAMS + 3)
*
* R/W BOUNDARY ELEMENT DATA
*
      READ(33,993) (IDATA(1),I=1,2)
      NBEL = IDATA(2)
      READ(33,992) A(1)
*
      READ(33,995) (A(1)(1:60),R1(I),I=1,NBEL)
995 FORMAT( A60,E10.4 )
      DO 40 I1 = 1,NPTYP(2)
          I = I1 + NPTYP(1)
          XB(DPI(I,3)) = R1(DPI(I,1))
      40 CONTINUE
*
      WRITE(35,997)
997 FORMAT(//' BOUNDARY ELEMENT DATA')
      WRITE(35,995) (A(1)(1:60),R1(I),I=1,NBEL)
*
* R/W LUMPED MASSES AND REST OF FILE
*
      READ(33,992) (A(1),I=1,12)
*
      RETURN
      END
*=====
```

```

*
      WRITE(5,994) (IDATA(I),(R(I,J),J=1,6),I=1,NPROP)
*
* R/W BEAM DATA
*
      READ(33,992) (A(I),I=1,NBEAMS + 3)
      WRITE(5,992) ( A(I),I=1,NBEAMS + 3)
*
* R/W BOUNDARY ELEMENT DATA
*
      READ(33,993) (IDATA(I),I=1,2)
      WRITE(5,993) (IDATA(I),I=1,2)
      NBEL = IDATA(2)
      READ(33,992) A(1)
      WRITE(5,992) A(1)
*
      READ(33,995) (A(I)(1:60),R1(I),I=1,NBEL)
995 FORMAT( A60,E10.4 )
      DO 40 I1 = 1,NPTYPN(2)
          I2 = I1 + NPTYPN(1)
          I = DPTYPN(2,I1)
          R1(DPI(I,1)) = XB(I2)
          DO 40 J1 = 1,DPI(I,4)
              J = J1 + DPI(I,5) - 1
              R1(DSLP(J,1)) = XB(I2) * SLRAT(J)
40 CONTINUE
*
      WRITE(5,995) (A(I)(1:60),R1(I),I=1,NBEL)
*
* R/W LUMPED MASSES AND REST OF FILE
*
      DO 50 I = 1,75
          READ(UNIT=33,FMT=992,END=52) A(1)
          WRITE(UNIT=5,FMT=992) A(1)
50 CONTINUE
*
52 RETURN
      END
=====

```

```

50 CONTINUE
*
* READ FREQUENCIES
*
      READ(6,993) (FR(I),I=1,NMT)
993 FORMAT(23X,F10.0)
*
      DO 60 I = LN1+NMT, LN2-1
        READ(6,992) JUNK
60 CONTINUE
*
* READ MODE SHAPES
*
      DO 70 I = 1, NMT
        DO 62 J = 1, 10
          READ(6,992) JUNK
62 CONTINUE
          DO 64 K = 1, NNDSPRD
            READ(6,994) (MSU(K,J,I), J=1,6)
994 FORMAT( 7X,6(2X,F12.0) )
            64 CONTINUE
          70 CONTINUE
*
* TRANSFORM INTO CURVILINEAR COORDINATES
*
      DO 80 I = 1, NMT
        DO 77 K = 42, 77, 1
          DO 77 J1 = 1, 4, 3
            J2 = J1 + 1
            TX = MSU(K, J1, I)
            TY = MSU(K, J2, I)
            MSU(K, J1, I) = TX * COS(TH(K)) - TY * SIN(TH(K))
            MSU(K, J2, I) = TX * SIN(TH(K)) + TY * COS(TH(K))
77 CONTINUE
          DO 78 K = 47, 71, 1
            DO 78 J1 = 1, 4, 3
              J2 = J1 + 1
              TX = MSU(K, J1, I)
              TY = MSU(K, J2, I)
              MSU(K, J1, I) = TX * COS(TH(K)) - TY * SIN(TH(K))
              MSU(K, J2, I) = TX * SIN(TH(K)) + TY * COS(TH(K))
78 CONTINUE
          DO 79 K = 49, 73, 1
            DO 79 J1 = 1, 4, 3
              J2 = J1 + 1
              TX = MSU(K, J1, I)
              TY = MSU(K, J2, I)
              MSU(K, J1, I) = TX * COS(TH(K)) - TY * SIN(TH(K))
              MSU(K, J2, I) = TX * SIN(TH(K)) + TY * COS(TH(K))
79 CONTINUE
80 CONTINUE
*

```

```

SUBROUTINE RDEXPD
  implicit real*8 (a-h,o-z)
*
* THIS SUBROUTINE READS THE EXPERIMENTAL DATA FROM
* DIRECT ACCESS FILE EXPDATA (TAPE 36).
*
  LOGICAL LARTGN
  INTEGER DMOD(10,0:6),DSTA(10,4,59),DSTASP(10,4,59)
  REAL*8 FU(10),MS(58,4,10),ERVEC(400),EVEC(400),WT(400),
* WTD(58,6)
*
  COMMON /DEXP/DMOD,DSTA,DSTASP,NM,NMT,IKOUNT,LN1,LN2,NNDSPRD,LARTGN
  COMMON /MSEXP/ FU,MS
  COMMON /VEC/ ERVEC,EVEC,WT,WTF,WTMS
  COMMON /WTD/ WTD
*
*
  II = 0
  DO 10 I = 1,NM
    II = II + 1
    I1 = DMOD(I,1)
    I2 = (I1-1) * 7 + 1
    READ( UNIT=36,FMT=9,REC=I2) FU(I)
    WT(II) = WTF
    DO 10 J = 1,DMOD(I,2)
      IREC = I2 + DMOD(I,J+2)
      READ( UNIT=36,REC=IREC,FMT=9) (MS(K,J,I),K=1,58)
9    FORMAT( 58(E10.4,3X))
      DO 10 K = 1,DSTA(I,J,1)
        II = II + 1
        MS(K,J,I) = MS(DSTA(I,J,K+1),J,I)
        WT(II) = WTD(DSTA(I,J,K+1),DMOD(I,J+2))
10 CONTINUE
*
  RETURN
  END

```

```

*
* DETERMINE BASE ERROR, fb
*
      call sapfunc( xb,n,fb,f(1,0),m )
*
      write(35,1) fb
1 format(//' Base Error = ',e12.6 )
      fbmin = fb * falpha
      do 5 j = 1,m
          bervec(j) = ervec(j)
5 continue
*
      if( itermx .lt. 0 ) then
          call endprog( xb, n, m )
      end if
*
* BEGIN LOOP TO CHECK BOUNDS, SCALE AND FIT PARABS
* FOR EACH PARAMETER
*
      write(35,4)
4 format(//// BOUNDS RESULTS'//// Param. increm. error   x(i)'/)
*
      ipn = 0
      do 20 i = 1,n
*
          call bounds( i,xb,n,fbmin,m )
          if( dbnd(1,i) .eq. 0 ) .or. (dbnd(2,i) .eq. 0 ) goto 19
          ipn = ipn + 1
*
* SCALE PARAMETER
*
          imax = max( abs(dbnd(1,i)), abs(dbnd(2,i)) )
          xmax = xb(i) * del(imax)
          call scafac( xalpha, x(0), xmax, scf(1,i), 2 )
*
* FIT PARABOLA TO (SCALED FUNCTION, MEASUREMENT) PAIRS
*
          do 12 j = dbnd(1,i),dbnd(2,i)
              x(j) = xsc( x(j), i )
              f1(j) = f(1,j)
12 continue
          npts = dbnd(2,i) - dbnd(1,i) + 1
*
          lrpt = .false.
          call parab( f1(dbnd(1,i)), x(dbnd(1,i)), npts, parco(1,1,ipn),
* 3, lrpt )
*
          lrpt = .true.
          do 14 k = 2,m
              do 13 j = dbnd(1,i),dbnd(2,i)
                  f1(j) = f(k,j)
13 continue

```

```

*      ' > 1.0 e+20 x value projected for parameter no. ',i2 )
      else
        sv(i) = (xnew - xb(i1)) / float(isdec)
        goto 44
      end if
*
* CONDENSE GRADIENT VECTOR AND HESSIAN MATRIX
*
      nn = nn - 1
      do 42 j = i,nn
        dp(j) = dp(j+1)
        g(j) = g(j+1)
        do 42 jj = 1,nn
          h(j,jj) = h(j+1,jj)
          h(jj,j) = h(jj,j+1)
        42 continue
      44 continue
*
      if( nn .lt. nnold ) goto 30
*
* GENERATE PARAMETER DIRECTORY MATRICES
*
      dp(nn+1) = -1
      call dirgen
*
* PERFORM LINE SEARCH
*
      istpmx = 10 * isdec
      fbold = fb
      call insrch( xb, sv, dp, n, nn, istpmx, fb, fvec, m )
*
      goto 2
*
*
      end

```

```

subroutine convch( iter, itermx, fb, fbold, delfmn, xb, n, m )
implicit real*8 (a-h,o-z)
real*8 xb(n)
*
* This subroutine checks to see if the convergence criteria
* have been satisfied. If so, LCONV is returned as .true.
*
*
* Check to see if max. no. of iterations have been exceeded
*
    if( iter .gt. itermx ) then
        write(35,2) itermx
2    format(///' *** MAX. NO. OF ITERATIONS( ',12,' ) EXCEEDED')
        call endprog( xb, n, m )
    else if( iter .eq. 1 ) then
        return
    else
        delf = abs( (fbold - fb) / fbold )
        if( delf .lt. delfmn ) then
            write(35,20) delf, delfmn
20    format(///' *** CONVERGENCE CRITERIA SATISFIED//
*        '    delf < delfmn (',e10.3,' < ',e10.3,')' )
            call endprog( xb, n, m )
        else
            return
        end if
    end if
*
*
return
end

```

```

      subroutine endprog( xb, n, m )
*
* This subroutine is called at the end of execution of the program.
* It calls sapfunc once more and writes out exper. and anal. measurements.
*
      implicit real*8 (a-h,o-z)
      LOGICAL LARTGN
      INTEGER DMOD(10,0:6),DSTA(10,4,59),DSTASP(10,4,59)
      integer nptyp(2), dpi(10,5), dslp(60,2), dptyp(2,10), nptypn(2),
* dp(11), nskip(2)
      REAL*8 FU(10),FR(10),MS(58,4,10),MSR(58,4,10),XB(N)
      REAL*8 ERVEC(400), FAC(10), FVEC(400), EVEC(400), WT(400)
*
      COMMON /MSR/ FR,MSR
      COMMON /MSEXP/ FU,MS
      COMMON /DEXP/DMOD,DSTA,DSTASP,NM,NMT,IKOUNT,LN1,LN2,NNDSPRD,LARTGN
      COMMON /VEC/ ERVEC,EVEC,WT,WTF,WTMS
      COMMON /FVEC/ FVEC
      common /dirpar/ nptyp, dpi, dslp, strat, nslp, dptyp, nptypn,dp,
* nskip
*
* SET PARAMETER DIRECTORY MATRICES FOR FULL "n" PARAMTERS
*
      do 1 i = 1,n
         dp(i) = i
1 continue
      call dirgen
*
      call sapfunc( xb, n, fb, fvec, m )
*
      write(35,2)
2 format('1', ' SUMMARY OF MEASUREMENTS'//
* ' ',14x,7(1h-), ' MEASUREMENT ',7(1H-)//
* ' Mode Station No. Experimental Analytical      Error')
*
      ii = 0
      do 10 i = 1,nm
         ii = ii + 1
         write(35,4) i,ii, fu(i),fr(i),ervec(ii)
4 format('/ ',i4,11x,i4,3(3x,g10.4))
         do 10 j = 1,dmod(i,2)
            do 10 k = 1,dsta(i,j,1)
               ii = ii + 1
               write(35,6) i,dsta(i,j,k+1),ii,ms(k,j,i),
* fvec(ii),ervec(ii)
6 format(' ',i4,3x,i4,4x,i4,3(3x,g10.4))
10 continue
*
      call deltap
*
      stop
      end

```

```

subroutine lnsrch( xb, sv, dp, n, nn, istpmx, fb, fvec, m )
  implicit real*8 (a-h,o-z)
*
* This subroutine performs a "line search" along the direction
* defined by the vector sv
*
*
integer dp(n)
real*8 x(10), f(0:50), xdum(10), coef(3), xb(n), sv(nn), fvec(m)
*
write(35,2)
2 format(///// LINE SEARCH RESULTS///// Step Error x(i)')
*
* PERFORM LINE SEARCH
*
istep = 0
f(0) = fb
*
20 istep = istep + 1
do 22 i = 1,nn
  i1 = dp(i)
  x(i) = xb(i1) + sv(i) * float(istep)
22 continue
*
call sapfunc( x, nn, f(istep), fvec, m )
*
write(35,21) istep, f(istep), (x(i),i=1,nn)
21 format(' ',i5,2x, e9.4,2x, 10(e9.4,2x) )
*
if( f(istep) .lt. f(istep-1) ) then
  if( istep .ge. istpmx ) then
    write(35,23) istepmx
23 format( /// *** error from LNSRCH:/'
*       ' max. no. of steps (' ,i4,') exceeded' )
    call endprog( xb, n, m )
  else
    goto 20
  end if
else
  if( istep .eq. 1 ) then
    write(35,24)
24 format(/// *** error from LNSRCH:/'
*       ' line search failed to reduce error' )
    call endprog( xb, n, m )
  end if
end if
*
* FIT PARABOLA THROUGH LAST 3 POINTS TO GET NEW X
*
xdum(3) = istep
xdum(2) = istep - 1
xdum(1) = istep - 2

```

```

      subroutine parabc( f, x, n, b, ithree, lrpt )
      implicit real*8 (a-h,o-z)
      *
      * This subroutine fits a parabola to the x, F(x) pairs of points
      * for each parameter x. The coefficients of the equation
      *  $y = B(1) + B(2)*x + B(3)*x*x$ 
      * are determined from a least squares formulation
      * If lrpt = .true. then matrix a is not recalculated
      *
      logical lrpt
      real*8 f(n), x(n), b(ithree)
      real*8 a(3,3),bd(3),as(3,3)
      *
      common /storag/ as
      *
      do 2 i = 1,3
         bd(i) = 0.
      2 continue
      *
      do 4 i = 1,n
         bd(1) = bd(1) + f(i)
         bd(2) = bd(2) + f(i)*x(i)
         bd(3) = bd(3) + f(i)*x(i)*x(i)
      4 continue
      *
      if( lrpt ) then
      *
         do 5 i = 1,3
            do 5 j = 1,3
               a(i,j) = as(i,j)
            5 continue
         *
         else
      *
      * Compute sums
      *
         do 6 i = 1,3
            do 6 j = 1,3
               a(i,j) = 0.
            6 continue
         *
         a(1,1) = n
         do 10 i = 1,n
            x1 = x(i)
            x2 = x1 * x1
            x3 = x2 * x1
            x4 = x3 * x1
         *
         a(1,2) = a(1,2) + x1
         a(2,2) = a(2,2) + x2
         a(2,3) = a(2,3) + x3
         a(3,3) = a(3,3) + x4

```

```

subroutine prtout( iter, fb, xb, n, dp, nn )
  implicit real*8 (a-h,o-z)
*
* This subroutine prints out to the log file the results of the
* last iteration
*
*
integer dbnd(2,10), dp(nn)
real*8 f(400,-4:4), x(-4:4), del(-4:4), xb(n), parco(3,400,10)
real*8 g(10), h(10,10)
character line*82
*
common /bnd/ f,x,del,dbnd
common /cgrdhsn/ parco, g, h
*
*
write(35,2) iter, fb
2 format( '1', ' Iteration', i2// ' ', ' Sum of Squarred Error: ',
* e14.7 //// )
*
write(35,4)
4 format( ' ', ' Parameter Base', 11x, 'Lower', 14x, 'Upper' /
* ' ', 4x, 'No.', 5x, 'Value', 10x, 'Bound', 14x, 'Bound', 5x,
* 'Normalized Slope' )
*
in = 0
do 10 i = 1, n
write( line, 6 ) i, xb(i)
6 format( ' ', 4x, i2, 3x, e10.4, 3x )
*
if( dbnd(1,i) .eq. 0 ) then
line(26:34) = 'Unbounded'
else
write( line(23:37), 7 ) xb(i)*del(dbnd(1,i)), dbnd(1,i)
7 format( e10.4, ' (', i2, ')' )
end if
*
if( dbnd(2,i) .eq. 0 ) then
line(44:52) = 'Unbounded'
else
write( line(41:55), 7 ) xb(i)*del(dbnd(2,i)), dbnd(2,i)
end if
*
if( (dbnd(1,i) .ne. 0) .and. (dbnd(2,i) .ne. 0) ) then
in = in + 1
write( line(60:82), 8 ) g(in) * xb(i)
8 format( e10.4 )
end if
*
write( 35, 9 ) line
9 format( a82 )
*

```

```

      subroutine scafac( alpha, x0, xmax, b, itwo )
      implicit real*8 (a-h,o-z)
*
* This subroutine computes the coefficients, B, to scale the parameter
* (so that it equals 1 at the base location and 1+alpha at xmax)
* The scaled parameter, xs, is related to the unscaled parameter, x,
* by the following equation:  $x_s = B(1) + B(2)\log(x)$ 
*
      integer iwork(2)
      real*8 b(itwo)
      real*8 a(2,2), bd(2)
*
      if( alpha .lt. 0. ) then
         b(1) = 0.
         b(2) = 1.
         return
      else
*
* SET UP SIMULTANEOUS EQUATIONS
*
         a(1,1) = 1.0
         a(1,2) = x0
         a(2,1) = 1.0
         a(2,2) = xmax
*
         bd(1) = 1.0
         bd(2) = alpha
*
* SOLVE EQUATIONS FOR B
*
         call solveq( a, bd, 2, 1, 2, iwork )
*
         do 10 i = 1,2
            b(i) = bd(i)
         10 continue
*
         return
*
      end if
*
      end
      function xsc( x, ip )
      implicit real*8 (a-h,o-z)
*
* This function returns the scaled value of x
*
      common /scf/ scf(2,10)
*
      xsc = scf(1,ip) + scf(2,ip) * x
*

```

## LIST OF CCEER PUBLICATIONS

Report No.	Publication
CCEER-84-1	Saiidi, M., and R. Lawver, "User's Manual for LZAK-C64, A Computer Program to Implement the Q-Model on Commodore 64," Civil Engineering Department, Report No. CCEER-84-1, University of Nevada, Reno, January 1984.
CCEER-84-1 Reprint	Douglas, B., Norris, G., Saiidi, M., Dodd, L., Richardson, J. and Reid, W., "Simple Bridge Models for Earthquakes and Test Data," Civil Engineering Department, Report No. CCEER-84-1 Reprint, University of Nevada, Reno, January 1984.
CCEER-84-2	Douglas, B. and T. Iwasaki, "Proceedings of the First USA-Japan Bridge Engineering Workshop," held at the Public Works Research Institute, Tsukuba, Japan, Civil Engineering Department, Report No. CCEER-84-2, University of Nevada, Reno, April 1984.
CCEER-84-3	Saiidi, M., J. Hart, and B. Douglas, "Inelastic Static and Dynamic Analysis of Short R/C Bridges Subjected to Lateral Loads," Civil Engineering Department, Report No. CCEER-84-3, University of Nevada, Reno, July 1984.
CCEER-84-4	Douglas, B., "A Proposed Plan for a National Bridge Engineering Laboratory," Civil Engineering Department, Report No. CCEER-84-4, University of Nevada, Reno, December 1984.
CCEER-85-1	Norris, G. and P. Abdollahiaee, "Laterally Loaded Pile Response: Studies with the Strain Wedge Model," Civil Engineering Department, Report No. CCEER-85-1, University of Nevada, Reno, April 1985.
CCEER-86-1	Ghusn, G. and M. Saiidi, "A Simple Hysteretic Element for Biaxial Bending of R/C in NEABS-86," Civil Engineering Department, Report No. CCEER-86-1, University of Nevada, Reno, July 1986.
CCEER-86-2	Saiidi, M., R. Lawver, and J. Hart, "User's Manual of ISADAB and SIBA, Computer Programs for Nonlinear Transverse Analysis of Highway Bridges Subjected to Static and Dynamic Lateral Loads," Civil Engineering Department, Report No. CCEER-86-2, University of Nevada, Reno, September 1986.
CCEER-87-1	Siddharthan, R., "Dynamic Effective Stress Response of Surface and Embedded Footings in Sand," Civil engineering Department, Report No. CCEER-86-2, University of Nevada, Reno, June 1987.
CCEER-87-2	Norris, G. and R. Sack, "Lateral and Rotational Stiffness of Pile Groups for Seismic Analysis of Highway Bridges," Civil Engineering Department, Report No. CCEER-87-2, University of Nevada, Reno, June 1987.
CCEER-88-1	Orie, J. and M. Saiidi, "A Preliminary Study of One-Way Reinforced Concrete Pier Hinges Subjected to Shear and Flexure," Civil Engineering Department, Report No. CCEER-88-1, University of Nevada, Reno, January 1988.
CCEER-88-2	Orie, D., M. Saiidi, and B. Douglas, "A Micro-CAD System for Seismic Design of Regular Highway Bridges," Civil Engineering Department, Report No. CCEER-88-2, University of Nevada, Reno, June 1988.
CCEER-88-3	Orie, D. and M. Saiidi, "User's Manual for Micro-SARB, a Microcomputer Program for Seismic Analysis of Regular Highway Bridges," Civil Engineering Department, Report No. CCEER-88-3, University of Nevada, Reno, October 1988.

- CCEER-89-1 Douglas, B., M. Saiidi, R. Hayes, and G. Holcomb, "A Comprehensive Study of the Loads and Pressures Exerted on Wall Forms by the Placement of Concrete," Civil Engineering Department, Report No. CCEER-89-1, University of Nevada, Reno, February 1989.
- CCEER-89-2 Richardson, J. and B. Douglas, "Dynamic Response Analysis of the Dominion Road Bridge Test Data," Civil Engineering Department, Report No. CCEER-89-2, University of Nevada, Reno, March 1989.